

Drying and hydration of proteins at high concentration

Jacob Bouman

Thesis committee

Promotor

Prof. Dr. E. van der Linden
Professor of Physics and Physical Chemistry of Foods
Wageningen University

Co-Promotors

Dr. R.J. de Vries
Associate Professor, Physical Chemistry and Soft Matter
Dr. P. Venema
Assistant Professor Physics and Physical Chemistry of Foods

Other members

Prof. Dr. E.J. Windhab, ETH Zürich
Prof. Dr. R.F Witkamp, Wageningen University
Prof. Dr. J.P.M. van Duynhoven, Wageningen University
Dr. Ir. A. Poortinga, Eindhoven, University of Technology

This research was conducted under the auspices of the Graduate School Vlag (Advanced Studies in Food Technology, Agrobiotechnology, Nutrition and Health Sciences)

Drying and hydration of proteins at high concentration

Jacob Bouman

Thesis

submitted in fulfillment of the requirements for the degree of doctor

at Wageningen University

by the authority of the Rector Magnificus

Professor A.P.J. Mol in the presence of the

Thesis Committee appointed by the Academic Board

to be defended in public

on Friday 13 November 2015

at 16:00 in the Aula.

Jacob Bouman

Drying and hydration of proteins at high concentration

161 pages

PhD thesis, Wageningen University, Wageningen, NL (2015)

With references, summaries in English and Dutch

ISBN: 978-94-6257-550-9

Contents

Chapter 1

General Introduction 9

Chapter 2

Coating formation during drying of β -lactoglobulin: gradual and sudden changes 19

Chapter 3

Hole and vacuole formation during drying of sessile whey protein droplets 49

Chapter 4

Extrusion-injection moulded zein matrices as controlled oral delivery system 69

Chapter 5

Controlled release from zein matrices: interplay of drug hydrophobicity and pH 95

Chapter 6

General discussion 123

Summary/Samenvatting 147

Acknowledgements 155

About the author 158

Publications 159

Overview of completed training activities 160



1. General Introduction

1.1. General introduction

Proteins are the building blocks of life and serve a wide range of essential functions in organisms. Not surprisingly, the use of proteins towards higher concentrations is of interest for food, pharmaceutical and medical applications. Nevertheless, the preparation of products with desired product properties can be challenging, when approaching higher protein concentrations. Therefore, in this thesis we investigate proteins at higher concentrations, especially focussing on their drying and hydration behaviour.

Proteins are large biopolymers, consisting of one or more long chain(s) of amino acid residues. The amino acid sequence of this chain is called the primary structure. This chain folds into a 3D-structure, which is described by its secondary, tertiary and quaternary structure. The protein folding is essential to its functionality. Many metabolic reactions in organisms are catalysed by enzymes, DNA is replicated by proteins and in cells proteins often facilitate active transport of e.g. glucose or ions. Even on a macroscopic scale protein functionality can be observed. For example, muscle contraction is essentially caused by the interplay of two proteins, actin and myosin. Protein folding is easily altered by e.g. heat, a change in pH or in ionic strength, as it is mainly held together by non-covalent interactions^[1]. This change in folding will cause a protein to lose its original function, however this can also give rise to new functionalities. Due to their range of functionalities, proteins are used in a wide variety of applications.

Recently, an increasing amount of applications and products are developed, where proteins are present at high concentration. For obese patients, a protein rich diet is often a successful way of losing weight as their strong satiating properties, protein rich food products can help to control food intake^{[2],[3]}. Here, especially plant based proteins are an increasing subject of investigation. Traditionally, in the western world, most of the protein intake originates from animals^[4]. Compared to plant based proteins, animal based proteins are a much less environmentally sustainable^[5]. Therefore, there is a growing demand for products rich in plant derived proteins, which are an important category of the so-called “superfoods”. Especially, when creating meat-like structures suitable for meat alternatives, it is essential to use proteins at high concentration. Some examples of the plant based proteins for food products are soy^[6], pea^[7] and quinoa^[8]. Another application of concentrated proteins is their use as a naturally derived barrier material. Here the proteins

are used as to make coatings or films^[9, 10], that can be used for food preservation. In addition, proteins at high concentration may be used to form microcapsules for nutritional purposes^[11]. The use of dense protein systems has been a topic of great interest for the pharmaceutical community as well. Especially in the field of drug delivery, the use of concentrated proteins have proven to be a useful slow release matrix in a wide range of applications^{[12, 13] [14]}

1.2. Protein dynamics at low water content

When approaching high concentrations, the dehydration of proteins becomes an issue. Water is considered to be essential for the folding of proteins and influences their stability, dynamics, and functionality^[15]. The hydration forces are responsible for packing and stabilization of the protein structure. Particularly, water participates in hydrogen bonding and in the screening of electrostatic interactions.^{[16], [15]} The majority of proteins is water soluble, but also non-soluble proteins still have some degree of hydration. By the loss of hydration, the protein's original functionality is often lost, and the folding can be irreversibly altered. Understanding the different stages of protein hydration is of major importance for both protein stability and their functionality. An important parameter is the so called monolayer moisture content which is defined as water content at which a substance is covered with a single layer of water molecules. In some studies, this parameter is regarded as a critical parameter above which enzyme activity is optimal and below which protein stability is optimal^[17, 18]. However, many different values exist for this parameter therefor also some ambiguity exist around the monolayer moisture content^{[18-20],[21]}. A lack in understanding might be due to the focus of a majority of studies on final properties in equilibrium conditions, leaving out the influence of the dynamics. The importance of the dynamical changes during drying is well reflected in many studies as drying conditions have been found to significantly influence final properties of protein systems^{[22],[23],[24],[25]}.

1.3. Applications: drying and hydration

A common way to prepare concentrated proteins is by solvent evaporation, a process commonly referred to as drying. Proteins in the dry state are physically, chemically and microbiologically more stable compared to proteins in the wet state^[18]. In many drying processes the protein solution is simply heated thereby evaporating the water. A disadvantage of this drying process is that it can alter the protein folding, as denaturation can occur during heating. Even at low temperatures the protein folding might due to

protein-protein interactions during to dehydration^[26]. A mild drying technique that is applied to minimize thermal denaturation is spray drying^[27]. In this process, solutions are dispersed into small drops in top of a spray drying tower. The atomisation causes a vast increase in the surface to volume ratio of the solution. Hot air is blown along these droplets, however, due to evaporative cooling the temperature in the droplet (i.e. the wet bulb temperature) remains relatively low. A process that can also minimise the dehydration damage is freeze drying. Here, a protein solution is rapidly frozen and subsequently subjected to a vacuum, which removes the ice by sublimation. The disadvantage of freeze drying compared to other drying techniques are the relatively high energy costs.

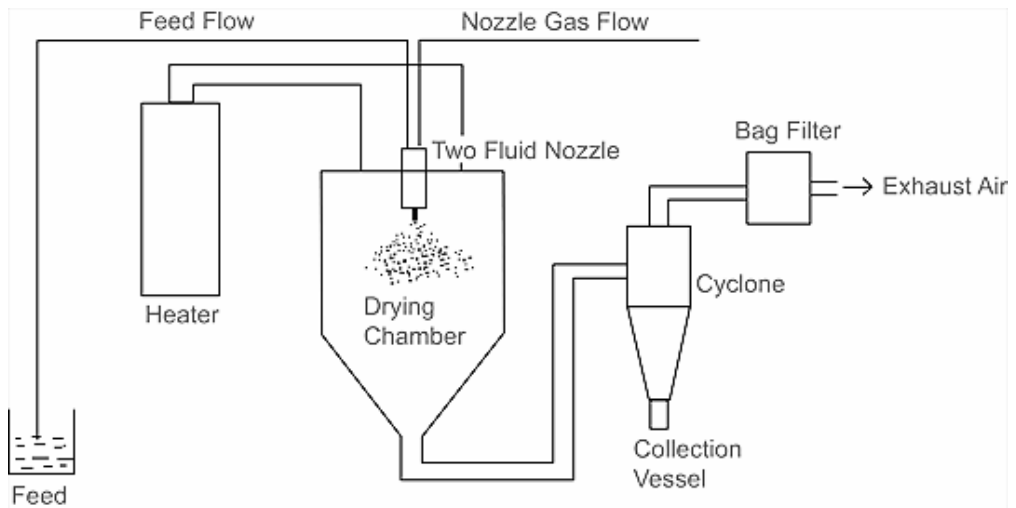


Figure 1: Schematic drawing of the spray drying process. A concentrated feed is atomised in the top of the tower and quickly dried by the gas flow also entering in the top of the tower. A cyclone and bag filter is used to collect the fines particle.^[27]

The hydration behaviour of proteins at low water content is also of importance for many applications. For powdered products, like infant formula, a good reconstitution behaviour is desired. Oppositely, when proteins are used for their barrier properties, their hydration should be as slow as possible. A protein source like whey protein can be used for both purposes. For many powdered applications the protein is kept in its native folding as making it overall more hydrophilic so it has quick hydration properties. In contrast, for films and coatings, it is often made more hydrophobic by denaturation, so it can function as a water barrier^[9]. A better understanding in how the protein hydrophobicity changes during

the drying and hydration, could result in developments in its functionality in many applications. In this thesis we focus on the use of two model proteins. We use whey protein, to study the drying process and we use the corn-derived protein zein, to study the hydration process.

1.4. Model proteins

1.4.1. Whey proteins

Whey protein is a mixture of globular proteins that after casein is the most abundant component in cow milk. Whey protein consists of four different proteins: β -lactoglobulin, α -lactalbumin, bovine serum albumin and immunoglobulins. Here β -lactoglobulin composes the majority of the protein present. Whey protein is water soluble and in solution heat denaturation already starts at approximately 65°C ^[16]. Traditionally, it was a waste product resulting from cheese production, while later it was found to have a high nutritional value, due to its amino acid composition. Whey protein is often used as dietary supplement and is an important ingredient in infant formula. Whey protein is one of the most investigated protein source and is therefore used as model system in this thesis.

1.4.2. Zein protein

Zein is a storage protein of corn and is organised in protein bodies located in the endosperm of the grain^[28]. Its main function is to provide a source of nitrogen during germination of the embryo. Traditionally, zein is a by-product from both starch and ethanol production. It consists of α -, β -, γ - and δ -zein, which are proteins with different molecular weight and modes of extraction^[29, 30]. The α -zein is the predominant protein, whose structure is a triple superhelix^[31]. The yellow colour of the powder is due to the lutein, localised in the non-polar interior of this helix. Several factors makes zein suitable for pharmaceutical applications. Zein can form tough, hydrophobic coatings that are stable against microbial degradation. Zein is soluble in aqueous ethanol, but not in water^[29]. In addition, it is biodegradable, biocompatible^[32, 33] and thermally stable up to $\sim 120^{\circ}\text{C}$ ^[34]. In this thesis we explore the potential of zein as a slow release agent for pharmaceutical drugs.

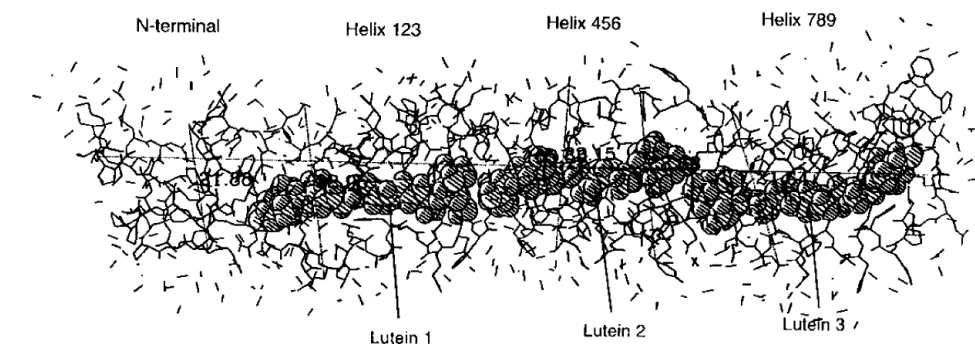


Figure 2: Structure of α -zein according to Momany^[31]. Solvent methanol molecules are noted as small lines. Lutein molecules are shown in space-filling representation.

1.5. Objective and outline of the thesis

In this thesis the dynamics of drying and hydration of proteins at low moisture content is studied. In **chapter 2** the dynamics of drying is studied on multiple lengthscales. Several in line techniques are used: diffusing wave spectroscopy, magnetic resonance imaging, IR-spectroscopy and dynamic vapour sorption. In **chapter 3**, the morphological changes of the drying of a whey protein solution droplet is monitored. Next to fundamental insight, also applications towards spray drying are discussed. In **chapter 4** the potential of a dense zein matrix as pharmaceutical excipient for the slow release of an active ingredient is investigated. Matrices are made by the use of hot-melt extrusion and injection moulding. Here also tune ability of drug release is considered. In **chapter 5** a wider range of drugs is used. Here both the effect of drug hydrophobicity and the electrical charge on release properties is studied. In the general discussion (**chapter 6**) the main findings of this thesis are discussed and further recommendations are presented.

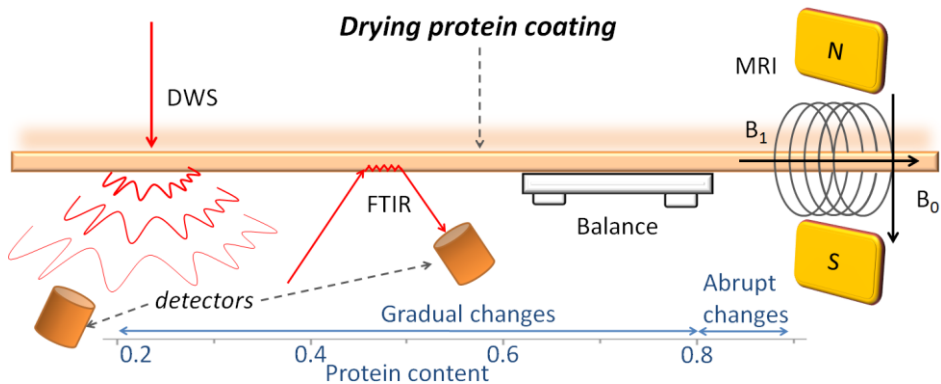
1.6. References

1. Michael Gromiha, M.; Saraboji, K.; Ahmad, S.; Ponnuswamy, M.N.; Suwa, M. Role of non-covalent interactions for determining the folding rate of two-state proteins. *Biophysical Chemistry* 2004, 107 (3), 263-272.
2. Westerterp-Plantenga, M.S.; Luscombe-Marsh, N.; Lejeune, M.P.G.M.; Diepvens, K.; Nieuwenhuizen, A.; Engelen, M.P.K.J.; Deutz, N.E.P.; Azzout-Marniche, D.; Tome, D.; Westerterp, K.R. Dietary protein, metabolism, and body-weight regulation: dose-response effects. 2006, 30 (S3), S16-S23.
3. Anderson, G.H.; Moore, S.E. Dietary Proteins in the Regulation of Food Intake and Body Weight in Humans. *The Journal of Nutrition* 2004, 134 (4), 974S-979S.

4. de Boer, J.; Hoek, A.; Elzerman, H. Social desirability: consumer aspects. in *Sustainable Protein Production and Consumption: Pigs or Peas?*; Springer, 2006; 99-127.
5. Pimentel, D.; Pimentel, M. Sustainability of meat-based and plant-based diets and the environment. *The American journal of clinical nutrition* 2003, 78 (3), 660S-663S.
6. Belloque, J.; García, M.; Torre, M.; Marina, M. Analysis of soyabean proteins in meat products: a review. *Critical Reviews in Food Science and Nutrition* 2002, 42 (5), 507-532.
7. Shand, P.; Ya, H.; Pietrasik, Z.; Wanasundara, P. Physicochemical and textural properties of heat-induced pea protein isolate gels. *Food Chemistry* 2007, 102 (4), 1119-1130.
8. Lorenz, K.; Coulter, L. Quinoa flour in baked products. *Plant Foods for Human Nutrition* 1991, 41 (3), 213-223.
9. Jooyandeh, H. Whey protein films and coatings: A review. *Pakistan Journal of Nutrition* 2011, 10 (3), 293-301.
10. John, M.K. Proteins as Raw Materials for Films and Coatings. in *Protein-Based Films and Coatings*; CRC Press, 2002.
11. Giroux, H.J.; Britten, M. Encapsulation of hydrophobic aroma in whey protein nanoparticles. *Journal of Microencapsulation* 2011, 28 (5), 337-343.
12. Paliwal, R.; Palakurthi, S. Zein in controlled drug delivery and tissue engineering. *Journal of Controlled Release* 2014, 189 (0), 108-122.
13. Georget, D.M.R.; Barker, S.A.; Belton, P.S. A study on maize proteins as a potential new tablet excipient. *European Journal of Pharmaceutics and Biopharmaceutics* 2008, 69 (2), 718-726.
14. Liu, X.; Sun, Q.; Wang, H.; Zhang, L.; Wang, J.Y. Microspheres of corn protein, zein, for an ivermectin drug delivery system. *Biomaterials* 2005, 26 (1), 109-115.
15. Levy, Y.; Onuchic, J.N. Water and proteins: a love-hate relationship. *Proceedings of the National Academy of Sciences of the United States of America* 2004, 101 (10), 3325-3326.
16. Haque, M.A.; Aldred, P.; Chen, J.; Barrow, C.J.; Adhikari, B. Comparative study of denaturation of whey protein isolate (WPI) in convective air drying and isothermal heat treatment processes. *Food Chemistry* 2013, 141 (2), 702-711.
17. Marcos, B.; Esteban, M.a.A.; López, P.; Alcalá, M.; Gómez, R.; Espejo, J.; Marcos, A. Monolayer values at 30°C of various spices as computed by the BET and GAB models. 1997, 204 (2), 109-112.
18. Bellissent-Funel, M. Collective effects in hydrated proteins. *Hydration processes in biology: theoretical and experimental approaches* 1999, 305 143.
19. Careri, G.; Gratton, E.; Yang, P.H.; Rupley, J.A. Correlation of IR spectroscopic, heat capacity, diamagnetic susceptibility and enzymatic measurements on lysozyme powder. *Nature* 1980, 284 (5756), 572-573.
20. Belton, P.S.; Colquhoun, I.J.; Grant, A.; Wellner, N.; Field, J.M.; Shewry, P.R.; Tatham, A.S. FTIR and NMR studies on the hydration of a high-Mr subunit of glutenin. *International Journal of Biological Macromolecules* 1995, 17 (2), 74-80.
21. De Jong, G.I.W.; Van den Berg, C.; Kokelaar, A.J. Water vapour sorption behaviour of original and defatted wheat gluten. *International Journal of Food Science & Technology* 1996, 31 (6), 519-526.

22. Alcantara, C.R.; Rumsey, T.R.; Krochta, J.M. Drying rate effect on the properties of whey protein films. *Journal of Food Process Engineering* 1998, 21 (5), 387-405.
23. Tapia-Blácido, D.R.; Sobral, P.J.A.; Menegalli, F.C. Effect of drying conditions and plasticizer type on some physical and mechanical properties of amaranth flour films. *LWT - Food Science and Technology* 2013, 50 (2), 392-400.
24. Denavi, G.; Tapia-Blácido, D.R.; Añón, M.C.; Sobral, P.J.A.; Mauri, A.N.; Menegalli, F.C. Effects of drying conditions on some physical properties of soy protein films. *Journal of Food Engineering* 2009, 90 (3), 341-349.
25. Soazo, M.; Rubiolo, A.C.; Verdini, R.A. Effect of drying temperature and beeswax content on physical properties of whey protein emulsion films. *Food Hydrocolloids* 2011, 25 (5), 1251-1255.
26. Cicerone, M.T.; Douglas, J.F. β -Relaxation governs protein stability in sugar-glass matrices. *Soft Matter* 2012, 8 (10), 2983-2991.
27. Patel, R.; Patel, M.; Suthar, A. Spray drying technology: an overview. *Indian Journal of Science and Technology* 2009, 2 (10), 44-47.
28. Cabra, V.; Vázquez-Contreras, E.; Moreno, A.; Arreguin-Espinosa, R. The effect of sulfhydryl groups and disulphide linkage in the thermal aggregation of Z19 α -zein. *Biochimica et Biophysica Acta (BBA) - Proteins and Proteomics* 2008, 1784 (7-8), 1028-1036.
29. Shukla, R.; Cheryan, M. Zein: the industrial protein from corn. *Industrial Crops and Products* 2001, 13 (3), 171-192.
30. Argos, P.; Pedersen, K.; Marks, M.; Larkins, B. A structural model for maize zein proteins. *Journal of Biological Chemistry* 1982, 257 (17), 9984-9990.
31. Momany, F.A.; Sessa, D.J.; Lawton, J.W.; Selling, G.W.; Hamaker, S.A.H.; Willett, J.L. Structural characterization of α -zein. *Journal of Agricultural and Food Chemistry* 2006, 54 (2), 543-547.
32. Breiteneder, H.; Mills, E.N.C. Plant food allergens - Structural and functional aspects of allergenicity. *Biotechnology Advances* 2005, 23 (6), 395-399.
33. Takagi, K.; Teshima, R.; Okunuki, H.; Sawada, J.I. Comparative study of in vitro digestibility of food proteins and effect of preheating on the digestion. *Biological and Pharmaceutical Bulletin* 2003, 26 (7), 969-973.
34. Selling, G.W. The effect of extrusion processing on Zein. *Polymer Degradation and Stability* 2010, 95 (12), 2241-2249.

The drying dynamics of protein coatings is of importance for many applications. The main focus of research so far is to investigate macroscopic properties of protein coatings, leaving drying dynamics virtually unexplored. An unique combination of techniques is used to monitor drying of a coating containing the protein β -lactoglobulin. The techniques used, cover both macroscopic and microscopic aspects of the drying process. For all water fractions amenable to diffusing wave spectroscopy analysis ($x_w > 0.2$ w/w), the tracer particles diffuse in the coating as in a Newtonian viscous medium. Magnetic resonance imaging shows both protein and water are distributed homogeneously over the coating during drying, up to water fractions above 0.2 w/w. When drying continues to lower water fractions, sudden transitions in drying behaviour are observed by both dynamic vapour sorption and IR-spectroscopy, which we suggest are due to changes in molecular interactions caused by dehydration of the protein backbone.



2. Coating formation during drying of β -lactoglobulin: gradual and sudden changes

¹Laboratory of Physical Chemistry and Soft matter and

²Physics and Physical Chemistry of foods, Wageningen

University, Wageningen, The Netherlands.

³School of Chemistry, University of East Anglia, Norwich,
United Kingdom.

⁴Department of Applied Physics, Eindhoven University of
Technology, Eindhoven, The Netherlands

This chapter is published as:

Bouman, J.^{1,2}; De Vries, R.¹; Venema, P.²; Belton, P.³; Baukh, V.⁴; Huinink, H. P.⁴; Van Der Linden, E.² Coating formation during drying of β -lactoglobulin: gradual and sudden changes. *Biomacromolecules* **2015**, 16 (1), 76-86.

2.1. Introduction

Due to a growing interest in environmentally friendly products, the use of proteins as a degradable material for films and coatings is increasingly explored. Some of the recently investigated applications include coatings of foods^[1, 2], tablets^[3] and bio plastics^[4]. Protein coatings are primarily made using the solvent casting method, where a protein solution is casted on a substrate and the finished coating is obtained after solvent evaporation. Alternatively, coatings can also be generated by solventless methods, such as compression molding or thermoplastic extrusion⁵. The latter coatings are generally recognized to have superior properties as compared to solvent casting-based coatings. Both methods require proteins with sufficient thermoplasticity^[5, 6], a condition typically not met by many globular proteins.

In the solvent casting method the coating gradually enters a more solid-like state during the drying process, causing dramatic changes in the physical properties of the coating. Often a plasticizer is added in order to increase the free volume of the proteins providing some macroscopic flexibility to the final coating. Most relevant for applications are the mechanical properties and the ability of the coatings to act as a selective barrier. Both these properties ultimately relate to the gradual loss of molecular mobility during coating drying. Considering barrier properties, the ability of a molecule to pass through a coating is related to mobility of the molecule inside the coating.

Previous research has predominantly focussed on the macroscopic properties of the finished films and coatings. Recent studies include oxygen and water permeability, tensile strength on a wide variety of films and coatings derived from both animal and plant proteins.^[4, 7] Given the wide variety of conditions and formulations where protein coatings can be developed, optimising coating functionality using only macroscopic techniques is a trial and error approach. A microscopic and dynamic approach could have added value, because it can provide an understanding of the mechanisms causing the different final properties.

Only a few studies investigated films and coatings on a microscopic and molecular scale to explain the macroscopic properties. When studying the influence of pH on soy protein-glycerol coatings, Guerrero^[8] found that the best mechanical properties are obtained at alkaline conditions. Using FTIR, the study found that unfolding of the protein is optimal at alkaline conditions, causing more intra- and inter-molecular bonds and hence better mechanical properties. In silk fibroin films^[9] it is shown that below the glass transition temperature T_g of silk proteins, the amide II region is affected upon water removal, while

the amide I region is only affected upon heating. The influence of plasticisation on Kaffarin coatings by glycerol has been particularly well examined using FTIR, NMR and DSC, and a relation between changes in protein mobility and conformation to changes in final mechanical properties of Kaffarin coatings is found ^[10].

Protein coating formation does not necessarily take place close to thermodynamic equilibrium, therefore the history of formation may have an impact on final properties. Indeed, in numerous studies on a variety of proteins, it has been shown that drying conditions have a strong effect on the final properties of coating and coatings^{[11] [12] [13] [14]}. For instance, Alcantara^[11] found that a faster drying rate generally increases final water vapour permeability and coating strength for whey protein isolates/glycerol coatings. Different microstructures in soy protein coatings are observed as a result of different drying conditions. This is related to different degrees of protein unfolding, which in turn is found to correlate with the mechanical and barrier properties of the different coatings^[13]. So far, the drying of protein coatings has been mostly approached and explained for specific proteins, with a strong tendency to focus mainly on the properties of finished coating properties, thereby neglecting the important role of the drying dynamics.

While some studies have investigated molecular mobility of finished protein coatings, the gradual loss of molecular mobility during the drying of protein coatings has been essentially unexplored. As we pointed out above, many drying conditions drive protein-solvent systems into non-equilibrium states, which could partially explain why different drying processes lead to different coatings properties. In order to gain more insight in the changes occurring before a protein coating attains its final characteristics, a more microscopic investigation of the drying process could be useful, especially when also the dynamics at microscopic scales can be taken into account. Such an approach might help understanding mechanical characteristics, the influence of process conditions and the stability of protein coatings over time.

Here we study the dynamics of the drying of beta-lactoglobulin (β -lg) solutions. The whey protein β -lg from bovine milk serves as a convenient model protein, because it is readily available in high purity and is widely studied, especially in food science. Moreover, whey protein based coatings have demonstrated excellent mechanical and barrier properties ^[15].

As explained, there is no prior work on the dynamic of drying protein coatings, but various techniques have been used to study loss of molecular mobility of drying coatings in other fields. Diffusing wave spectroscopy (DWS) has been used as a technique to monitor

particle mobility during drying colloidal suspensions. ^{[16, 17] [18]} The GARField approach for magnetic resonance imaging (MRI) is used to monitor water uptake of multilayer coatings and paints^[19]. Based on their success in these studies, it is our objective to apply these techniques for the first time to drying protein coatings. FTIR has been successfully used before to identify molecular transitions in other drying protein systems, therefore we also apply it on drying β -lg coatings. First, the drying kinetics is explored using DVS, and subsequently, DWS, FTIR and MRI are used to study the drying dynamics.

2.2. Materials and methods

2.2.1. Material.

Bovine β -lactoglobulin (β -lg, purity $\geq 90\%$ w/w) is supplied by Sigma Aldrich. In order to remove any salts from the protein, it is dissolved and dialysed against demineralised water for 3 days at 5°C in the dark using a 3.5 kDa membrane. The water is refreshed until no increase in conductivity is found. After dialysis the solution is frozen using liquid nitrogen and freeze-dried. For each of the experiments a 20% (w/w) solution is prepared by adding demineralised water to the protein powder. The solutions is gently stirred and left for at least 3 hours before use to allow for complete hydration.

2.2.2. Equilibrating coatings under controlled relative humidity (RH).

20% (w/w) β -lg solutions were spread on microscope glass plates. The initial coating thickness (I_0) i.e. the thickness at the start is ~ 0.5 -1 mm. The glass plates are placed in desiccators containing saturated salt solutions (MgCl , K_2CO_3 , KI , NaCl , KBr , KCl , KNO_3 and K_2SO_4) creating relative humidities ranging from 33% to 97%, a common range where in practice many systems are exposed to. A small dish containing 1 g thymol is added to each desiccator to avoid microbial growth. After 3 weeks of equilibration the FTIR spectra are measured. It should be noted that this experiment is different from the dynamic drying experiments, since for this experiment only coatings equilibrated under steady state conditions are investigated

2.2.3. Diffusing wave spectroscopy (DWS).

DWS is used to continuously monitor the viscosity of the drying protein coating via the motion of highly scattering monodisperse polystyrene microspheres (diameter: 600 nm)(Optibind[®] Thermo Scientific[™], Indianapolis, Indiana, USA), which are added until a 1% (w/w) concentration is reached. In Figure 3, a schematic overview of the DWS setup is shown. A He-Ne laser beam (20mW), operating at a wavelength of 633 nm, is expanded in width (2.0 mm diameter) and guided through a quarter lambda plate, by which the polarisation direction of the light can be varied. The beam is guided vertically through the coating using a mirror and below the coating the light is passed through a Glan Thompson polariser, to filter out the light that has not multiple scattered within the coating. Before placing the sample, the transmitted beam is minimized by rotating the quarter lambda plate in front of the laser. Behind the polariser the scattered light from the coating is collected using a single-mode optical fiber, while the transmitted beam of non-scattered light is directed into a photo diode. By measuring the intensity of the transmitted beam the sample turbidity is monitored, providing the transparency of the sample. The light from the single mode fiber is directed into 2 photomultiplier tubes (ALV/SO-SIPD, ALV, Germany) by using a beam splitter. The photomultipliers convert the optical intensity into TTL pulses that are directed into a correlator (ALV-6010, ALV, Germany), from which the intensity autocorrelation function is determined.

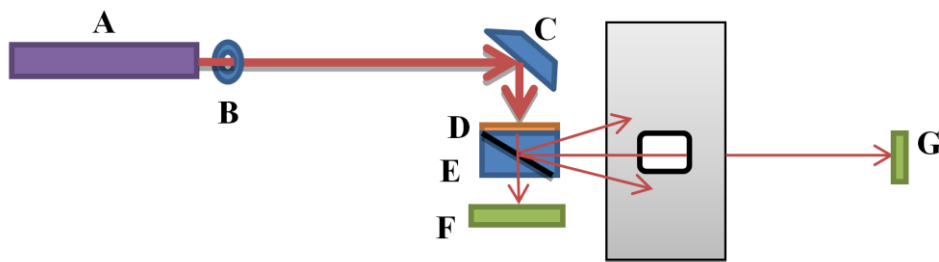


Figure 3. DWS setup schematic view. A: He Ne laser; B: beam expander and quarter wave plate; C: mirror; D: sample coating; E: polarising cube; F: diode for directly transmission; G: Single mode fiber.

During experiments the intensity autocorrelation function of multiply scattered light, $g_2(t)$ is measured. Light scattered from the system is supposed to be completely randomized and its path can be described by diffusion theory.^[20] In ergodic systems $g_2(t)$ is related to the

motion of the scatterers by the following equation^[21], where the last equality follows from the Siegert relation.^[22]

$$g_2(t) - 1 = \beta \left(\int_0^\infty P(s) \exp\left(-\frac{1}{3} X(t) \frac{s}{l^*}\right) ds \right)^2 = \beta |g_1(t)|^2 \quad [1]$$

In this equation β is a constant, smaller than one, determined primarily by the collection optics, l^* is the mean free path length of the photons, $P(s)$ is the path-length distribution function of paths of lengths, and the term $X(t)$ represents the average contribution of a moving scatterer to the de-phasing of a light path.^[21] The path length distribution function $P(s)$ of equation 1 depends on the geometry used. For light transmitted through a slab-shaped sample, that is much wider than it is thick^[21, 22], it has been shown that, using an incident beam of arbitrary width, equation 1 reduces to the following expression:^[21, 23]

$$g_1(t) = C \int_0^\infty e^{-(\xi^2 - Q^2) \left(\frac{\delta}{4}\right)^2} D(\xi, \varepsilon, \zeta) \xi e^{-(1-\zeta)\xi} d\xi \quad [2]$$

In this equation C is a normalization constant chosen so that $g_1(0) = 1$; $Q(t) \equiv (L/l^*) \sqrt{X(t)}$; $\varepsilon \equiv 2l^*/3L$; $\zeta \equiv z_0/L \approx l^*/L$ and $\delta \equiv d/L$, where d is the Gaussian diameter of the illuminating light beam and L is the thickness of the sample cell. The function $D(\xi, \varepsilon, \zeta)$ is given by:

$$D(\xi, \varepsilon, \zeta) = \frac{2\varepsilon[(1+\varepsilon\xi) - (1-\varepsilon\xi)e^{-2\zeta\xi}]}{(1+\varepsilon\xi)^2 - (1-\varepsilon\xi)^2 e^{-2\zeta\xi}} \quad [3]$$

The $X(t)$ is the mean square displacement of the scatterers reflecting their mobility in the matrix. For pure diffusive Brownian motion we have $X(t) = 6t/\tau_0$, with $\tau_0 \equiv 1/Dk_0^2$.^[20, 21] In the latter equality D ($D = k_B T / 6\pi\eta a$) is the diffusion coefficient of the scatterers with radius a , dispersed in a continuous phase with viscosity η and $k_0 = 2\pi n/\lambda$ with n the refractive index of the solvent and λ the wavelength of the laser. When elastic properties of the matrix start to influence the mobility of the matrix the mean square displacement of the scatterers are expected to obey $X(t) = 6t^b/\tau_0$. When b is smaller than 1, the matrix is shows elastic behaviour. When $b=1/2$ a gel is formed.

The suspension is spread on a glass plate and retained by a Teflon ring (inner diameter 14mm, thickness 5mm). A coating with an initial thickness of 4 mm is positioned in the DWS setup and air-dried ($T = 20 \pm 1^\circ\text{C}$ and $\text{RH} = 30 \pm 5\%$) and the intensity autocorrelation curves are obtained during drying. Simultaneously, an identically prepared second coating is air-dried, being positioned on a weight balance directly next to the DWS setup. For this coating the weight loss is measured over time. The water fraction of the coating is determined by measuring the weight directly after the DWS run and after drying the coating for 2 days at 110°C .

2.2.4. Attenuated Total Reflection Fourier Transform Infrared Spectroscopy (ATR-FTIR)

Infrared spectroscopy is an efficient analytical method providing information on the protein-water interaction and the influence of the water on the conformation of the protein. The IR spectra of the samples are collected using a FTIR spectrophotometer (IFS66/S model from Bruker Optics limited, Coventry, UK) with a mercury/cadmium/telluride detector. Dried β -lg solution coatings are directly placed on a single-reflection diamond ATR (attenuated total reflectance) accessory (Specac, Orpington, UK); this modification allows the coating to be examined as is, without the need for grinding. For each sample 64 scans are acquired with a resolution of 2 cm^{-1} . All measurements are performed in duplicate. Additionally, online drying measurements are performed, where a 20% (w/w) β -lg solution coating is spread out and dried on the crystal plate while measurements are taken every 3 minutes

2.2.5. Differential Vapour Sorption (DVS)

Water desorption data is measured using a high performance water sorption analyser (Q5000 SA, TA Instruments, Zellik, Belgium). This instrument is equipped with a sensitive symmetrical thermo balance (100 mg dynamic mass range) monitoring the sample mass. The humidity control chamber generates a specific relative humidity (RH) by mixing a constant flow of dry nitrogen gas with a second nitrogen stream containing water vapour. A desorption isotherm is measured at different RH (93%, 85%, 80%, 75%, 69%, 50%, 30%, 20%, 10%, 5%) at a temperature of 20°C . The instrument maintained a constant RH until the change in water content is less than 0.002% (w/w) per minute during a 10-min period. The water fraction is determined by drying the coating in an oven for 48hr at 110°C . The desorption data is fitted with the Guggenheim–Anderson–de Boer^[24-26] equation (GAB),

which is a semi-empirical equation to describe desorption isotherm for water activities until 0.85.

The GAB equation is given by:

$$m_c^1 = \frac{m_0 c k_b a_w}{(1 - k_b a_w)(1 - k_b a_w + c k_b a_w)} \quad [4]$$

Here m_0 denotes the monolayer water content, a_w the water activity i.e. the partial vapor pressure of water in a substance divided by the standard state partial vapor pressure of water, m_c^1 the water content (g/100g solid), c the so-called Guggenheim constant and k_b is a constant compensating for multilayer formation. This equation is used to obtain the value for the monolayer content m_0 .

Next to the desorption isotherm, a drying curve is determined with the same instrument, where the coating is dried at 20°C and 0% RH. From this drying curve the mass loss due to evaporation is determined. For higher water fractions this mass loss is determined by the difference between 2 data points. However, for lower water fractions, in order to reduce the noise, the mass loss is determined by the difference between multiple data points. After this experiment the final water fraction is determined by drying the coating in an oven for 48hr at 110°C. Mass fractions are converted to volume fraction with the use of β -lg density (ρ) determination at different water fraction performed in an earlier study^[27]. Between water mass fraction 0-0.12 sample density is estimated at 1.25. For water mass fractions higher than 0.12 density is estimated using a linear data fit: $\rho = -0.29 \cdot x_w + 1.29$. Coating thickness values are obtained by dividing the volume by the surface area.

2.2.6. Nuclear Magnetic Resonance Imaging (NMR Imaging)

This section only briefly discusses NMR imaging principles and measurements of coating formation during drying of the protein solution. For more details of NMR imaging measurements and relaxation analysis we refer to the literature.^{[19] [28]}

The NMR setup that we used is designed to measure ¹H-nuclei and utilizes the GARField approach^[29] to measure with high spatial resolution within thin layers. The magnetic field strength of the setup is 1.5 T and the gradient is 41 T/m. The NMR signal is obtained with an Ostroff-Waugh-like pulse sequence, with a flipping angle nominally equal to 90°^{[30] [31]}. The measurements are performed with echo time values $t_e = 50 \mu s$ and $100 \mu s$. The acquisition time is 40 μs , meaning that the spatial resolution is ca. 12 μm . As a result a number of spin-echoes are obtained, which are corrected with a reference signal, which is

measured for a 0.01M aqueous CuSO₄ solution. For the details of the signal correction see Ref ^[32]. When N distinct ¹H nuclei pools are present in the sample the signal of n -th echo reads:

$$S_n(x) = \sum_{k=1}^N I_k(x) \exp\left(-\frac{nt_e}{T_{2k}(x)}\right) \left(1 - \exp\left(-\frac{t_r}{T_{1k}}\right)\right) \quad [5]$$

Where $I_k(x)$ [-] is amplitude of the contribution to the signal of k -th pool in the sample. T_{1k} [s] is the transverse relaxation time of ¹H nuclei in the k -th pool. T_{1k} [s] is the longitudinal relaxation time of the k -th pool. The intensity I_k is proportional to the number of the protons in the k -th pool. The correction with the reference signal implies that $I_k = \rho_k / \rho_{ref}$, where ρ_k $\left[\frac{mol}{m^3}\right]$ is concentration of the protons in k -th pool and ρ_{ref} $\left[\frac{mol}{m^3}\right]$ is density of protons in the reference. Since the reference is an aqueous 0.01 M CuSO₄ solution, $\rho_{ref} = 1/9$ mol/cm³, which is equal to the density of protons in liquid water. Therefore, the concentration of protons in the sample can be calculated with the following expression:

$$\rho_k = \rho_{ref} \cdot I_k \quad [6]$$

The repetition time t_r in the measurements is 0.5 s and the signal is averaged 2048 times during water uptake. First, the signal is measured with $t_e = 100$ μ s, then with $t_e = 50$ μ s. This sequence is continued and, thus the process is measured with two echo times.

In order to place protein solution in the NMR setup, glass cups are used. The cups had bottom with a thickness of 110 μ m. The diameter of the cups is 1.1 cm and the height is ca. 1 cm. Approximately 0.4 ml of protein solution is added to the cup, resulting in a liquid coating of 1.2 mm at the beginning of the measurement. A protein solution with D₂O is also measured in order to distinguish signal of water from signal of protein. Temperature and relative humidity are respectively 21 \pm 4°C and 32 \pm 4%.

2.2.7. Overview

In Table 1, an overview is provided of the initial coating thickness (I_0), the coating thickness at the start of the experiment, and the coating surface area for the different techniques used. Different initial thicknesses are due to limitations of the techniques used.

Table 1: Overview of initial β -lg coating thicknesses and surface area used in the different drying experiments

Technique	I_0 (mm)	A (mm ²)
FTIR	1.0	10
DWS	4.0	154
DVS	0.8	15
MRI	0.4	100

2.3. Results and discussion

2.3.1. Desorption isotherm

Figure 4 shows the desorption isotherm for a β -lg solution coating at 20°C obtained using DVS. The sigmoidal shape is typical for so-called type II isotherms^[33], which are usually observed for hydrophilic polymers^[34, 35]. In previous research^[36], a nearly identical sorption isotherm for β -lg powders is found, suggesting that equilibrium is attained in these experiments and that hysteresis effects are minimal. The curve in Figure 4 is a fit using the 3-parameter Guggenheim-Anderson-de Boer^[24-26] (GAB) isotherm, from which the fit parameters can be found in Table 2. The fit parameter m_0 , is typically interpreted as a value for the monolayer water content (g/100g dry), which is required for hydration of the proteins by a single water monolayer. We use it as a water fraction x_w (w/w) value $m_0 = 0.08$. this value is comparable to values found for many other proteins^[37, 38]. Although the monolayer water content is recognised to be a crucial parameter for food materials^{[39] [40]}, it also remains a fitting parameter and doesn't necessarily demarcate differences in drying behavior.

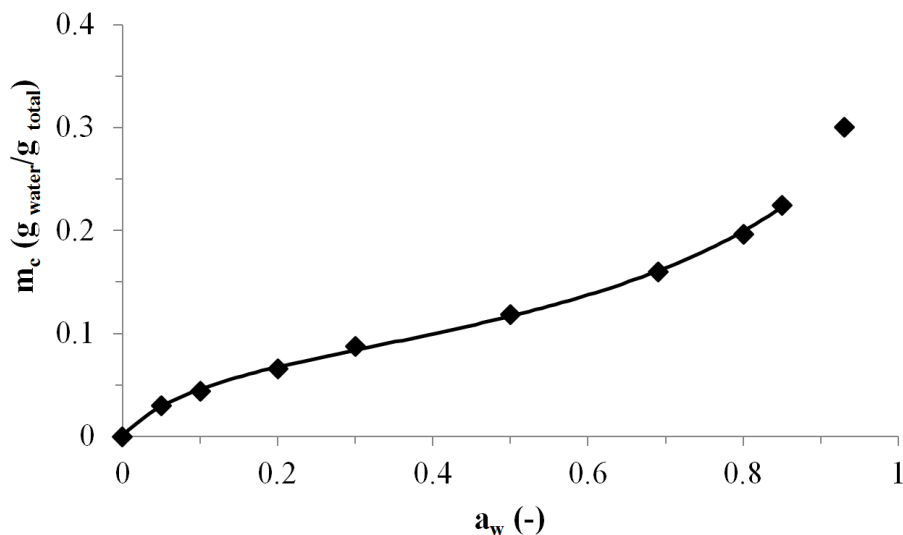


Figure 4. Desorption isotherm of β -lg solution at 20°C. Water content (m_c) against water activity (a_w). Experimental data points are denoted by the black diamonds while the solid line is a fit to the data points using the GAB equation. The optimal fit is found using the parameters given in Table 2.

Table 2: GAB fit parameters for the desorption isotherm for β -lg solution at 20°C

parameter	value	unit
m_0	$8.7 \pm .3$	(g/100g dry)
k_b	$0.83 \pm .01$	-none
c	11 ± 1.5	-none

2.3.2. Drying kinetics and homogeneity of drying coatings

For all drying coatings we observed that the upper contact line moved down while the coating kept adherent to the glass surface. At the end of drying (below $x_w=0.2$) also many thin fractures appeared over the entire film. Visual observation shows that the coating remains transparent during the drying process, suggesting that no phase separation occurs. Inhomogeneous drying of the coating in the direction perpendicular can still be compatible with transparent coatings. When the evaporation of water from the coating is significantly faster than the homogenization of the gradients in protein concentration in the perpendicular direction by diffusion, inhomogeneous drying may result. In other directions

drying is assumed to be homogeneous, because with a disc with a large diameter /thickness ratio the loss from the sides will be minimal. Additionally, the sides contained within the edges of the sample holder, will prevent sideways evaporation. A first indication of whether drying in the perpendicular direction is homogeneous, comes from measuring the drying kinetics (water fraction against drying time) for coatings. The coatings used had an initial thickness $I_0 \approx 0.8$ mm, which is close to the coating thickness used in further experiments.

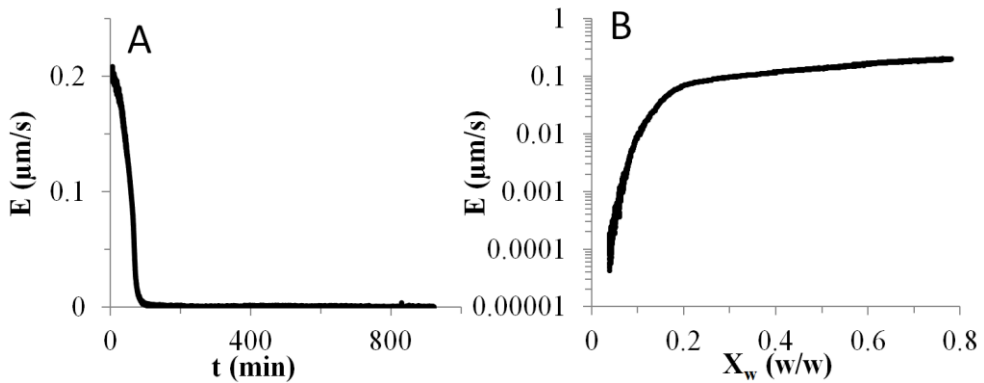


Figure 5. Evaporation rate of a drying β -Ig coatings measured using DVS. A) Evaporation rate (E) against drying time (t) B) Evaporation rate (E) against water fraction (x_w). Initial coating thickness (I_0)= 0.8 mm , initial protein concentration: 20% (w/w), temperature $T=20^\circ\text{C}$ and relative humidity $\text{RH}=0\%$

The evaporation rate E (decrease of coating thickness per unit time) as a function of drying time is determined using DVS. The β -Ig coating has an initial water fraction of 0.8 and is dried at $\text{RH}=0\%$ and $T=20^\circ\text{C}$ (see figure 3A). The corresponding evaporation rate E as a function of water fraction x_w is shown in figure 3B. At the beginning of drying, the evaporation rate E is almost constant and very close to zero order down to a water fraction of $x_w \approx 0.2$, followed by a sharp drop at lower water fractions. Note that the sharp drop in evaporation rate occurs well before reaching the monolayer water fraction $x_w = 0.08$, as fitting parameter from the sorption isotherm.

Inhomogeneous drying is expected to occur when the evaporation rate E is large compared to the rate at which diffusion homogenizes concentration gradients in the coating. Following Routh and Russel^[41] and others^{[42] [43] [44]}, we introduce the Peclet number Pe to identify regimes where drying may be expected to be homogeneous ($Pe \ll 1$) from regimes where drying may be expected to be inhomogeneous ($Pe \gg 1$):

$$Pe = \frac{I_0 E}{D} \quad [7]$$

Here D is the diffusion coefficient of the protein in the coating and I_0 is the initial thickness of the coating. The protein β -lg has a reported diffusion constant (at high water fractions) of $D_0 = 9.5 \cdot 10^{-11} \text{ m}^2 \text{ s}^{-1}$ at a concentration of 3.3 g/L, pH 7 and 0.003 M NaCl ^[45]. The dependence of protein diffusion constants on water fraction x_w has been studied using a range of methods, but only for water fractions x_w larger than approximately 0.65^[46, 47]. A useful empirical expression for extrapolating to lower water fractions is the expression proposed by Nesmelova et al. ^[48]:

$$\frac{D}{D_0} \approx \left(\frac{\phi}{\phi}\right)^3 \quad [8]$$

Where ϕ is the protein volume fraction, and $\hat{\phi}$ is a characteristic volume fraction separating the “dilute” from the “concentrated” regime. The parameter $\hat{\phi}$ somewhat depends on the type of protein, but typically is in the range 0.1-0.15. For β -lg, the concentration dependence of the diffusion constant has not been determined and to estimate Pe , we use a typical value of $\hat{\phi} = 0.13$. Next, we use a density of 1.25 g cm^{-3} to convert protein volume fractions into water fraction. As seen in figure 3b, for $x_w > 0.2$, the evaporation rate is nearly constant, $E \approx 0.1 \mu\text{m/s}$. With these numbers, also displayed in Table 3, we find that in the semi-dilute regime ($x_w \approx 0.8$), $Pe = 6$, and increases to $Pe = 7 \cdot 10^1$ for $x_w \approx 0.5$. For still lower water fractions, we cannot really be sure about the validity of Eq. (8), but it is clear that we should take into account the possibility that for our protein coatings, drying is inhomogeneous in the perpendicular direction. Next we turn to an experimental determination of the water distribution in the perpendicular direction, and hence of the homogeneity of the coating, based on nuclear magnetic resonance imaging.

Table 3: Calculated diffusion coefficients (D) and pecllet (Pe) values of β -lg coatings at different evaporation rates (E) and volume fractions (ϕ)

ϕ	$D \text{ (m}^2 \text{ s}^{-1}\text{)}$	$E \text{ (}\mu\text{m/s)}$	Pe
0.2	$2.6 \cdot 10^{-11}$	0.20	6
0.3	$7.7 \cdot 10^{-12}$	0.18	$2 \cdot 10^1$
0.4	$3.3 \cdot 10^{-12}$	0.17	$4 \cdot 10^1$
0.5	$1.7 \cdot 10^{-12}$	0.14	$7 \cdot 10^1$

2.3.3. Thin layer MRI

To investigate how water and protein mobility changes and how water redistributes in the protein coating during drying, the process is measured with high resolution NMR imaging. Previously, this technique is successfully used for measuring drying and water uptake by thin polymeric coatings^[19, 28]. Protein drying in D₂O and H₂O solution is measured in order to identify protons of protein and of water during the coating formation.

First, we consider the distribution of protons during drying of the H₂O solution. Signal profiles are obtained during drying for two echo times: $t_e = 50 \mu\text{s}$ (Figure 6A) and $t_e = 100 \mu\text{s}$ (Figure 6B). The profiles for echo time $t_e = 100 \mu\text{s}$ are measured first, followed by the measurements with echo time $t_e = 50 \mu\text{s}$. The measurement time for a single profile is 20 min, hence the time for measuring both profiles is 40 min. The drying process is followed for 8 hours .

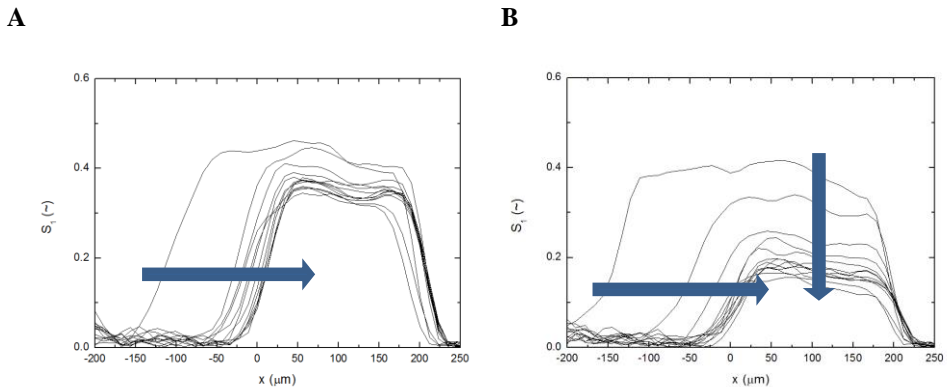


Figure 6. MRI concentration profiles of a drying β -Ig protein coating. Signal of first echo (S_1) against coating thickness (x) A) echo time $t_e = 50 \mu\text{s}$ B) $t_e = 100 \mu\text{s}$. The time between subsequent profiles is 40 minutes. The profiles with $50 \mu\text{s}$ echo time show shrinkage of the protein coating but little signal level change, whereas the profiles for $100 \mu\text{s}$ echo time show both shrinkage and signal decrease. Temperature $T = 21 \text{ }^\circ\text{C}$, relative humidity $\text{RH} = 33\%$.

A first observation is that no gradients develop in the signal $S_1(x)$ in the x -direction. This suggests that at least within the spatial resolution of the thin layer MRI method (approximately $12 \mu\text{m}$), no significant inhomogeneity in the local protein concentration develops during coating drying, despite the rather high Peclet numbers estimated above, supposedly occurring at lower water fractions. It may still be possible that inhomogeneous drying causes the formation of a thin coating of increased protein fraction at the air/water interface, that is beyond the resolution of the thin layer MRI.

A second observation is that the signal for $t_e = 50 \mu\text{s}$ changes little, whereas at $t_e = 100 \mu\text{s}$, signal intensity decreases with drying time. This implies that at $50 \mu\text{s}$, the amount of visible protons stay at the same level, while at $100 \mu\text{s}$ their number decreases as drying progresses. A signal loss due to T_1 relaxation is found at the start of the experiment at $T_1 \approx 0.65 \text{ s}$. This value and the repetition time of 0.5 s suggests that at the start, already about 50% of the signal is lost due to T_1 relaxation.

In order to investigate the relative contributions of water and protein to the NMR signal, we analyze signal decays for H_2O and D_2O solutions during drying. For H_2O solutions signal decays are averaged over the coating thickness. In the case of a D_2O solution, a signal decay from a single point in the profiles is taken. Note that for a D_2O solution, the initial thickness is different compared to the H_2O solution measurements, so we can only compare changes in the relaxation behaviour, but not in drying kinetics. An analysis of the signal decay using an inverse Laplace transform shows a maximum of two T_2 components in the signal. In order to estimate the T_2 values and proton populations of the T_2 components, signal decays are fitted with single and bi-exponential functions. The evolution of T_2 values with drying time is shown in Figure 7A for $t_e = 50 \mu\text{s}$ and in Figure 7B for $t_e = 100 \mu\text{s}$. The proton populations of the components are shown in Figure 7c for $t_e = 50 \mu\text{s}$ and Figure 7d for $t_e = 100 \mu\text{s}$.

First, we consider the difference between T_2 relaxation at the beginning of the experiment, i.e. at the first data point. Both solutions in the beginning have two T_2 relaxation components at both echo time values (Figure 7A and Figure 7B). In the case of the $100 \mu\text{s}$ echo time this component has disappeared by the second sampling point. An important difference can be observed between the populations of the long T_2 component of the H_2O and D_2O samples (Figure 7C and Figure 7D). This implies that the short T_2 component represents only the protein protons, whereas both water and protein contribute to the long T_2 component. Additionally, for both solutions the T_2 values of the both components are smaller at $t_e = 100 \mu\text{s}$ than at $t_e = 50 \mu\text{s}$. This is due to echo time dependency of the relaxation times, which can be due to dipolar interactions or self-diffusion of the measured species. The influence of dipolar interactions on T_2 reflects the mobility of the species: higher mobility means larger T_2 values.

In order to investigate how a change in mobility of the measured species is reflected in the measurements, we consider the evolution of the T_2 components during drying. The T_2

relaxation times of both components decrease with drying, which is observed as a decrease in both T_2 values (Figure 7A) and as a decrease of the relaxation time of the longer T_2 component and disappearance of the shorter T_2 component (Figure 7B). The decrease in T_2 values can be a consequence of a decrease of the protein and water mobilities or a consequence of an increased diffusion. In our case, we conclude that loss of water and a decrease of protein mobility causes the decrease in T_2 values, as during drying diffusion should certainly not increase.

Next, in order to estimate the actual water and protein concentrations from the NMR data, we consider the evolution of the proton populations (Figure 7C and Figure 7D). The populations of the short T_2 component increases during drying (Figure 7C). This is the result of an increase of the protein fraction as drying progresses. The population of the long T_2 component changes little in the case of a D_2O solution (from ca. 9 mmol/cm^3 to ca. 8 mmol/cm^3), whereas a significantly decrease is found in the case of the H_2O solution. This implies that the contribution of protein to the population of the long T_2 component changes little, and the decrease in its population is mainly a consequence of water evaporation. For an estimate of how water and protein concentrations change during drying, we subtract the concentration of mobile protein protons, 8 mmol/cm^3 from the intensity of the long T_2 component. The resulting concentration of water protons is converted into the visible water concentration. Likewise, total protein proton concentrations are calculated as a sum of the intensity of the short T_2 component in $50 \mu\text{s}$ data (i.e. the less mobile protein protons) and the concentration of water mobile protein protons: 8 mmol/cm^3 . The resulting visible concentration of protein and water are shown in Figure 8.

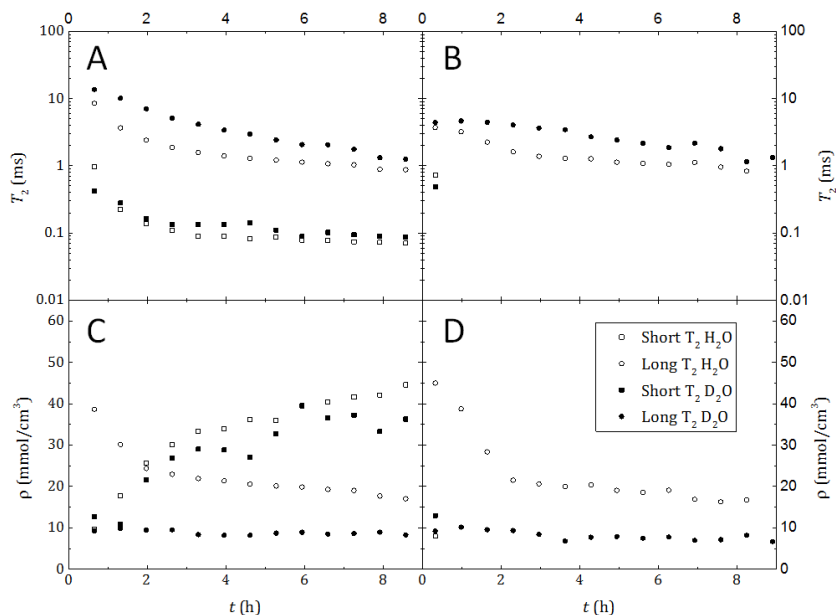


Figure 7. The time evolution of T_2 relaxation times during β -Ig coating drying. Time (h) is plotted against T_2 relaxation time (T_2) for the upper graphs ((A) and (B)) and against proton population (ρ) for the lower graphs ((c) and (d)). Echo times (t_e) for left ((A) and (C)) and for right ((B) and (D)) are respectively 50 and 100 μ s. The T_2 components of the signal decays of H₂O (open symbols) and D₂O (solid symbols) protein solutions. The squares show the evolution of the components of the short T_2 component and the circles show the evolution for the long T_2 component. Temperature $T=21$ °C, relative humidity RH = 33%.

Initially, the visible water concentration is approx. 0.35 g/cm^3 . However, the T_1 measurements of H₂O protein solution showed that the T_1 value is 0.65 s at the beginning of the experiment. This means that for the used repetition time of 0.5 s, approx. half of the signal is lost, which is equivalent to ca. 0.4 g/cm^3 of water. Assuming that water loses signal due to T_1 and not the protein, the water concentration at the beginning of the drying process is approx. 0.75 g/cm^3 , which is close to amount of water in the solution before drying. The rate of drying changes after approx. 2 hours, at a water concentration of ca. 0.15 g/cm^3 . At the end of the measurement, the water concentration has decreased to 0.1 g/cm^3 .

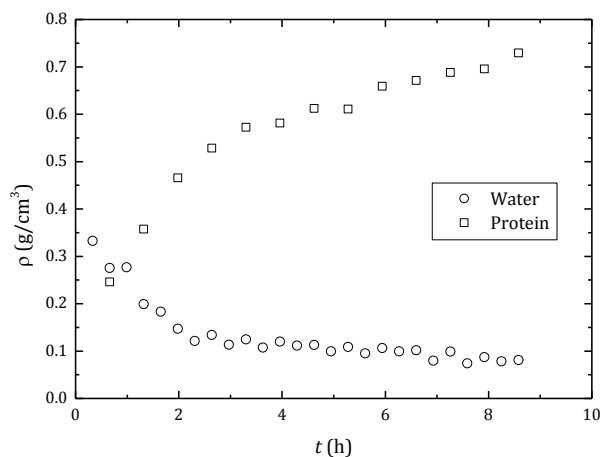


Figure 8. The calculated densities of visible water (circle) and protein (squares) as a function of time for a drying β -Ig coating.

The high resolution NMR imaging show that the drying process occurs homogeneously on length scales within the resolution of the technique. The initial drying rate is fast, but slows down below a visible water concentration of 0.15 g/cm^3 . After this point the visible water concentration slowly decreases over the next 6 hours to 0.1 g/cm^3 . This drying behaviour is qualitatively comparable to the DVS results, where a clear change in drying behaviour is found at a water fraction around $x_w=0.2$. Converting concentrations of visible water to actual values of water fraction is not entirely accurate, because of possible signal loss due to the T_1 relaxation as discussed earlier in this paragraph. Nevertheless it could provide us an approximate indication of the water fraction at which MRI picks up a change in drying rate. We know that the density of the concentrated β -Ig system is approx. 1.24 g/cm^3 . From this we convert the value of 0.15 g/cm^3 to a water fraction of $x_w=0.12$. Although it is a considerably lower value, it is still in the same range as the water fraction x_w as found in DVS. Therefore, we conclude that the MRI and DVS results are at least consistent with each other, but more precise MRI results, and more detailed analysis of the MRI data is required to achieve a possible quantitative agreement. Both protein and water become less mobile as drying progresses, as shown by relaxation analysis of the NMR signal. Two populations of protein protons with different mobilities are observed. The

fraction of the lower mobility protons is decreasing during drying, reflecting loss of protein molecular mobility.

2.3.4. Infrared-Spectroscopy

The DVS and NMR experiments indicate that the drying of the coating for water fractions above $x_w=0.2$ is distinctly different from drying at lower water fractions. We expect that this must be related in some way to the hydration of the protein molecules. In order to probe the protein hydration during drying in more detail, in particular at lower water fractions, we use ATR-FTIR. This technique is sensitive to small changes in molecular vibrations such as those caused by conformational changes and changes in hydration. When analysing proteins, the amide I band (1600 to 1690 cm^{-1}) and the amide II band (1480-1575 cm^{-1}) are considered to be the most informative. The amide I band is primarily (70-80%) due to C=O stretching and is closely correlated to conformational changes, while the amide II band, due to a combination of NH bending and CN stretching, is much less sensitive to conformational changes and more to hydration ^[49].

Figure 9 shows spectra of the amide I and II bands of a coating of β -lg as a function of drying time. The Amide I band does not show any significant changes during drying, suggesting that at least for these drying conditions and drying times, no conformational changes take place in the secondary structure of β -lg. Any changes that do take place may also be obscured (at least in part) by the water peak at 1644 cm^{-1} , especially towards higher water fractions. On the other hand, the amide II band shows clear changes during drying, that may be related to changes in protein hydration. During part of the drying process, peaks became visible in the amide II region occur at 1541 cm^{-1} and 1535 cm^{-1} and these are chosen to follow the state of hydration of the proteins. To correct for changes in optical contact during drying, we use the absorbance peak around 1515 cm^{-1} that is generally attributed to the ring vibrations of the Tyrosine (Tyr) side chain as a reference. These vibrations are relatively insensitive to conformational changes ^[37] and the 1515 cm^{-1} peak should therefore be a reliable internal standard.

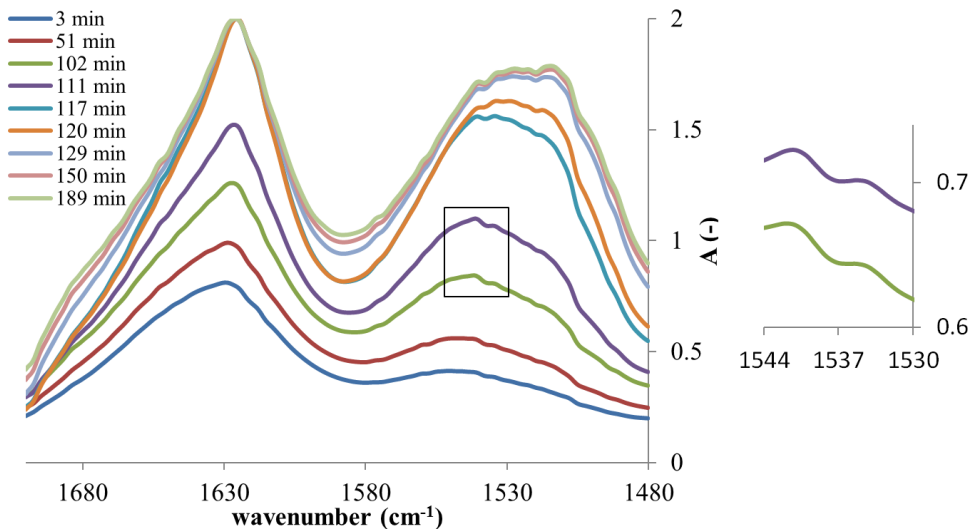


Figure 9. FTIR spectra of a drying β -Ig coating. Wavenumbers are plotted against absorbance (A), focussing on the amide I and II bands. Drying times (in minutes) are shown in the legend. Absorbance values increase while drying progresses. Initial β -Ig concentration 20% (w/w), $T= 22\text{ }^{\circ}\text{C}$ and $\text{RH}=35\%$. Inserts displays section of spectrum showing peaks at the 1535 and 1541 cm^{-1} bands.

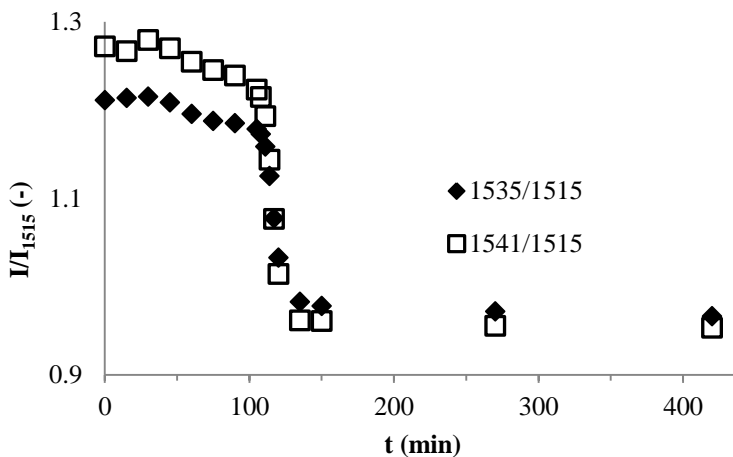


Figure 10: Band intensity ratios from FTIR spectra for a drying β -Ig coating. Intensity ratio selected band/ 1515 cm^{-1} (I/I_{1515}) against time (t). Selected band 1535 cm^{-1} represented by diamonds and 1541 cm^{-1} represented by squares. Initial concentration 20% (w/w) β -Ig, $T= 22\text{ }^{\circ}\text{C}$ and $\text{RH}=35\%$

Figure 10 shows the scaled absorbance peak values at 1541 cm^{-1} and 1535 cm^{-1} (scaled by the reference at 1515 cm^{-1}) as a function of drying time. Clearly, for drying times between

105 and 130 minutes, a steep change is visible in the intensity ratio, while hardly a change occurs after 130 minutes of drying. In order to plot the FTIR results as a function of water fraction x_w , spectra are taken from β -lg coatings that are equilibrated at different relative humidities. Figure 11 shows the normalized intensities at 1535 cm^{-1} and 1541 cm^{-1} as a function of water fraction.

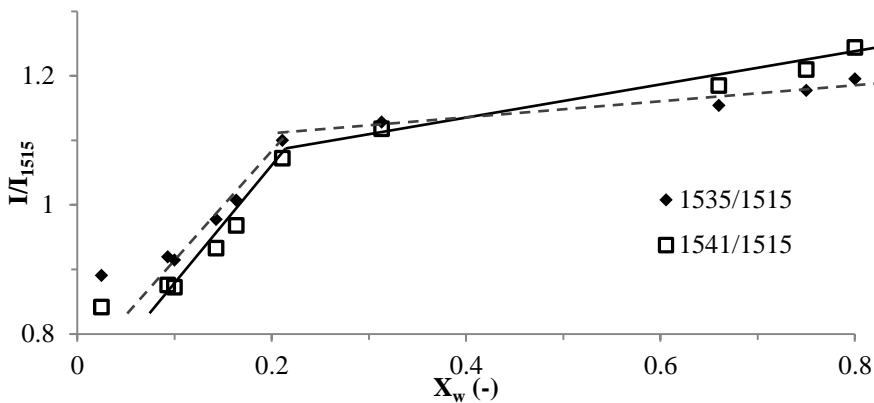


Figure 11. Band intensity ratios from FTIR spectra from equilibrated β -lg coating at $22\text{ }^\circ\text{C}$. Intensity ratio selected band/ 1515 cm^{-1} (I/I_{1515}) against water fraction (x_w). Selected band 1535 cm^{-1} represented by diamonds and 1541 cm^{-1} represented by squares.

In agreement with the previous DVS results, a distinct transition in protein hydration appears to take place in between water fractions $x_w = 0.1$ and $x_w = 0.2$. For water fractions $x_w > 0.2$, the N-H environment apparently does not change with water fraction, suggesting that hydrogen bonding associated with this group is saturated beyond $x_w = 0.2$. Similar results are found for hydrated gluten^[37] and lysozyme^[50]. As noticed before, the amide II region is associated with N-H bending and C=O stretching. When hydrating β -lg with D_2O it is shown that the amide II peak shifts to the right, while the signal on its original position practically vanishes^[51]. This suggests that the backbone of the protein interacts almost entirely with the D_2O molecules. We can assume this hydration of the protein backbone will occur as well when dissolved in water. From calculations we find that if we designate 1 molecule of water for each N-H and C=O group on the backbone of a protein molecule, this protein would have a water fraction of $x_w = 0.26$, close to the water fraction of $x_w = 0.2$ which we find in both the FTIR, MRI and DVS results. In a dry state the hydrogen bonds are present between the C=O and N-H groups inside proteins, but also between them, resulting in a rigid and immobile structure. When these hydrogen bonds are replaced by water

molecules, the protein mobility could significantly increase. This likely causes a different behaviour on macroscopic scales as well. In the next section, these results will be compared with the drying behaviour on a larger length scale, using DWS to study the mobility of rather large tracer particles (600nm) in the drying protein coatings.

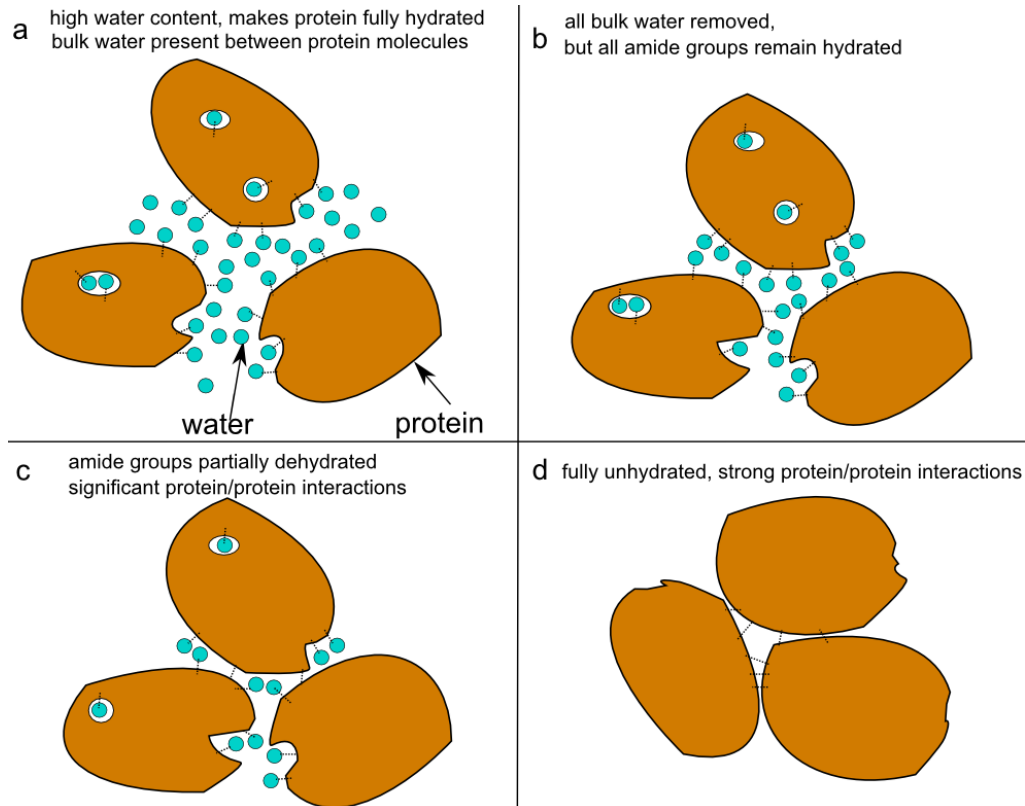


Figure 12: Illustration showing concentrated proteins from a hydrated (a) to a unhydrated (d) protein backbone. (b) represents the transition point at $x_w=0.2$. During dehydration water-protein hydrogen bonds are replaced by protein-protein hydrogen bonds resulting in decrease molecular mobility.

2.3.5. Diffusing Wave Spectroscopy

β -lg coatings containing 1% latex particles (600nm) as tracer particles are air dried. During the drying process the autocorrelations functions in transmission mode are obtained. A selection of representative autocorrelation functions during drying are shown in Figure 13. The decay becomes slower at longer drying times, reflecting the decrease of mobility of the latex tracer particles. Interestingly, the shape of the curves remains almost unchanged with

increasing drying times. All decay curves are close to a simple mono-exponential decay and can be fitted to:

$$(g_2 - 1) = \exp(-\Gamma t^b) \quad [8]$$

We find that at most drying times the parameter b remains close to 1, indicating a simple diffusive motion of the tracer particles in a Newtonian viscous medium of increasing viscosity.

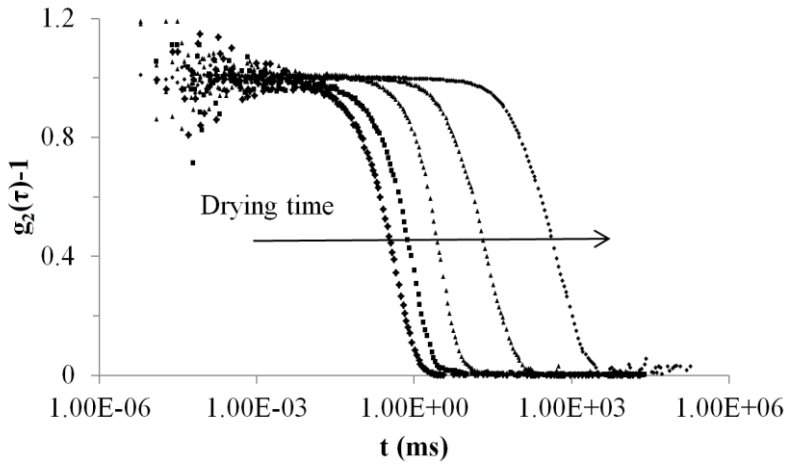


Figure 13. Time autocorrelation curves $(g_2 - 1)$ of a drying β -Ig coating ($X_{w,t=0} = 0.2$). Drying times are $t=5$ min, 100 min, 220 min, 300 min and 400 min, while drying continues the curves shift to the right.

If drying had been significantly heterogeneous, we would have expected to see multiple relaxation times, or a spread of relaxation times, both leading to values of the parameter b in eq.8, that would be significantly different from 1^[18]. This confirms the earlier conclusion from thin layer MRI, that drying mainly occurs homogeneously. The presence of a thin layer of high protein content at the air-water interface that would only account for a small fraction of the total coating volume, would probably go unnoticed in the DWS experiment, so we cannot exclude that possibility. At water fractions $x_w < 0.2 \pm 0.02$, the samples become more transparent, since the optical contrast is reduced due to water evaporation, thereby concentrating the protein. For this regime, there is no multiple scattering anymore, and we can no longer usefully apply DWS. This leaves the question unanswered, whether there are macroscopic changes to the coating properties when x_w decreases below 0.2. This

regime might possibly be explored by using tracer particles with a very high refractive index, like titanium dioxide particles.

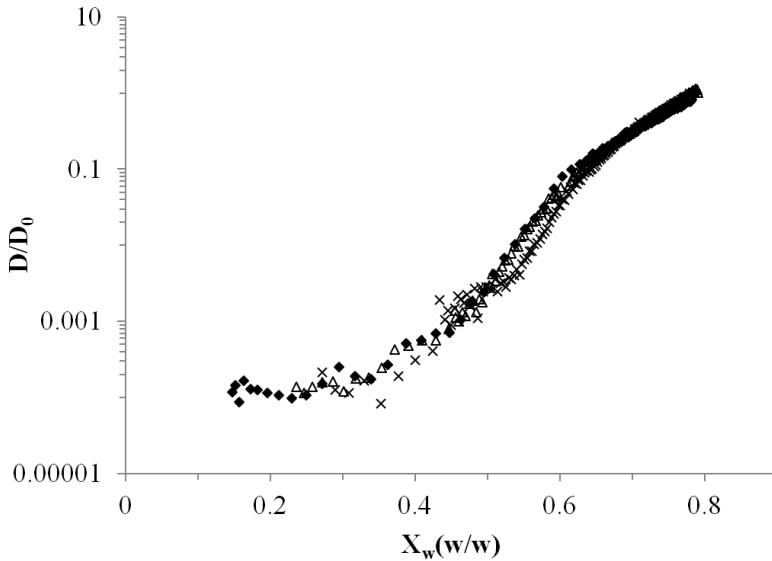


Figure 14. Tracer particle diffusivity during drying a β -lg coating at 20 °C and RH 30%. Scaled diffusion coefficient (D/D_0) against water fraction x_w . D_0 is the diffusion coefficient of latex particles at the start of the drying of the coating, which is at water fraction $x_w = 0.8$.

Figure 14 shows that the scaled diffusion coefficient D/D_0 of the tracer particles decreases approximately by 4 orders of magnitude when the water fraction is reduced from $x_w = 0.8$ to $x_w = 0.2$. The absence of a sudden decrease in scaled diffusion coefficient indicates, that no sharp kinetic arrest occurred during the drying of the coating. We continue to observe diffusion of the large tracer particles down to the lowest water fractions for which the DWS measurements can still be performed.

2.4. Conclusions

Despite the fact that estimated values for Peclet numbers are rather high, we find no evidence from either thin coating NMR or DWS that drying is significantly inhomogeneous in the direction perpendicular to the drying β -lg coating. However, both techniques would presumably not detect a thin protein layer at the air-water interface with that is significantly different from the bulk of the coating. DWS shows a gradual increase in viscosity for all water fractions amenable to this technique (down to approximately $x_w = 0.2$). Similarly, DVS shows a gradual decrease in evaporation rate, and FTIR shows a gradual decrease in

protein hydration based on changes in the amide II peak. Water concentration profiles as determined by MRI show gradual changes in time for all depths. Only for water fractions below around $x_w = 0.2$, the water evaporation rate drops drastically as observed by DVS. On a molecular scale we observe quite abrupt changes associated with the FTIR response of N-H and C=O groups, which we argue are due to changes in molecular mobility caused by dehydration of the protein backbone

Other authors have previously used differential scanning calorimetry (DSC) to locate thermal glass transitions in β -lg powders containing different water fractions^[36]. However, signals that are observed and attributed to the glass transition are very small. Using modulated temperature differential scanning calorimetry (MTDSC) on equilibrated β -lg coatings with water fractions between $x_w = 0.05$ and $x_w = 0.29$, we have been unable to locate a thermal glass transition in our protein coatings.

The experimental results points to a picture of dried β -lg coatings that under many practical conditions are non-glassy, very high viscosity liquids. As a result, we may expect the (very slow) permeation of even rather large particles down to very low water fractions, ($x_w \approx 0.2$). Proteins being much smaller than the tracer particles used in DWS, may be expected to be even more mobile. In practical terms this may imply that over long storage times, some coated materials could mix with dried protein coatings.

Our novel combination of on-line techniques applied to drying protein coatings also show promise for investigations of other protein coating systems. Issues that could be addressed using our approach include the influence of plasticisers or the environmental conditions on the drying kinetics from molecular to macroscopic scales.

2.5. Acknowledgements

This work is part of the Industrial Partnership Programme (IPP) Bio(-Related)Materials of the Stichting voor Fundamenteel Onderzoek der Materie (FOM), which is financially supported by the Nederlandse Organisatie voor Wetenschappelijk Onderzoek (NWO). The IPP BRM is co-financed by the Top Institute Food and Nutrition and the Dutch Polymer Institute.

2.6. References

1. Scramin, J.A.; de Britto, D.; Forato, L.A.; Bernardes-Filho, R.; Colnago, L.A.; Assis, O.B.G. Characterisation of zein-oleic acid films and applications in fruit

- coating. *International Journal of Food Science and Technology* 2011, 46 (10), 2145-2152.
2. Ramos, Ó.L.; Santos, A.C.; Leão, M.V.; Pereira, J.O.; Silva, S.I.; Fernandes, J.C.; Franco, M.I.; Pintado, M.E.; Malcata, F.X. Antimicrobial activity of edible coatings prepared from whey protein isolate and formulated with various antimicrobial agents. *International Dairy Journal* 2012, 25 (2), 132-141.
 3. Elzoghby, A.O.; Abo El-Fotoh, W.S.; Elgindy, N.A. Casein-based formulations as promising controlled release drug delivery systems. *Journal of Controlled Release* 2011, 153 (3), 206-216.
 4. Wang, L.Z.; Liu, L.; Holmes, J.; Kerry, J.F.; Kerry, J.P. Assessment of film-forming potential and properties of protein and polysaccharide-based biopolymer films. *International Journal of Food Science and Technology* 2007, 42 (9), 1128-1138.
 5. Zhang, H.; Mittal, G. Biodegradable protein-based films from plant resources: A review. *Environmental Progress & Sustainable Energy* 2010, 29 (2), 203-220.
 6. Mangavel, C.; Rossignol, N.; Perronnet, A.; Barbot, J.; Popineau, Y.; Guéguen, J. Properties and Microstructure of Thermo-Pressed Wheat Gluten Films: a Comparison with Cast Films. *Biomacromolecules* 2004, 5 (4), 1596-1601.
 7. Sánchez, A.C.; Popineau, Y.; Mangavel, C.; Larré, C.; Guéguen, J. Effect of Different Plasticizers on the Mechanical and Surface Properties of Wheat Gliadin Films. *Journal of Agricultural and Food Chemistry* 1998, 46 (11), 4539-4544.
 8. Guerrero, P.; de la Caba, K. Thermal and mechanical properties of soy protein films processed at different pH by compression. *Journal of Food Engineering* 2010, 100 (2), 261-269.
 9. Hu, X.; Kaplan, D.; Cebe, P. Dynamic Protein–Water Relationships during β -Sheet Formation. *Macromolecules* 2008, 41 (11), 3939-3948.
 10. Gao, C.; Stading, M.; Wellner, N.; Parker, M.L.; Noel, T.R.; Mills, E.N.C.; Belton, P.S. Plasticization of a Protein-Based Film by Glycerol: A Spectroscopic, Mechanical, and Thermal Study. *Journal of Agricultural and Food Chemistry* 2006, 54 (13), 4611-4616.
 11. Alcantara, C.R.; Rumsey, T.R.; Krochta, J.M. Drying rate effect on the properties of whey protein films. *Journal of Food Process Engineering* 1998, 21 (5), 387-405.
 12. Tapia-Blácido, D.R.; Sobral, P.J.A.; Menegalli, F.C. Effect of drying conditions and plasticizer type on some physical and mechanical properties of amaranth flour films. *LWT - Food Science and Technology* 2013, 50 (2), 392-400.
 13. Denavi, G.; Tapia-Blácido, D.R.; Añón, M.C.; Sobral, P.J.A.; Mauri, A.N.; Menegalli, F.C. Effects of drying conditions on some physical properties of soy protein films. *Journal of Food Engineering* 2009, 90 (3), 341-349.
 14. Soazo, M.; Rubiolo, A.C.; Verdini, R.A. Effect of drying temperature and beeswax content on physical properties of whey protein emulsion films. *Food Hydrocolloids* 2011, 25 (5), 1251-1255.
 15. Khwaldia, K.; Perez, C.; Banon, S.; Desobry, S.; Hardy, J. Milk Proteins for Edible Films and Coatings. *Critical Reviews in Food Science and Nutrition* 2004, 44 (4), 239-251.
 16. Brun, A.; Dihang, H.; Brunel, L. Film formation of coatings studied by diffusing-wave spectroscopy. *Progress in Organic Coatings* 2008, 61 (2–4), 181-191.

17. Narita, T.; Beauvais, C.; Hébraud, P.; Lequeux, F. Dynamics of concentrated colloidal suspensions during drying - Aging, rejuvenation and overaging. *European Physical Journal E* 2004, 14 (3), 287-292.
18. Breugem, A.J.; Bouchama, F.; Koper, G.J.M. Diffusing wave spectroscopy: A novel rheological method for drying paint films. 2005, 88 (2), 135-138.
19. Baukh, V.; Huinink, H.P.; Adan, O.C.G.; Erich, S.J.F.; Van Der Ven, L.G.J. NMR imaging of water uptake in multilayer polymeric films: Stressing the role of mechanical stress. *Macromolecules* 2010, 43 (8), 3882-3889.
20. Wu, X.L.; Pine, D.J.; Chaikin, P.M.; Huang, J.S.; Weitz, D.A. Diffusing-wave spectroscopy in a shear flow. *Journal of the Optical Society of America B* 1990, 7 (1), 15-20.
21. Gopal, A.D.; Durian, D.J. Shear-Induced "Melting" of an Aqueous Foam. *Journal of Colloid and Interface Science* 1999, 213 (1), 169-178.
22. Wyss, H.M.; Romer, S.; Scheffold, F.; Schurtenberger, P.; Gauckler, L.J. Diffusing-Wave Spectroscopy of Concentrated Alumina Suspensions during Gelation. *Journal of Colloid and Interface Science* 2001, 241 (1), 89-97.
23. Brown, W. *Dynamic light scattering: the method and some applications.* Clarendon Press, 1993.
24. Anderson, R.B.; Hall, W.K. Modifications of the Brunauer, Emmett and Teller Equation III. *Journal of the American Chemical Society* 1948, 70 (5), 1727-1734.
25. Boer, J.H. *The dynamical character of adsorption.* Clarendon Press, 1953.
26. Guggenheim, E.A. *Applications of Statistical Mechanics.* Clarendon Press, 1966.
27. McMeekin, T.L.; Groves, M.L.; Hipp, N.J. Partial specific volume of the protein and water in beta-lactoglobulin crystals. *Journal of Polymer Science* 1954, 12 (1), 309-315.
28. Baukh, V.; Huinink, H.P.; Adan, O.C.G.; Erich, S.J.F.; Van Der Ven, L.G.J. Water-polymer interaction during water uptake. *Macromolecules* 2011, 44 (12), 4863-4871.
29. Glover, P.M.; Aptaker, P.S.; Bowler, J.R.; Ciampi, E.; McDonald, P.J. A Novel High-Gradient Permanent Magnet for the Profiling of Planar Films and Coatings. *Journal of Magnetic Resonance* 1999, 139 (1), 90-97.
30. Ostroff, E.D.; Waugh, J.S. Multiple spin echoes and spin locking in solids. *Physical Review Letters* 1966, 16 (24), 1097-1098.
31. Mansfield, P.; Ware, D. NMR spin dynamics in solids. I. Artificial line narrowing and zeeman spin-spin relaxation in the rotating frame. *Physical Review* 1968, 168 (2), 318-334.
32. Baukh, V.; Huinink, H.P.; Adan, O.C.G.; Erich, S.J.F.; van der Ven, L.G.J. Predicting water transport in multilayer coatings. *Polymer* 2012, 53 (15), 3304-3312.
33. Lowell, S.; Shields, J.E. *Powder surface area and porosity.* Springer, 1991.
34. Yasuda, H.; Stannett, V. Permeation, solution, and diffusion of water in some high polymers. *Journal of Polymer Science* 1962, 57 (165), 907-923.
35. Detallante, V.; Langevin, D.; Chappey, C.; Métayer, M.; Mercier, R.; Pinéri, M. Water vapor sorption in naphthalenic sulfonated polyimide membranes. *Journal of Membrane Science* 2001, 190 (2), 227-241.
36. Zhou, P.; Labuza, T.P. Effect of water content on glass transition and protein aggregation of whey protein powders during short-term storage. *Food Biophysics* 2007, 2 (2-3), 108-116.

37. Almutawah, A.; Barker, S.A.; Belton, P.S. Hydration of gluten: A dielectric, calorimetric, and fourier transform infrared study. *Biomacromolecules* 2007, 8 (5), 1601-1606.
38. De Jong, G.I.W.; Van den Berg, C.; Kokelaar, A.J. Water vapour sorption behaviour of original and defatted wheat gluten. *International Journal of Food Science & Technology* 1996, 31 (6), 519-526.
39. Rahman, M.S. State diagram of foods: Its potential use in food processing and product stability. *Trends in Food Science & Technology* 2006, 17 (3), 129-141.
40. Marcos, B.; Esteban, M.a.A.; López, P.; Alcalá, M.; Gómez, R.; Espejo, J.; Marcos, A. Monolayer values at 30°C of various spices as computed by the BET and GAB models. 1997, 204 (2), 109-112.
41. Routh, A.F.; Russel, W.B. Deformation Mechanisms during Latex Film Formation: Experimental Evidence. *Industrial & Engineering Chemistry Research* 2001, 40 (20), 4302-4308.
42. Sadek, C.; Tabuteau, H.; Schuck, P.; Fallourd, Y.; Pradeau, N.; Le Floch-Fouéré, C.; Jeantet, R. Shape, Shell, and Vacuole Formation during the Drying of a Single Concentrated Whey Protein Droplet. *Langmuir* 2013, 29 (50), 15606-15613.
43. Narita, T.; Hebraud, P.; Lequeux, F. Effects of the rate of evaporation and film thickness on nonuniform drying of film-forming concentrated colloidal suspensions. *The European physical journal. E, Soft matter* 2005, 17 (1), 69-76.
44. Vehring, R.; Foss, W.R.; Lechuga-Ballesteros, D. Particle formation in spray drying. *Journal of Aerosol Science* 2007, 38 (7), 728-746.
45. Bon, C.L.; Nicolai, T.; Kuil, M.E.; Hollander, J.G. Self-diffusion and cooperative diffusion of globular proteins in solution. *Journal of Physical Chemistry B* 1999, 103 (46), 10294-10299.
46. Tokuyama, M.; Moriki, T.; Kimura, Y. Self-diffusion of biomolecules in solution. *Physical Review E* 2011, 83 (5), 051402.
47. Balbo, J.; Mereghetti, P.; Herten, D.P.; Wade, R.C. The shape of protein crowders is a major determinant of protein diffusion. *Biophysical Journal* 2013, 104 (7), 1576-1584.
48. Nesmelova, I.V.; Skirda, V.D.; Fedotov, V.D. Generalized concentration dependence of globular protein self-diffusion coefficients in aqueous solutions. *Biopolymers* 2002, 63 (2), 132-140.
49. Wellner, N.; Belton, P.S.; Tatham, A.S. Fourier transform IR spectroscopic study of hydration-induced structure changes in the solid state of ω -gliadins. *Biochemical Journal* 1996, 319 (3), 741-747.
50. Careri, G.; Gratton, E.; Yang, P.H.; Rupley, J.A. Correlation of IR spectroscopic, heat capacity, diamagnetic susceptibility and enzymatic measurements on lysozyme powder. *Nature* 1980, 284 (5756), 572-573.
51. Dong, A.; Matsuura, J.; Allison, S.D.; Chrisman, E.; Manning, M.C.; Carpenter, J.F. Infrared and Circular Dichroism Spectroscopic Characterization of Structural Differences between β -Lactoglobulin A and B \dagger . *Biochemistry* 1996, 35 (5), 1450-1457.

Morphological development from droplet to particle, during drying, has a strong influence on powder structure and functionality. We study the evolving morphological properties of whey protein droplets during single sessile droplet drying experiments, as a well-controlled model for spray drying. Sessile drying droplets are visualised with a camera and subjected to varying drying conditions such as temperature, initial protein concentration, presence of airflow and droplet rotation. The final particles are imaged by SEM and X-ray tomography. Under all conditions used, the droplets initially shrink steadily while at some point a hole nucleates. Next a vacuole develops and until finally a rigid particle is obtained. The location of the hole is found to be strongly dependent on the presence and the direction of the applied air flow. We hypothesise that in the early drying stage a skin forms, which becomes more rigid when the hole nucleates. The hole forms at the position where the local modulus of the skin layer is minimal and/or at the point below the skin where the local pressure is minimal, and that after the hole has nucleated, the vacuole develops mainly by evaporation of water through the hole.

3. Hole and vacuole formation during drying of sessile whey protein droplets

¹Laboratory of Physical Chemistry and Soft matter
Wageningen University, Wageningen, The Netherlands.

²Physics and Physical Chemistry of foods, Wageningen
University, Wageningen, The Netherlands.

³Laboratory of Food Process Engineering, Wageningen
University, Wageningen, The Netherlands.

This chapter is submitted as:

Bouman, J. ^{1,2}; De Vries, R. ¹; Venema, P. ²; Van Der Linden, E. ²; Schutyser M.A.I. ³ Hole and vacuole formation during drying of sessile whey protein droplets.

3.1. Introduction

Drying processes do not only remove water, but also have large influence on final product properties. Simple models for industrial drying processes can be used to gain detailed insight into various aspects of drying. For example, the drying behaviour of thin films has been studied to examine the influence of drying conditions on product properties such as film stiffness, flexibility and permeability^{[1],[2],[3]}. Also, the drying of single droplets has been investigated in relation to the properties of powders prepared by spray-drying^[4, 5]. Droplet drying during spray drying involves dehydration and solidification, which may be accompanied by the development of various mechanical stresses. These processes are believed to have a significant impact on the final product properties and in this way co-determine the optimal conditions for a spray drying process that provides both stable operation and the required product quality.

During drying, removal of solvent becomes increasingly difficult because the matrix from which the solvent has to be extracted both concentrates and solidifies. The increase in rigidity of the matrix during drying is crucial, since it has a large influence on particle morphology, which in turn is an important determining factor for attributes of the final powder such as particle size, bulk density, and reconstitution behaviour.^[6-8]

In industrial spray drying processes, many droplets are dried simultaneously with a large distribution in droplet size, residence time and temperature history. Such processes are not well suited to gain insight in the underlying mechanisms of drying. Instead, many studies employ single droplet drying experimentation to study droplet drying under well-defined drying conditions^{[9],[10]}. Different single droplet drying approaches have been developed, such as for example acoustic levitation^[11], pending or suspended droplet^{[12], [13]}, and sessile droplet drying^[14]. These techniques have been used to characterise drying kinetics^[15], enzyme inactivation^{[16], [17]}, protein denaturation^[18] and the final particle morphology^[19]. Most single droplet studies do not focus on particle morphology development. Only one recent study focusses on the drying of whey protein using a pending single droplet approach^[13]. While this study provides interesting data on the drying of droplets in stagnant air, it is less representative for spray drying. For mimicking spray drying, a convective airflow should be applied, as is done in a previous study that used sessile droplets^[14]. In this approach a sessile droplet is positioned on a hydrophobic surface to retain the spherical droplet shape and subsequently the droplet is dried with a convective air flow at a set

drying air temperature and relative humidity. The latter parameters are known to affect particle morphology^[4, 6, 20], which we monitored with a camera during drying.

The objective of this study is to exploit the sessile droplet drying platform to characterise particle morphology development during drying of whey protein isolate droplets. Whey protein isolate (WPI) is chosen as a model system for protein drying, as it is a well-characterised protein product and it is applied as an ingredient in a wide range of foods. Morphological changes are studied as function of several drying parameters such as air temperature, airflow, and initial droplet protein concentration. Fully dried protein particles are then subjected to more extensive imaging using scanning electron microscopy (SEM) and x-ray tomography (XRT). We find that a key event in the drying is the formation of a hole, from which subsequently, a vacuole develops. Finally, based on our experimental observations, we hypothesise on the physical mechanisms behind the sequence of events that we observe for WPI droplet drying.

3.2. Materials and methods

3.2.1. Sessile droplet drying experiments

Protein solutions are prepared by adding whey protein isolate (WPI) powder (Davisco Foods International Inc. Le Sueur, MN, USA) to de-mineralised water. The solutions are prepared at concentrations of 5, 10, 20 and 30% (w/w). Sessile droplets are deposited on a hydrophobic surface using a micro-dispenser as described by Perdana et al. (Figure 15)^[17] The hydrophobic surface consists of a polypropylene membrane (Akzo Nobel Faser Ag., The Netherlands) positioned on a metal sample holder. The droplet is dried by temperature-controlled air streaming from the tunnel. The temperature at the droplet position is monitored with a thermocouple Type K (NiCr–NiAl; RS Component, United Kingdom). A μ Eye 1480ME CCD camera (Imaging Development Systems GMBH, Germany) is used to image the droplet shape during drying. Experiments are performed using dry air (relative humidity RH=0%) heated to temperatures, near the droplet, between 20°C and 80°C with a streaming velocity of the air of about 0.20 m/s. Image analysis on the data is performed using imageJ.

3.2.2. Laboratory-scale spray drying experiments

Similar to the sessile droplet drying experiments solutions are prepared at concentrations of 20 % (w/w). The liquid samples are spray dried in a Buchi B-290 spray dryer (Buchi

Labortechnik AG, Switzerland). Dry air (RH = 0%) is used while the inlet and outlet spray drying temperature is set to 160 °C and 80 °C, respectively.

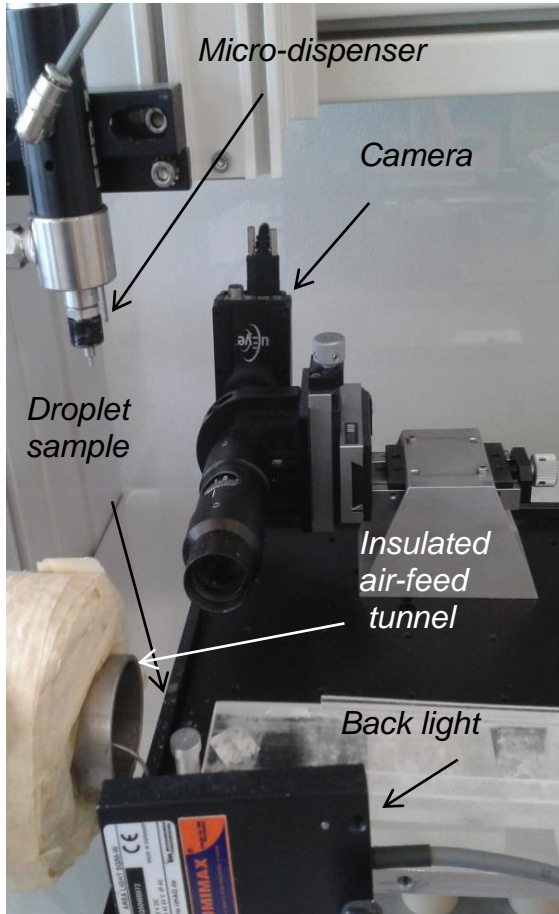


Figure 15. The experimental set-up used for drying of sessile single droplets.

3.2.3. Droplet analysis, microscopy and X-ray tomography

Images obtained during the droplet drying experiments are analysed with Image-J analysis software. Initial droplet shrinkage and subsequent vacuole formation are quantified to calculate initial evaporation rates. After the drying is finished, the protein particles are collected and studied using a Phenom G2 pure desktop electron microscope. Additionally, XRT images are taken using a Phoenix v[tome]x m (General Electric, Wunstorf, Germany). This technique allows for non-invasive measurement of the 3D structure of objects at a

spatial resolution of $1\mu\text{m}$. A 3D image of a fixed particle can be reconstructed from a large series of two-dimensional radiographic images taken around the axis of rotation^[21].

3.3. Results and discussion

Time series of images of drying WPI droplets are shown in Figure 16 for different drying temperatures. The droplets had an initial concentration of 20% (w/w) WPI and a radius of 0.5 mm. The temperature of the airflow is fixed. During the first stage of the drying process, the droplets just shrink, but after a while a hole nucleates at the downstream side of the air flow. Subsequently, it can be clearly observed that a front moves inwards into the droplet and a vacuole develops. Although the radius of the particle slowly continues to decrease, it is expected that the evaporation of water from the droplet is mainly taking place from the vacuole through the hole. After hole formation, the radius of the particle decreases much more slowly. phase, and the final phase of vacuole development and shell formation in more detail.

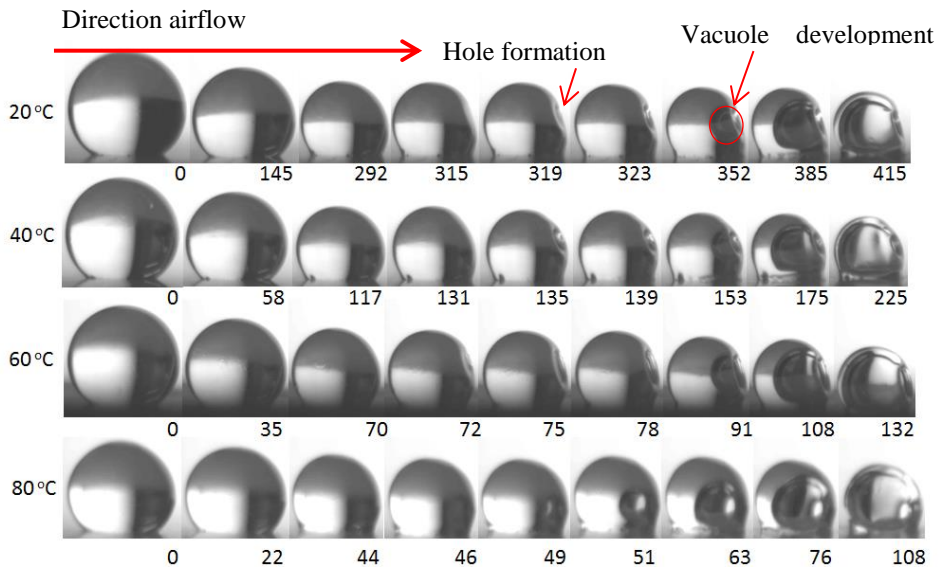


Figure 16. Time series of drying droplets with an initial radius of 0.5 mm and an initial WPI concentration of 20% (w/w). The droplets are dried with an airflow coming from the left with a streaming velocity of 0.2 ms^{-1} at temperatures ranging from 20°C to 80°C. Time (s) after droplet disposition is displayed in the right-bottom corner of each image and temperature T (°C) on the left in front of each series.

This strongly suggests that hole formation is correlated with the formation of a more rigid skin at the surface of the droplet, and that hole formation occurs at spot where the rigidity

of the skin is minimal and/or where the mechanical stresses are maximal. Eventually, a hollow particle is obtained with a rigid outer shell and a single hole. In the next sections we study the initial drying phase, the skin- and hole formation

3.3.1. Initial drying

We observed that all air temperatures lead to a qualitatively similar morphological development including hole formation in the downstream direction of the airflow, the development of a vacuole and the final formation of a solid shell. First, images are analysed to determine the decrease in droplet radius until the moment of hole formation. In Figure 17A the radius squared value of the droplets are shown for different temperatures and found to decrease linearly with drying time, thus following the radius-square-law^[22]:

$$\frac{r^2(t)}{r_0^2} = 1 - \frac{\kappa}{r_0^2} t \quad [1]$$

Here r is the droplet radius (m), r_0 is the initial droplet radius and κ is the evaporation rate of the water (m²/s). Evaporation rates (κ) are determined from the slope of the lines characterising the steady state evaporation prior to hole formation.

3.3.2. Skin formation

In Figure 18 the droplet radius is shown for different air temperatures at the moment of hole formation. A clear correlation is observed between air temperature and droplet radius at the moment of hole formation. Air temperature influences the water evaporation water which will be discussed later. The actual droplet temperatures, which is expected to be close to the wet bulb temperature, can be derived from the relevant energy balance^[14] with the use of the evaporation values (κ) obtained earlier:

$$\Delta T = \frac{\rho_L H_{vap}}{4\pi\lambda} \kappa \quad [2]$$

Here H_{vap} is the heat of evaporation (J/kg), ρ_L is droplet density which for the early stages of drying we approximated to the water density (kg/m³), ΔT is the difference between air temperature and droplet temperature (K) and λ is the heat conductivity of the vapour(W/m/K). From equation (2) we estimate that the droplet temperature varied from 8 °C at a drying air temperature of 20 °C to 25 °C at a drying air temperature of 80 °C.

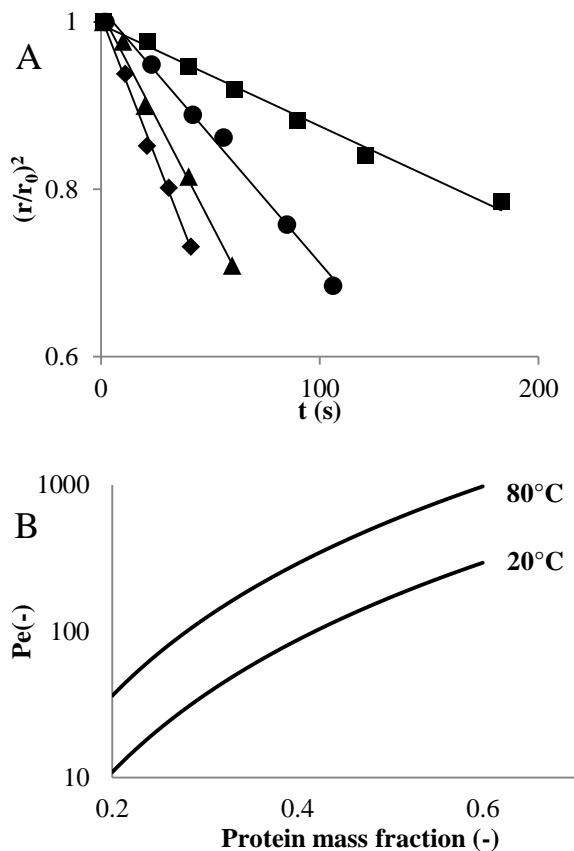


Figure 17. A) Decrease in radius squared of the droplets over time for different temperatures. Squares: 20°C, triangles: 40°C, circles: 60°C and diamonds: 80°C. Lines are fitted to the experimental data. B) Peclet number during drying of whey droplets versus their protein mass fraction. Airflow temperatures are 20°C, and 80°C. The initial droplet radius $r_0 = 0.5$ mm and the air velocity is 0.2 ms^{-1} in both graphs.

For whey proteins, the sol-gel transition occurs above $414 \text{ g/L}^{[23]}$ (at 20°C), corresponding to a protein concentration of approximately 40% (w/w). Therefore, if bulk properties are to determine the moment of hole formation, we would expect it for the droplets (starting concentration 20% (w/w)) to occur at a normalised droplet radius of 0.8. However, as can be observed from Figure 18, the hole formation occurs at much smaller droplet radii. After hole formation, the outer radius of the particles decreases much more slowly. This strongly suggests that the moment of hole formation is determined not by a change in mechanical properties of the bulk of the droplet, but rather by a change of the mechanical properties of the droplet surface. Indeed, it is frequently assumed that at some stage during drying a more

rigid skin can develop at the droplet surface. Meerdink (1995) and others relate skin formation to differential diffusion of solution components away from the surface of the droplets^[6, 13,24]. Whereas solutes are initially uniformly distributed in the droplet, the solute concentration near the surface may start to rise sharply due to water evaporation at the surface. As a consequence, solutes tend to diffuse towards the centre, but because of their low diffusivity they accumulate at the droplet surface. This is assumed to give rise to skin formation. The dimensionless number governing whether drying is uniform or not is the Peclet number, which is defined as the ratio of evaporation rate and solute diffusivity^[6]:

$$Pe = \frac{\kappa}{8D_i} \quad [3]$$

Here, D_i is the diffusion coefficient of the solute in the liquid phase. If $Pe \gg 1$, the evaporation dominates over diffusional transport, and drying is non-uniform, leading to skin formation.

In order to estimate Peclet numbers during the drying of whey protein droplets, we need values for the protein diffusion constants at high protein volume fractions. Ample data is available for dilute systems, i.e. for $x_w < 0.65$ (w/w)^[25,26, 27], but not for the dense systems that we are dealing with here. Therefore we use the empirical expression by Nesmelova et al. that is found to be appropriate for dense protein systems^[28]:

$$\frac{D}{D_0} = \left(\frac{\hat{\varphi}}{\varphi}\right)^3 \quad [4]$$

where φ is the protein volume fraction (-), and $\hat{\varphi}$ is a characteristic protein volume fraction demarcating the “dilute” from the “concentrated” regime. The parameter $\hat{\varphi}$ depends on the type of protein, but is typically between 0.1-0.15 (v/v) for proteins. For D_0 , we use a value previously reported^[29] for dilute β -lactoglobulin (β -lg), $D_0 = 9.5 \cdot 10^{-11} \text{ m}^2 \text{ s}^{-1}$. Nesmelova et al. do not report a value of $\hat{\varphi}$ for β -lg, so we use an average of the values they report for similar globular proteins: $\hat{\varphi} = 0.13$. For converting volume fractions to mass fractions, we use a density of $1.25 \cdot 10^6 \text{ g/m}^3$. With the use of κ -values calculated from Figure 17A, Peclet numbers are estimated for our protein drying conditions (these κ -values can also be found in Figure 18). These are given in Figure 17B. Clearly, already from the start of the drying process $Pe \gg 1$ and therefore drying is indeed expected to be inhomogeneous, favouring the formation of a skin at some stage during the drying process.

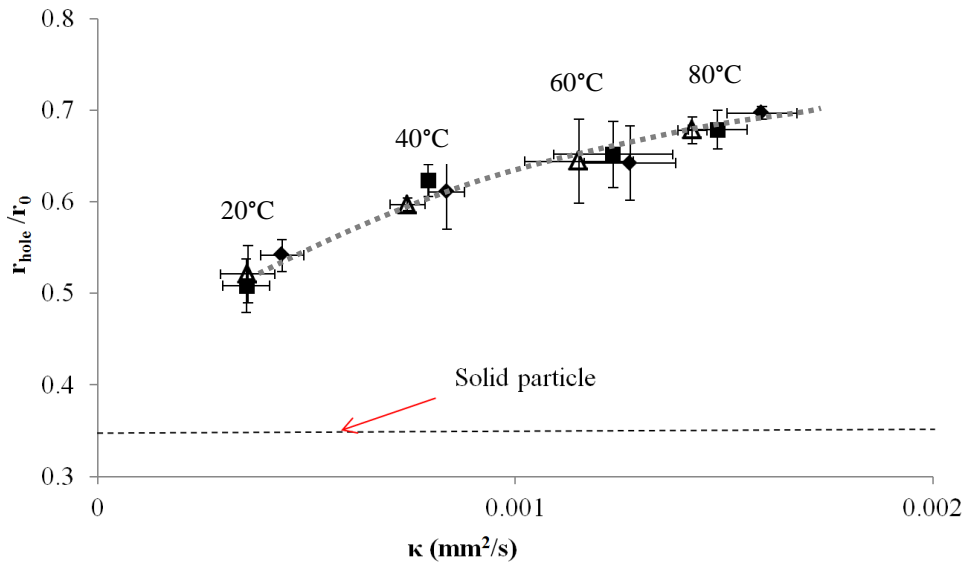


Figure 18. Average normalised droplet radius (r_{hole}/r_0) at the moment of hole formation is plotted versus evaporation rate κ (m^2/s) for different initial droplet radii (r_0). Initial radii are 0.75mm(◆), 0.5mm(■) and 0.25mm(Δ). The drying temperatures related to the different data points are displayed in the figure. Dotted curve is drawn to guide the eye.

The evaporation rate κ (Figure 18) is practically independent of initial droplet size, in agreement with the radius square law for the initial stage of drying and clearly correlates with the droplet size at which hole formation occurs. This is in line with the different values for Peclet we have found. Higher evaporation rates will result in higher Peclet values (assuming that the diffusion coefficient D remains constant), meaning stronger inhomogeneous drying. This will lead to more rapid accumulation of proteins on the surface, enhancing the skin formation.

At a later stage in the drying process, when the evaporation rate decreases, the temperature inside the droplets increase above the wet-bulb temperature, heat-induced protein aggregation near the surface might be an additional contribution to the development of the skin. This could provide additional integrity to the particle, and should decrease shrinkage as compared to particles for which heat-induced gelation temperatures are not reached. In an earlier study heat-induced gelation is hypothesised to cause skin formation for drying gelatin droplets^[30].

3.3.3. Hole formation

The images (Figure 16) show the formation of a hole in the surface of the droplet. The formation of hollow particles during single droplet drying has been observed previously for whey proteins^[6, 19, 31, 32]. However, the development of a hole *prior to* vacuole formation has not been observed for proteins earlier to the best of our knowledge. From the images, it can be observed that the hole develops from the outside to the inside of the droplet, i.e. it ‘sinks’ into the surface of the droplet. This is in contrast to earlier studies that describe holes being formed from the inside to the outside, i.e. so-called “blow holes”^{[19, 33], [34], [7]}. For these cases it is suggested that directly after skin formation, liquid trapped inside may reach boiling temperature and vapour bubble nucleation can occur. This leads to rapid volume expansion due to liquid-vapour transition and a sudden pressure increase^[35], resulting in hole formation at the weakest point of the skin^[12]. The latter is clearly not expected for our rather low drying temperatures.

In one study, the actual size of glycoprotein powder particles just after skin formation is measured but no sign of droplet inflation is reported^[6]. For that case, hole formation is suggested to be related to drying of the interior of the particles, causing the inward movement of the locally elastic skin^[6, 33]. This is in line with the time series of the images obtained during sessile droplet experiments (Figure 16). These images clearly show an inward movement of the skin rather than an outward movement. In another study^[36] on drying of polymer films, also an inward bend of the surface is observed followed by the formation of bubbles below the surface. This is explained by continued solvent evaporation after skin formation, thus creating a lower pressure below the skin, exerting a stress on the skin that eventually leads to an inward bend. No collapse of the skin is reported in this study. In other studies drying of droplets containing colloidal particles is monitored^[37, 38]. In one³⁷ the drying of droplets of a suspension containing micron-sized polystyrene particles, skin formation and subsequent surface buckling are observed. This is explained by the argument that non-uniform drying lead to close packing of particles until inter-colloidal repulsions resists further shrinkage. During further evaporation droplet an under-pressure developed in the droplet exerted a compressive capillary stress on the particle skin contributing to a sol-gel transition and subsequent buckling and crumpling of the shell. Despite similarities between the drying of the polystyrene suspensions and the WPI solution no hole is formed in the outer shell in the former case. Possibly, due to the larger

size of the colloids as compared to the proteins, in the case of the colloids, the skin much more rapidly developed the mechanical strength to withstand the formation of a hole. In the second study³⁹ hole formation and vacuole formation, (there mentioned as buckling and invagination) is observed for much smaller colloidal silica particles (15 nm). The hole development is explained to be driven by a pressure difference between the inside and the outside of the particle. Further development of the vacuole is hypothesised to be determined by the competition between bending and stretching deformations. The behaviour of the latter systems shows similarities with the one in this study, which could suggest that there could be a similarity between the globular proteins and these larger hard spheres.

3.3.4. Vacuole and shell formation

From the XRT images presented in Figure 19 we conclude that the final shell thickness is uniform across the particle. Since protein is still being deposited as the remaining solvent evaporates through the hole, one might have expected a somewhat thicker shell further away from the hole, but apparently this is a minor effect.

Next, we have quantified the loss of volume from the shrinking droplets after hole formation (Figure 20). In the initial stage of drying, the evaporation rate is constant. Remarkably, even after hole nucleation, there is no abrupt change in the drying rate. Only once the outer shell starts rigidify, the drying rate starts to decrease. As water diffusivity decreases with protein concentration^[39], we expect diffusion through the skin to decrease, especially when the skin rigidifies. Clearly, the hole- and subsequent vacuole formation contribute to a high and relatively constant drying rate, since the hole acts as an evaporation vent. This is also evident from the fact that after hole formation, a clear receding liquid front inside the droplet can be observed (Figure 16).

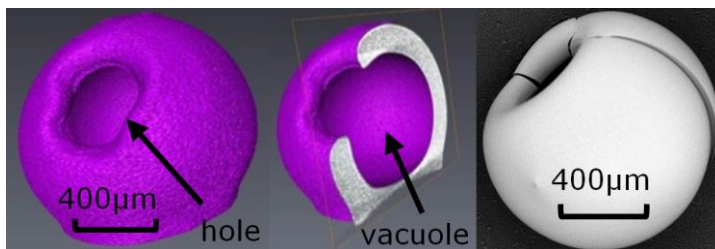


Figure 19. XRT images and a SEM image of a dried particle. Initial droplet radius is 0.75 mm and initial concentration of WPI solution is 20% (w/w).

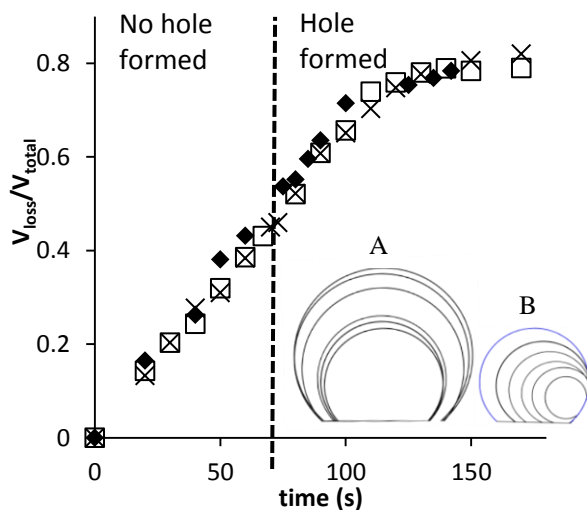


Figure 20. WPI droplet evaporation represented by the normalised volume loss ($V_{\text{loss}}/V_{\text{total}}$) as a function of time. Initial WPI concentration is 20 % (w/w), initial droplet radius is 0.5 mm, air temperature is 60°C and airflow speed is 0.2 ms^{-1} . The vertical dashed line marks the moment when the hole nucleates. Insert: A. examples of image analysis used to calculate volume loss from droplet shrinkage B. Hole nucleation and growth of a vacuole

3.3.5. Different stages during the drying of a single sessile droplet of WPI

In Figure 21, based on the experimental results we discriminate the following stages occur during sessile protein droplet drying. 1) In the initial stage, the protein distribution in the droplet is still homogeneous. The evaporation rate at the downstream side of the air flow is slightly lower than at the upstream side. 2) Initially proteins absorb to the interface of the droplet mainly by their surface activity, while at a later stage the accumulation rate at the interface increases due to the increasing Peclet number. Thereby an elastic skin is formed, that is thinner at the downstream side, since the Peclet number is also smaller on the downstream side. 3) After a certain period, the skin becomes sufficiently rigid to stop further shrinkage of the droplet. The evaporation continues through the skin, which creates a local pressure minimum below the surface of the droplet at the point downstream side, where the thickness of the skin layer is also minimal. 4) The rapid increase in surface area of the vacuole prevents the formation of a rigid skin inside the vacuole and 5) this surface area provides an efficient way for further evaporation. 6) hollow particle with a hole in the surface is formed. Possibly also another mechanism could explain the formation at the hole at the downstream side. This explanation is related to small temperature differences that can

develop in the droplet due to differences in local evaporation rates³². As a result a surface tension gradient develops across the droplet, which again induces Marangoni flow within the droplet from the downstream direction to the upstream direction. The net effect will be that the skin at the downstream side will be thinner compared to that at the upstream side.

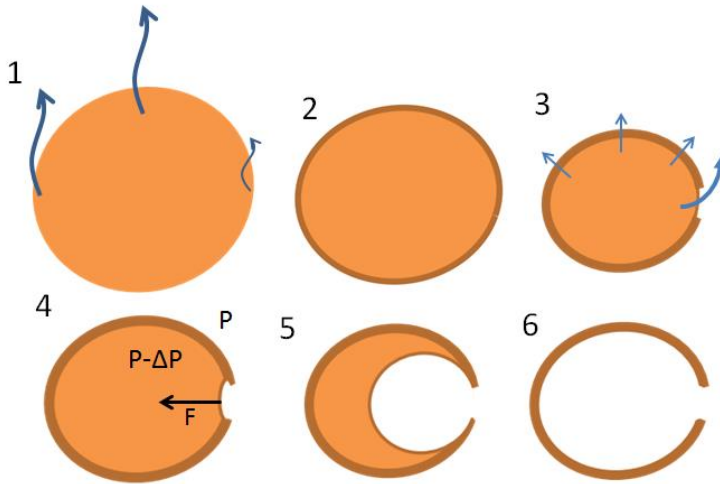


Figure 21: Schematic representation of a drying sessile droplet with whey proteins displayed in 6 steps.

3.3.6. Influence of the direction of the convective airflow on hole formation

We found that a hole is formed at the surface of the droplet at the downstream side of the airflow. To investigate what happens without the presence of convective airflow, sessile droplets are dried in stagnant air at room temperature. The initial radius of the droplets is 0.5 mm, while the initial protein concentration is 20% (w/w) WPI. We observed (Figure 22A), that drying the droplets in stagnant air is approx. 4 times slower than drying with previously applied airflow. When drying in stagnant air the hole is formed on top of the droplet (cf. Figure 22A + B). At the moment of hole formation it shows that the droplet shape is still spherical. Bond numbers^[40] are determined (given a surface tension of 48 mN/m^[41]) to be at least a factor smaller than one (0.11 for the largest droplets), suggesting that surface tension dominates the shape over gravity preventing a minimum in Gaussian curvature on top of the particle. However, we suggest that gravity may still play an essential role, since it causes the bulk liquid to form a local minimum in pressure below the skin on

top of the particle. This may result in an increased local stress thereby causing a hole to develop on top of the droplet. In a recent study on a similar system, no clear hole formation is observed¹³. However in this study, instead of a sessile droplet, a pending droplet geometry is used, where the droplet is hanging on a surface patterned with cylindrical pillars. Because for a pending droplet gravity would cause the local minimum in pressure to develop at the droplet-surface interface, it is not in disagreement with the idea that in stagnant air gravity is the main determining factor for hole formation in the case of stagnant air drying of sessile protein droplets.

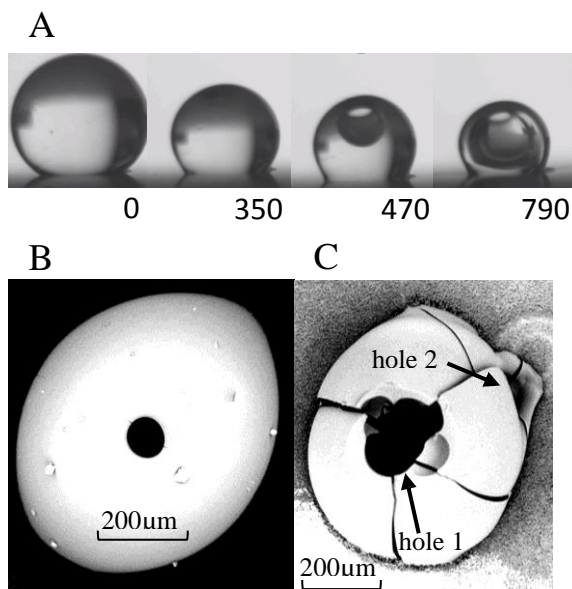


Figure 22. A) Images of a 20% (w/w) WPI solution droplet drying without convective airflow. Initial droplet radius is 0.5 mm, air temperature is 25 °C and relative humidity is 33% B) SEM top view of the final particle. C) SEM of final particle of a WPI droplet dried while rotating at a speed of 55 rpm. Initial WPI concentration is 20% (w/w), initial droplet radius is 0.5mm, air temperature T is 100°C and airflow speed is 0.2 ms⁻¹

3.3.7. Relation to spray drying

During spray drying droplets are suspended in air and are subject to rotational motion. To investigate the influence of rotation on hole formation, we subjected a sessile droplet to a rotational motion during drying in an airflow. We found that hole formation still occurs during rotation and occasionally even two holes in the shell are formed. In Figure 8C a SEM image is shown of the shell of a droplet that is rotated at 55 rpm during drying in an

airflow. During rotation the holes are not formed at the top of the particle, but mostly at locations close to the equator. Clearly, when the droplet is being rotated, the drying is more uniform, making the position of the thinnest skin unpredictable.

In order to investigate how single droplet drying relates to spray drying we investigate morphologies of spray dried protein particles. In Figure 23 a SEM image of lab-scale spray dried WPI solution is shown. It can be observed that most of these particles, show similarities with SDD dried particles i.e. spherical shell morphology with a hole and vacuole. Additionally it is observed that several particles have multiple holes, which is similar with the results from the rotated SDD particles see Figure 22C.

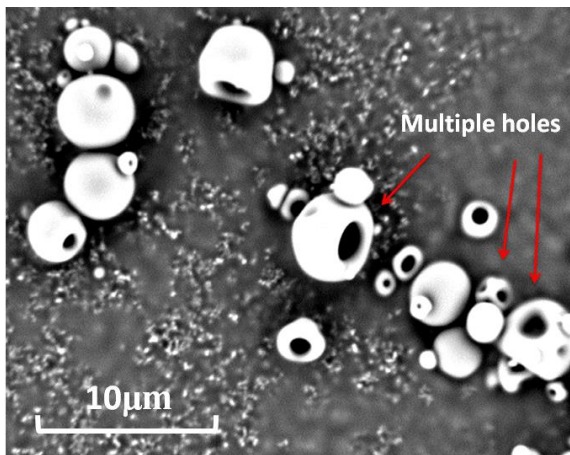


Figure 23: SEM image of lab scale spray dried WPI. Initial concentration, inlet and outlet spray are respectively 20% (w/w) 160 and 80 °C

3.3.8. Initial concentration and surface buckling

It is expected that the shell morphology of the dried particles is also influenced by the initial protein concentration. We therefore investigated droplet drying at different initial whey protein concentrations. In Figure 24, images of droplets at the moment of hole formation are displayed. The droplets have different initial protein concentrations (5%, 10%, 20%, 30% (w/w)). For droplets with an initial concentration of 5% and 10% (w/w) surface deformations are found, and the shells showed large deformations from spherical. These deformation are similar to surface buckling, dimpling or wrinkling described earlier^{[42],[33]}. These are typically explained in terms of a critical surface rigidity, below which the droplet cannot maintain its spherical shape during further drying.

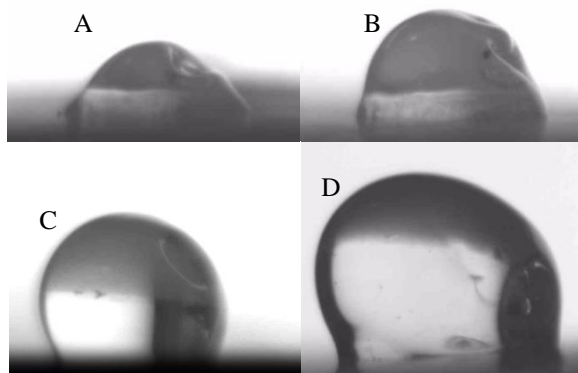


Figure 24: Video images of droplets with varying initial WPI concentrations at the specific moment of hole formation. Initial WPI concentrations: A) 5% (w/w), B) 10% (w/w), C) 20% (w/w) and D) 30% (w/w). Initial droplet radius is 0.5 mm, Temperature is 100°C and airflow speed is 0.2 ms⁻¹

3.4. Conclusion

A sessile single droplet drying setup has allowed us to accurately monitor hole- and subsequent vacuole formation during the drying of whey protein solutions. The initial rate of drying until hole formation is found to be governed by the radius squared law. The hole formation that we observe is explained by inward collapse of the skin (‘sink-hole’) rather than by a sudden vapour pressure increase inside droplet (‘blow-hole’). The direction of air flow is found to determine the location of the hole. In stagnant air the hole is formed on top of the droplet. In case of rotating droplets in an air flow, holes or even multiple holes are formed at positions close to the equator, but never at the top of the droplet. We hypothesise that hole formation happens at the point with the thickness of the skin is minimal and/or where stresses induced by drying are largest. Hole formation prior to vacuole formation increases the drying rate by increasing the overall surface area available for evaporation. For spray drying this is advantageous since drying will be shorter while the rapid evaporation keeps the temperature of the droplet lower, minimising thermal degradation. If due to higher temperatures, evaporation is fast this will result in larger particle size and subsequently in powders with a lower bulk density, which may be disadvantageous again. Further investigations will be directed towards a better understanding of the mechanism of

hole, vacuole and shell formation and towards developing strategies to control these phenomena during spray drying.

3.5. Acknowledgements

This work is part of the Industrial Partnership Programme (IPP) Bio(-Related)Materials of the Stichting voor Fundamenteel Onderzoek der Materie (FOM), which is financially supported by the Nederlandse Organisatie voor Wetenschappelijk Onderzoek (NWO). The IPP BRM is co-financed by the Top Institute Food and Nutrition and the Dutch Polymer Institute. We thank Erik Sewalt and Jun Qui for their contributions to this work.

3.6. References

1. Alcantara, C.R.; Rumsey, T.R.; Krochta, J.M. Drying rate effect on the properties of whey protein films. *Journal of Food Process Engineering* 1998, 21 (5), 387-405.
2. Denavi, G.; Tapia-Blácido, D.R.; Añón, M.C.; Sobral, P.J.A.; Mauri, A.N.; Menegalli, F.C. Effects of drying conditions on some physical properties of soy protein films. *Journal of Food Engineering* 2009, 90 (3), 341-349.
3. Jooyandeh, H. Whey protein films and coatings: A review. *Pakistan Journal of Nutrition* 2011, 10 (3), 293-301.
4. Fang, Y.; Rogers, S.; Selomulya, C.; Chen, X.D. Functionality of milk protein concentrate: Effect of spray drying temperature. *Biochemical Engineering Journal* 2012, 62 (0), 101-105.
5. Alamilla-Beltrán, L.; Chanona-Pérez, J.J.; Jiménez-Aparicio, A.R.; Gutiérrez-Lopez, G.F. Description of morphological changes of particles along spray drying. *Journal of Food Engineering* 2005, 67 (1-2), 179-184.
6. Vehring, R.; Foss, W.R.; Lechuga-Ballesteros, D. Particle formation in spray drying. *Journal of Aerosol Science* 2007, 38 (7), 728-746.
7. Hassan, H.M.; Mumford, C.J. Mechanisms of Drying of Skin-Forming Materials; the Significance of Skin Formation and a Comparison Between Three Types of Material. *Drying Technology* 1996, 14 (7-8), 1763-1777.
8. Walton, D.E.; Mumford, C.J. Spray Dried Products—Characterization of Particle Morphology. *Chemical Engineering Research and Design* 1999, 77 (1), 21-38.
9. Adhikari, B.; Howes, T.; Bhandari, B.R.; Truong, V. Experimental studies and kinetics of single drop drying and their relevance in drying of sugar-rich foods: A review. *International Journal of Food Properties* 2000, 3 (3), 323-351.
10. Schutyser, M.A.I.; Perdana, J.; Boom, R.M. Single droplet drying for optimal spray drying of enzymes and probiotics. *Trends in Food Science and Technology* 2012, 27 (2), 73-82.
11. Fu, N.; Woo, M.W.; Chen, X.D. Single Droplet Drying Technique to Study Drying Kinetics Measurement and Particle Functionality: A Review. *Drying Technology* 2012, 30 (15), 1771-1785.
12. Walton, D.E.; Mumford, C.J. The Morphology of Spray-Dried Particles: The Effect of Process Variables upon the Morphology of Spray-Dried Particles. *Chemical Engineering Research and Design* 1999, 77 (5), 442-460.

13. Sadek, C.; Tabuteau, H.; Schuck, P.; Fallourd, Y.; Pradeau, N.; Le Floch-Fouéré, C.; Jeantet, R. Shape, Shell, and Vacuole Formation during the Drying of a Single Concentrated Whey Protein Droplet. *Langmuir* 2013, 29 (50), 15606-15613.
14. Perdana, J.; Fox, M.B.; Schutyser, M.A.I.; Boom, R.M. Mimicking Spray Drying by Drying of Single Droplets Deposited on a Flat Surface. *Food and Bioprocess Technology* 2013, 6 (4), 964-977.
15. Chen, X.D.; Lin, S.X.Q. Air drying of milk droplet under constant and time-dependent conditions. *AIChE Journal* 2005, 51 (6), 1790-1799.
16. Yamamoto, S.; Sano, Y. Drying of enzymes: enzyme retention during drying of a single droplet. *Chemical Engineering Science* 1992, 47 (1), 177-183.
17. Perdana, J.; Fox, M.B.; Schutyser, M.A.I.; Boom, R.M. Single-Droplet Experimentation on Spray Drying: Evaporation of a Sessile Droplet. *Chemical Engineering & Technology* 2011, 34 (7), 1151-1158.
18. Haque, M.A.; Aldred, P.; Chen, J.; Barrow, C.J.; Adhikari, B. Comparative study of denaturation of whey protein isolate (WPI) in convective air drying and isothermal heat treatment processes. *Food Chemistry* 2013, 141 (2), 702-711.
19. Walton, D.E. The morphology of spray-dried particles a qualitative view. *Drying Technology* 2000, 18 (9), 1943-1986.
20. Gaiani, C.; Morand, M.; Sanchez, C.; Tehrany, E.A.; Jacquot, M.; Schuck, P.; Jeantet, R.; Scher, J. How surface composition of high milk proteins powders is influenced by spray-drying temperature. *Colloids and Surfaces B: Biointerfaces* 2010, 75 (1), 377-384.
21. Herman, G.T. *Fundamentals of computerized tomography: image reconstruction from projections*. Springer, 2009.
22. Jakubczyk, D.; Kolwas, M.; Derkachov, G.; Kolwas, K.; Zientara, M. Evaporation of Micro-Droplets: the " Radius-Square-Law" Revisited. *Acta Physica Polonica-Series A General Physics* 2012, 122 (4), 709.
23. Sadek, C.; Pauchard, L.; Schuck, P.; Fallourd, Y.; Pradeau, N.; Le Floch-Fouéré, C.; Jeantet, R. Mechanical properties of milk protein skin layers after drying: Understanding the mechanisms of particle formation from whey protein isolate and native phosphocaseinate. *Food Hydrocolloids* 2015, 48 8-16.
24. Meerdink, G.; van't Riet, K. Modeling segregation of solute material during drying of liquid foods. *AIChE Journal* 1995, 41 (3), 732-736.
25. Tokuyama, M.; Moriki, T.; Kimura, Y. Self-diffusion of biomolecules in solution. *Physical Review E* 2011, 83 (5), 051402.
26. Balbo, J.; Mereghetti, P.; Herten, D.P.; Wade, R.C. The shape of protein crowders is a major determinant of protein diffusion. *Biophysical Journal* 2013, 104 (7), 1576-1584.
27. Parker, R.; Noel, T.R.; Brownsey, G.J.; Laos, K.; Ring, S.G.; Ring, S. The nonequilibrium phase and glass transition behavior of β -lactoglobulin. *Biophysical Journal* 2005, 89 (2), 1227-1236.
28. Nesmelova, I.V.; Skirda, V.D.; Fedotov, V.D. Generalized concentration dependence of globular protein self-diffusion coefficients in aqueous solutions. *Biopolymers* 2002, 63 (2), 132-140.
29. Bon, C.L.; Nicolai, T.; Kuil, M.E.; Hollander, J.G. Self-diffusion and cooperative diffusion of globular proteins in solution. *Journal of Physical Chemistry B* 1999, 103 (46), 10294-10299.

30. Hassan, H.M.; Mumford, C.J. Mechanisms of Drying of Skin-Forming Materials. II. Droplets of Heat Sensitive Materials. *Drying Technology* 1993, 11 (7), 1751-1764.
31. Sadek, C.; Tabuteau, H.; Schuck, P.; Fallourd, Y.; Pradeau, N.; Le Floch-Fouere, C.; Jeantet, R. Shape, Shell, and Vacuole Formation during the Drying of a Single Concentrated Whey Protein Droplet. *Langmuir* 2013, 29 (50), 15606-15613.
32. Farid, M. A new approach to modelling of single droplet drying. *Chemical Engineering Science* 2003, 58 (13), 2985-2993.
33. Vehring, R. Pharmaceutical Particle Engineering via Spray Drying. 2008, 25 (5), 999-1022.
34. Littringer, E.M.; Paus, R.; Mescher, A.; Schroettner, H.; Walzel, P.; Urbanetz, N.A. The morphology of spray dried mannitol particles — The vital importance of droplet size. *Powder Technology* 2013, 239 (0), 162-174.
35. Vicente, J.; Pinto, J.; Menezes, J.; Gaspar, F. Fundamental analysis of particle formation in spray drying. *Powder Technology* 2013, 247 (0), 1-7.
36. Araia, S.; Doi, M. Skin formation and bubble growth during drying process of polymer solution. *European Physical Journal E* 2012, 35 (7).
37. Sugiyama, Y.; Larsen, R.J.; Kim, J.-W.; Weitz, D.A. Buckling and Crumpling of Drying Droplets of Colloid–Polymer Suspensions. *Langmuir* 2006, 22 (14), 6024-6030.
38. Boulogne, F.; Giorgiutti-Dauphine, F.; Pauchard, L. The buckling and invagination process during consolidation of colloidal droplets. *Soft Matter* 2013, 9 (3), 750-757.
39. Bouman, J.; De Vries, R.; Venema, P.; Belton, P.; Baukh, V.; Huinink, H.P.; Van Der Linden, E. Coating formation during drying of β -lactoglobulin: Gradual and sudden changes. *Biomacromolecules* 2015, 16 (1), 76-86.
40. Hager, W.H. Wilfrid Noel Bond and the Bond number. *Journal of Hydraulic Research* 2012, 50 (1), 3-9.
41. Gonzalez-Tello, P.; Camacho, F.; Guadix, E.; Luzón, G.; González, P. Density, viscosity and surface tension of whey protein concentrate solutions. *Journal of Food Process Engineering* 2009, 32 (2), 235-247.
42. Xu, H.; Melle, S.; Golemanov, K.; Fuller, G. Shape and Buckling Transitions in Solid-Stabilized Drops†. *Langmuir* 2005, 21 (22), 10016-10020.
43. Pauchard, L.; Allain, C. Buckling instability induced by polymer solution drying. *Europhysics Letters* 2003, 62 (6), 897-903.

The purpose of this study is to evaluate the potential of zein as a sole excipient for controlled release formulations prepared by hot melt extrusion. Physical mixtures of zein, water and crystalline paracetamol are hot melt extruded (HME) at 80°C and injection moulded (IM) into caplet forms. HME-IM Caplets are characterised using differential scanning calorimetry, ATR-FTIR spectroscopy, scanning electron microscopy and powder X-ray diffraction. Hydration and drug release kinetics of the caplets are investigated and fitted to a diffusion model. For the formulations with lower drug loadings, the drug is found to be in the non-crystalline state, while for the ones with higher drug loadings paracetamol is mostly crystalline. Release is found to be largely independent of drug loading but strongly dependent upon device dimensions, and predominately governed by a Fickian diffusion mechanism, while the hydration kinetics shows the features of Case II diffusion. In this study a prototype controlled release caplet formulation using zein as the sole excipient is successfully prepared using direct HME-IM processing. The results demonstrated the unique advantage of the hot melt extruded zein formulations on the tuneability of drug release rate by alternating the device dimensions.

4. Extrusion-injection moulded zein matrices as controlled oral delivery system

¹Laboratory of Physical Chemistry and Soft matter and

²Physics and Physical Chemistry of foods, Wageningen University, Wageningen, The Netherlands.

³School of Chemistry, University of East Anglia, Norwich, United Kingdom.

⁴School of Pharmacy, University of East Anglia, Norwich, United Kingdom.

This chapter is published as:

Bouman, J.^{1,2}; Belton, P.³; Venema, P.²; van der Linden, E.²; de Vries, R.¹; Qi, S.⁴ The development of direct extrusion-injection moulded zein matrices as novel oral controlled drug delivery systems *Pharmaceutical Research*. 2015, 1-12.

4.1. Introduction

Controlled release oral drug delivery systems have many advantages over conventional formulations. These systems have no constraint on the drug release rate, including reduced dosing frequency, enhanced bioavailability and subsequently reduced side-effects by maintaining a long period of a steady drug plasma concentration ^[1]. Therefore the use of controlled release formulations often contributes to the improved patient adherence to the treatment and overall therapeutic outcome. However, good control of the drug release rate is challenging and polymeric excipients are often used for this purpose ^[2]. Although there is a wide range of synthetic polymers that may be used for a controlled release purpose, some naturally derived polymers have the advantages of being biocompatible as well as environmentally sustainable and often inexpensive. Therefore, much interest has been directed towards finding more natural polymers as suitable excipients for drug delivery formulations including controlled drug release systems. Recently zein, a mixture of natural proteins found in maize, has been explored for its potential applications in drug delivery ^[3-5].

Zein is a main component in the by-products of both the wet milling and dry milling process to obtain ethanol from maize ^[6]. It contains a mixture of α , β , γ and δ zein proteins which forms both hydrophobic and hydrophilic domains allowing it to behave as a polymeric amphiphile^[7]. It is not readily soluble in water which is likely due to strong protein-protein interactions^[8]. Compared to other proteins, zein has a good heat and pH stability^[9]. It is highly biocompatible^[10, 11], low cost and has versatile physical and mechanical properties that are suitable for being used in many different forms of drug delivery systems. For example, zein has been already successfully applied in the preparation of drug-loaded microspheres ^[3], films ^[4] and tablets ^[5]. In addition, the swellable but non-dissolvable nature of zein makes it a suitable candidate as excipient for controlled release drug delivery systems.

Being relatively heat-stable, zein has proven to be a good candidate for hot melt extrusion^[12, 13], which is a thermal processing that is being increasingly adopted for the preparation of pharmaceutical solid dispersion based formulations. It has been reported that zein its structure only begin to change at temperatures above 120°C, which is likely to be due to protein cross linking by disulphide bonds ^[9]. The use of extrusion techniques to

process zein is well known in the food industry^[12, 13], but the potential for the preparation of pharmaceutical products has not been widely explored. The aim of this work is to develop new oral controlled release caplets with tuneable release rates, with zein as the sole excipient using a simple two-step processing, hot melt extrusion (HME) in combination with injection moulding (IM). The use of HME in combination with IM is a novel and effective way to create tuneable matrix dosage forms with precise shape and dimensions^[14, 15], which is critical for the systems in which the drug release rate is highly controlled by both.

During extrusion zein is heated above the glass transition temperature (T_g) and forms a viscoelastic system^[9] generating a single matrix phase providing potentially superior properties compared to those prepared by tablet pressing, where particles are only pressed together forming an inhomogeneous system. Paracetamol is used as a model drug because it is well characterised, pH stable and stable at the extrusion temperatures applied in this study^[16]. The physical states of the model drug and its distribution is characterised by differential scanning calorimetry (DSC), Fourier transform Infra-red spectroscopy (FTIR) and powder X-ray diffraction (PXRD). Dissolution studies are performed to investigate the influence of dissolution medium, drug loading and caplet dimension on the release kinetics. Hydration behaviour of the caplets is monitored and the potential impacts on drug release kinetics are evaluated.

4.2. Materials and methods

4.2.1. Materials

Purified zein protein (Acros organics, Geel, Belgium) is ground using a kitchen blender with 15s grinding alternated with 20s cooling down to minimise temperature increases due to frictional forces. The particle size of the grounded zein powder is measured between 40-200 μm to ensure good mixing with the crystalline model drug, paracetamol (Sigma-Aldrich, Gillingham, UK), which had similar particle size.

4.2.2. Hot melt extrusion and injection moulding

Ground zein powder is mixed with distilled water (10-12% of weight mixture) in a glass mortar and pestle in order to lower its glass transition temperature (T_g) and allow the hot

melt extrusion at relatively low temperature. Different amounts of paracetamol are added to the zein-water mixture to obtain the mixes for formulations with drug loading ranging from 4.4-45.1% (w/w). The ternary mixes (zein-water-model drug) are ground again prior to extrusion. A feeding batching size of 5-10g is processed using a HAAKE™ Minilab extruder (Thermo Fisher, Karlsruhe, Germany) with a co-rotating twin screw. The extrusions are performed at a temperature of 80 °C and screw speed of 100 rpm. A pre-heated injection moulding cylinder (80 °C) is attached to the extruder to collect the extrudates and keep them at 80°C. The injection moulding process is performed at 80°C, under high pressure of 300-500 bar into a caplet mould using a HAAKE™ MiniJet Pro Piston Injection Moulding System (Thermo Fisher, Karlsruhe, Germany). After the IM sequence, the mould is placed on aluminium foil positioned on dry ice for a rapid cooling. The caplet (5.9x4.4x19.7mm) is then ejected out of the mould and stored in a sealed container at ambient conditions. After processing, the moisture contents of the caplets are determined using thermogravimetric analysis (TGA) to be between 12% and 14% (w/w) for the samples with drug loadings between 45.1% to 4.4% (w/w).

4.2.3. Differential Scanning Calorimetry (DSC)

DSC experiments are conducted using a Q2000 MTDSC (TA Instruments, Newcastle, DE, U.S.). Full range calibration is performed prior to the sample testing. For the DSC samples, a caplet slice is cut and milled into smaller particles using mortar and pestle. Prior to the DSC measurements, all samples are dried in a 70°C oven for 3 days, to minimize the effect of water evaporation during a DSC run. A standard heat-cool-heat sequence is applied to each sample. 10.00 °C/min heating rate and 5.00°C/min cooling rate are applied for all samples. In the DSC cell a nitrogen purge at a flow rate of 50 mL/min is used. Analysis is performed using TA Universal Analysis software. To measure the amount of crystalline paracetamol present, melting enthalpies are compared with the melting enthalpy of pure crystalline paracetamol form I, which is experimentally measured as 181±0.7 J/g.

4.2.4. Attenuated Total Reflection Fourier Transform Infrared Spectroscopy (ATR-FTIR)

ATR-FTIR spectra of the samples are collected using an FTIR spectrometer (IFS66/S model from Bruker Optics limited, Coventry, UK) with a mercury/cadmium/telluride

detector. The samples (both outer surface and cross-section of caplet/extrudate) are directly placed on a single-reflection diamond ATR (attenuated total reflectance) accessory (Specac, Orpington, UK). 64 scans are acquired for each sample with a resolution of 2 cm^{-1} .

4.2.5. Powder X-Ray Diffraction (PXRD)

PXRD measurements are taken using a Thermo Scientific™ ARL™ X'TRA Powder Diffractometer (Ecublens, Switzerland) fitted with a Cu (copper) x-ray tube. The following operating conditions are used: voltage, 45kV; current, 40mA; step size, 0.01° and acquisition time of 0.5-1.0 s/step.

4.2.6. Scanning electron microscopy (SEM)

Prior to SEM imaging, fractured caplet pieces are sputter coated with Au/Pd. The images of the morphologies of the surface and cross section of the caplets/extrudates are taken using a Phillips XL20 SEM (Phillips Electron Optics, Netherlands).

4.2.7. Swelling and hydration studies

The swelling behaviour of the formulations is investigated using an imaging based method. Several cylindrical pieces of drug-loaded zein extrudate with similar diameters ($\pm 0.5\text{mm}$) are immersed in a dissolution bath containing 0.1M HCl solution at 37°C with 50 rpm paddle rotation speed. At regular time intervals, a piece is removed and cut in half, so a cross section became visible. Pictures are taken using a Thorlabs DCC1645C - High Resolution CMOS Camera (Thorlabs GmbH, Dachau/Munich, Germany). Hydrated zein matrix is opaque, whereas dry zein extrudates are yellow in colour. Using the colour change as a marker, the rate of hydration is estimated by measuring the change of the thickness of the hydrated layer with time. Image are analysed using Image-J software.

The hydration of the caplets is investigate using a conventional weighing method. Drug-loaded caplets are immersed in a dissolution bath containing dissolution media (either HCl or phosphate buffer) at 37°C with 50 rpm paddle rotation speed. At regular time intervals, the sample is removed from the dissolution bath. Excess water is gently removed using a piece of paper towel before weighing the sample. After measuring the weight of the sample, it is immediately returned to the solution. The weight change of the sample is monitoring over a period of 54 hours in both HCl (pH 1) and phosphate buffer (pH 6.8).

4.2.8. Dissolution studies

Caplets (diameter 5.9 mm) are carefully cut into slices by the use of a razor blade. Slice thicknesses are 2.4 ± 0.05 mm for most experiments, except for one experiment where slice thickness is varied. In this experiment a slice thicknesses of 1.1 ± 0.05 mm and 4.5 ± 0.05 mm are used additionally. Slice thicknesses and weights are measured using an electronic calliper and a microbalance respectively. Dissolution experiments are performed using the paddle method with 900 ml dissolution media at 37.0 ± 0.5 °C and 50 rpm rotation speed of the paddles. Release kinetics are measured at regular time intervals. 10 ml samples are taken and measured UV/vis spectrophotometer (S-22 Boeco, Boeckel and Co., Hamburg, Germany) at 270 nm corresponding to the λ_{\max} of paracetamol.

4.3. Results and Discussion

4.3.1. Effect of hot melt extrusion on zein structure

Zein is thermally stable at temperatures up to 120°C, so the extrusion temperature of 80°C is not expected to affect the protein conformation significantly^[9]. However the combined stressing effect of increased temperature and shear force during HME may still alter the secondary structure of zein protein. To investigate this, ATR-FTIR spectroscopy is used to compare both untreated zein powder and extruded drug-free zein. Prior to the measurement, both samples are dried for 1 week in a desiccator at 0% relative humidity (RH), to minimise the disruption of water peaks on the ATR-FTIT spectra of zein (water peak is broad and can overlap with the amide peak of zein protein). The deconvoluted and second derivative spectra of the amide I region, from 1580 cm^{-1} to 1700 cm^{-1} , of both samples are displayed in Figure 25. From the second derivative results a clear absorption peak can be observed in both samples around 1650 cm^{-1} , which is in line with earlier published data suggesting that the secondary structure of zein protein is dominated by α -helices^[17]. In addition, peaks can be observed at 1615, 1631, 1681 and 1692 cm^{-1} , which are also reported for zein^[5] and are typically assigned to β -sheets^[18]. For the extruded samples, the 1650 cm^{-1} peak is less pronounced while the other peaks are increased. This suggests that during extrusion some of the α -helical structure is lost, while more β -sheets are formed, which is consistent with other studies on processed zein^[5]. These changes in protein structure may be significant,

since it has been reported that secondary structure can influence the drug release mechanism from zein based formulations ^[19]. In this case intermolecular β -sheets could induce a network structure, potentially slowing down the water penetration and release of the incorporated drug. Although secondary structure of zein may have been slightly altered after HME, there is no evidence of degradation, indicating that the extrusion conditions used are appropriate for the purpose of this study. This agrees well with the literature data in which zein protein crosslinking and chain cleavage are reported to occur at temperature above 120 and 180°C, respectively^[9]. ATR-FTIR results of the HME zein matrix showed no significant changes after the follow-on injection moulding process (data not shown). Therefore it is reasonable to conclude that both the HME and IM as performed in this study leads to no degradation and little structure changes in the zein protein.

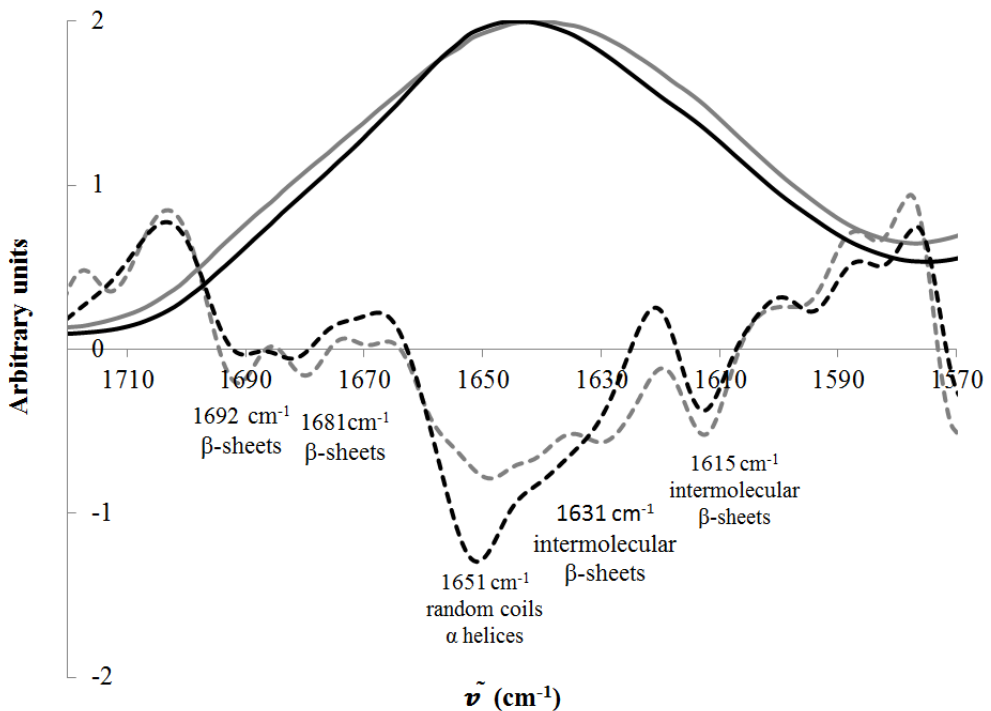


Figure 25: ATR-FTIR spectra for dried zein powder (DZP) and dried ground zein extrudates (DGZE). Solid lines are the baseline corrected spectra of DZP (dark) and DGZE (grey). Dashed lines are the secondary derivatives of DZP (dark) and DGZE (grey). Detailed assignments of different forms of secondary structures of zein protein are shown in the secondary derivative spectra.

4.3.2. Microstructural and physicochemical characterisations of drug-loaded zein caplets and extrudates

The physical state of the model drug in the zein matrix after extrusion and injection moulding may influence drug release behaviour and the caplet storage stability. When the drug is in an amorphous state or molecularly dispersed in zein, it can exhibit greater apparent solubility and can subsequently increase the dissolution rate of the drug in the formulation ^[20]. Therefore the processed samples are studied using SEM, PXRD and DSC to confirm the physical state of the model drug in the caplets. Figure 26 shows the SEM images of the caplets surfaces and cross-sections. Between the sample with a low drug loading (8.8%) and high drug loading (45.1%), clear differences especially in the surface morphology can be observed. Relatively smooth surfaces without the presence of particle features can be seen for the caplets with low drug loading for both the surface and the cross-section. The samples with a high drug loading (45.1%) show rough outer surface, with visible particles in size of ~20 μm . These particles may be crystalline paracetamol or phase separated domains containing drug and/or zein. To confirm the nature of these particles, further characterisation using DSC and PXRD are carried out and are discussed in the later sections. When comparing the caplet surface with the inner cross-section, for the sample with 45.1% paracetamol loading, more particles are seen in the inner core of the caplets.

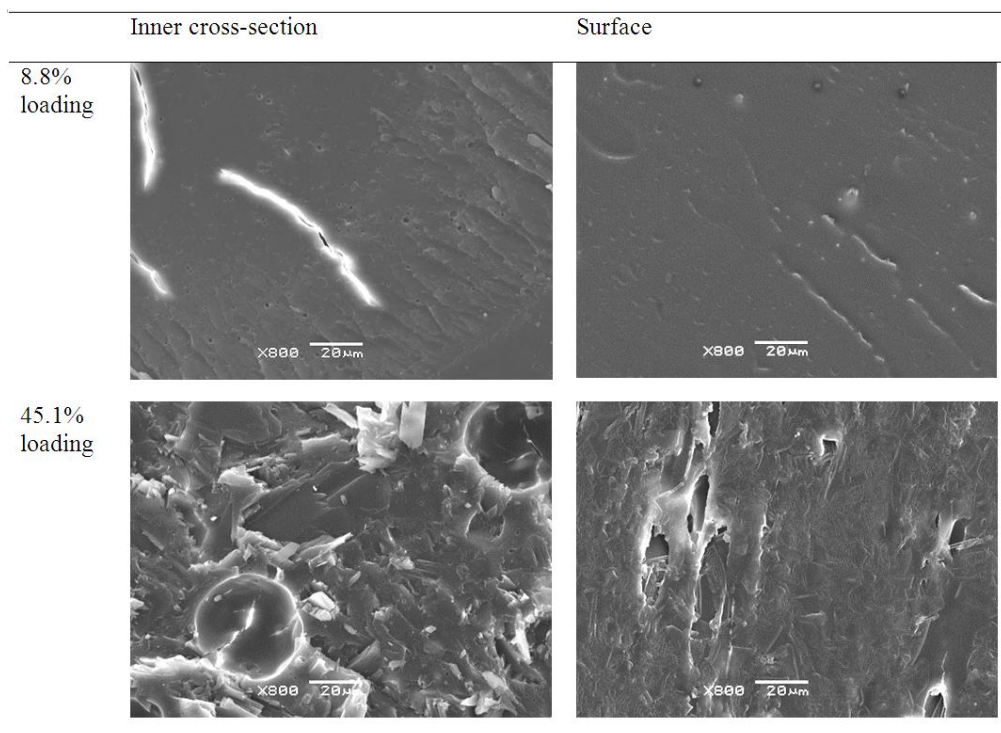


Figure 26: SEM images of the cross-sections of the inner core and outer surfaces of the caplets with two different loadings.

Figure 27 shows the presence of clear crystalline drug diffraction peaks for the samples with high drug loadings (22.2% and 45.1%), whereas only single halo is observed for the samples with relatively low drug loadings (4.4% and 8.8%) indicating these samples being fully amorphous dispersions. This suggests the presence of crystalline paracetamol in the samples with high drug loadings (22.2% and 45.1%), which supports the interpretation that the particles seen in SEM are paracetamol crystals. The powder X-ray diffraction peaks from the caplets with 45.1% paracetamol loading are highly comparable to the diffraction pattern of pure crystalline paracetamol form I indicating the presence of high quantity of crystalline paracetamol form I. Although some peaks in this sample show anomalous intensity in comparison to the PXRD pattern of pure paracetamol form I, they do not resemble with other polymorphic forms of paracetamol^[21]. However for the 22.2% sample, in addition to the diffraction peaks of form I, new peaks are found at 22.2° and 45.2°. These peaks are consistent with earlier reported PXRD diffraction pattern of crystalline

paracetamol form III^[21, 22]. This result indicates the presence of a mixture of crystalline forms I and III in the caplets with 22.2% drug loading. The presence of paracetamol form III is further confirmed by the DSC results.

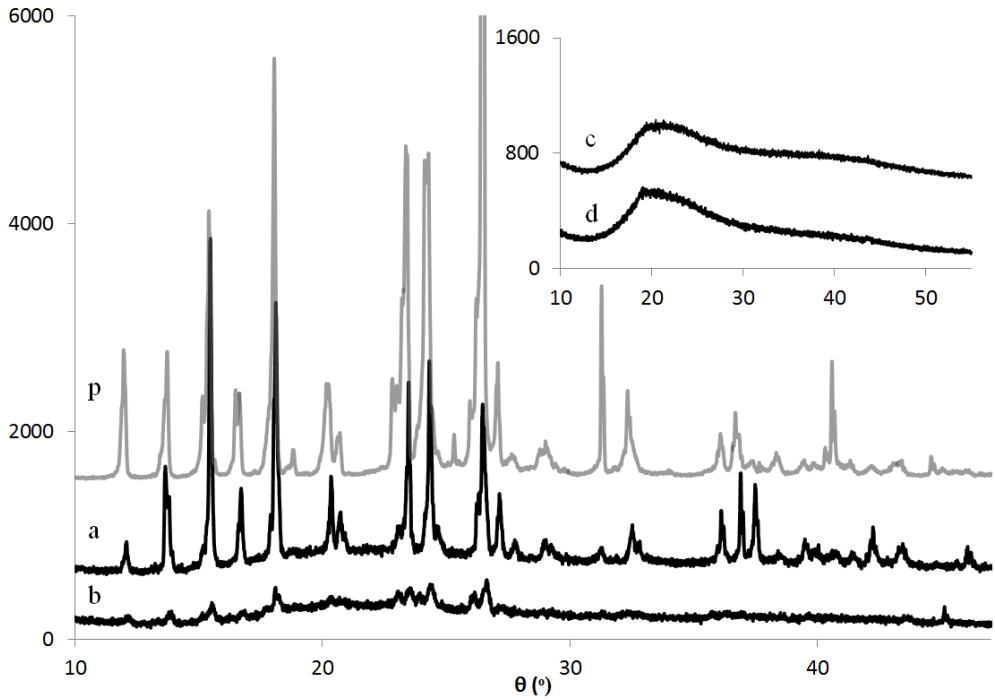


Figure 27: PXRD spectra of dried zein/paracetamol caplet slices with a) 45.1%, b) 22.2%, c) 8.8% and d) 4.4% drug loadings compared with p) crystalline paracetamol form I powder.

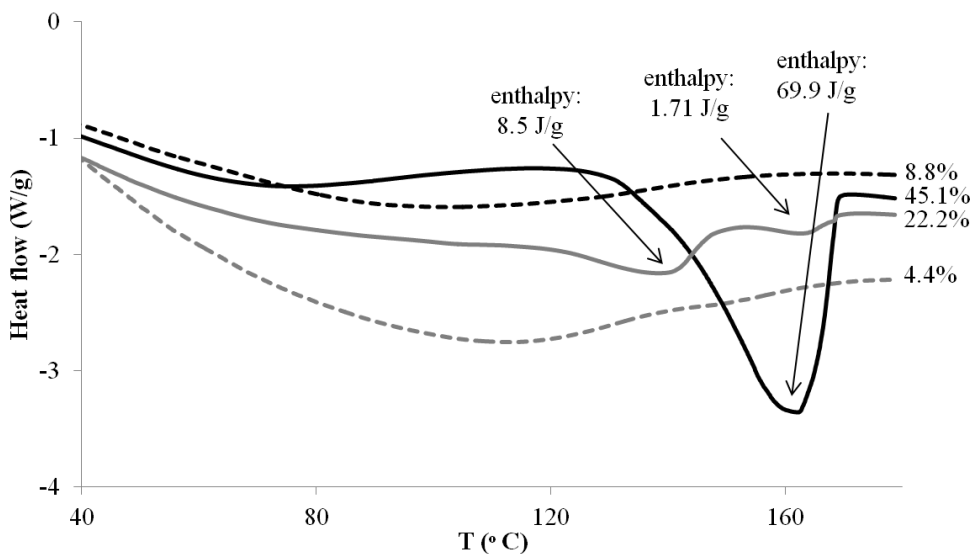


Figure 28: DSC thermograms of the dried zein/paracetamol caplets. Caplets with 4.4% paracetamol loadings (grey dashed line); 8.8% (black dashed line); 22.2% (grey solid line) and 45.1% (black solid line).

Figure 28 shows the DSC results of the caplets with a range of different drug loadings. All loadings show a broad endothermic transition around 100°C, which is likely due to moisture loss. Since zein absorbs moisture, it is likely to be taken up from the environment when preparing the sample prior to the DSC runs. For the samples with higher paracetamol loadings (22.2% and 45.1%), melting peaks of crystalline paracetamol can be observed, which are absent for the formulations with lower drug loadings (4.4% and 8.8%). This is in agreement with the PXRD results suggesting the amorphous nature of the formulations with low drug loadings and the presence of crystalline drug in the formulations with high drug loadings. For the 22.2% paracetamol loaded caplet, two endothermic peaks can be observed. One peak is at 163°C, which is around the expected paracetamol form I melting temperature, and the other at 140°C, which is at the reported melting temperature for paracetamol form III^[23]. This is in agreement with the PXRD results indicating the presence of form III in the 22.2% paracetamol loaded samples. Single broad melting with a peak temperature of 163°C can be seen in the DSC thermograph of the sample with 45.1% drug loading. Using the melting enthalpy of pure crystalline paracetamol (181 ± 0.7 J/g for form I paracetamol), it is possible to estimate the amount of crystalline paracetamol in the sample.

The caplet containing 45.1% paracetamol loading shows a melting enthalpy of 69.9 J/g. This suggests that approximately 85.7% (w/w) of paracetamol present in this sample is in the crystalline form I. For the sample with 22% drug loading, the measured melting enthalpy of the 163°C peak is 1.7 J/g, indicating that only about 4.3% of the paracetamol is in crystalline form I. The estimated melting enthalpy of the form III paracetamol is 8.5 J/g suggesting about 23.2% of the paracetamol is present in form III as calculated from the earlier reported form III melting enthalpy being 165 J/g^[23].

We hypothesise that there may be limited dissolution of the paracetamol in the water (10-12% w/w) used during the pre-mixing prior to extrusion. However as the water is mixed with zein prior to the adding of paracetamol, majority of water is expected to contribute to the zein hydration instead of drug dissolution. Nevertheless it is reasonably to predict that a small quantity of paracetamol may be dissolved during the pre-mixing stage and molecularly dispersed in the partially hydrated zein. Further loss of paracetamol crystallinity might be due to the dissolution into the plasticised (by water) zein matrix during extrusion at the processing temperature above the T_g of the zein/water matrix^[24]. Under this circumstance, the drug-polymer solubility may play an important role in inhibiting the recrystallization of molecularly dispersed drug in the polymer matrix. The fact that the formulations with low drug loadings (4.4 and 8.8%) showed no sign of the presence of crystalline drug indicates that these two drug loadings are likely to be at or below the solubility of paracetamol in zein processed by HME-IM. The model drug is likely to be present as molecular dispersion or phase separate amorphous drug-rich domains in the processed formulations. However, the presence of crystalline paracetamol in the 22.2% drug loaded caplets suggests that this drug loading is likely to be above the drug-polymer solubility, which leads to the rapid drug recrystallization after HME-IM. The dissolved paracetamol during HME-IM may reach the saturation of paracetamol in zein and rapidly recrystallize on cooling. It is highly likely that the recrystallization into metastable form III occurred prior to the solid state transformation of form III into the stable form I. Initial recrystallization into metastable polymorphic form is common and has been reported for paracetamol^[25]. Therefore both polymorphic form I and III are detected in the caplets with 22.2% drug loading. In the 45.1% sample, a significant amount of paracetamol crystalline form I is detected in the processed formulation. We suspect that some of the form I crystals remained un-dissolved in the matrix during the HME-IM at 80°C and these

form I crystals can act as nucleus and promote the polymorphic conversion of form III into form I. Therefore only form I is observed in the DSC and PXRD results of the 45.1% samples. The confirmation of the presence of crystalline paracetamol by 45.1% caplets by both DSC and PXRD results suggests that the particles observed in the SEM images of the sample are highly likely to be crystalline paracetamol particles.

4.3.3. Hydration kinetics of drug-loaded zein extrudates

The zein-based extrudates and caplets developed in this study are single-unit matrix systems, which do not exhibit disintegration behaviour prior to dissolution. The drug release is accompanied by the swelling (expansion in volume) and hydration (water uptake) of the formulations. They play an important role in modulating the drug release. Therefore the kinetics of the swelling (measuring the volume change v.s. time) and hydration (measuring the weight change v.s. time) behaviour of the formulations is studied. During hydration and swelling, zein loses its distinct yellow colour and turns pale. This property is used to follow the swelling kinetics of drug-loaded zein extrudates during dissolution. At various time intervals, piece of the extrudate are removed and cut in half, so a fresh cross section could be revealed. From these cross sections the wet pale outer layer, whose thickness increased with time, became visible, as displayed in Figure 29a which is the result of the extrudates with 8.8% drug loading. Using image analysis, normalised values for the inner radius and the outer radius are obtained (Figure 29b). Similar images with a slower rate of swelling are obtained for the extrudates immersed in phosphate buffer (data not shown).

The extrudate swells up to approximately 1.5 times its original size after 48 hours immersion in HCl. It can also be observed that the colour gradient between the pale outside and the darker inner core remains sharp. This sharp boundary between the swelled outer layer and relatively dry inner glassy polymer core is typical for Case II diffusion, in which this boundary moves at a constant velocity^[26, 27]. This is reasonably consistent with the data presented in Figure 29b, in which the rates of changes of the thickness of the outer layer and inter core are linear. Different models have been proposed in literature to explain this phenomenon^[26, 27]. For example, Thomas and Windle (TW) model considers that the swelling of the outer plasticized polymer (by water in this case) shell is driven by osmotic pressure and the movement of the sharp diffusion front is controlled by the coupling of

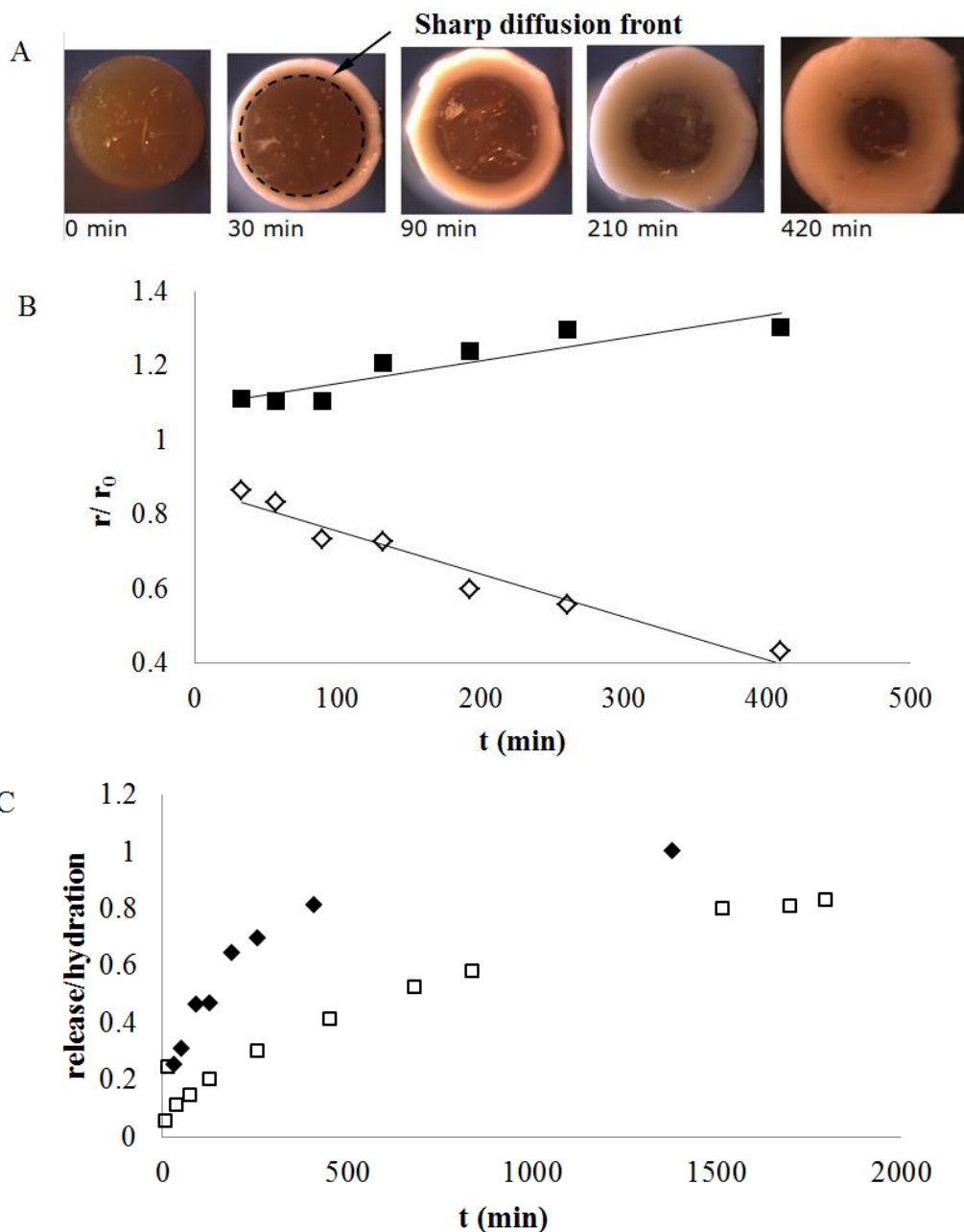


Figure 29: Swelling results of the cylindrical extrudates with 8.8% drug loading immersed in 0.1M HCl. A) The cross-section images of the extrudates after different hydration times; B) image analysis results: initial radius/measured (r/r_0) versus time (t) (outer radius: ■ and inner radius: ◇); C) drug release (□) and hydration (◆) fractions are plotted against time for cylindrical extrudate with 8.8% drug loading in 0.1 M HCl

osmotic-pressure-driven swelling and nearly Fickian diffusion in the glassy polymer core^[27]. Recently the sharp diffusion front is also explained by a ‘change of state’ theory, in which it assumes that when the freely diffused small solvent molecules reach the glassy polymer core (diffusion front) they are partially immobilised (via adsorption or binding) at the surface of the holes and micro-voids of glassy polymer. The significant reduction on the mobility of the small molecules at the boundary interface results the sharp diffusion front^[28]. In either case the observable swelling and water uptake phenomena are the same.

The water uptake by the drug-loaded zein-based formulations is further quantified using the conventional weighing method. It can be seen in Figure 6 that caplets in HCl solution take up almost twice the amount of water compared to the ones immersed in phosphate buffer. The de-amidation of the glutamine and asparagine could occur in the acidic media and cause the zein network to loosen up and allow more water to be incorporated into the swollen zein matrix^[29].

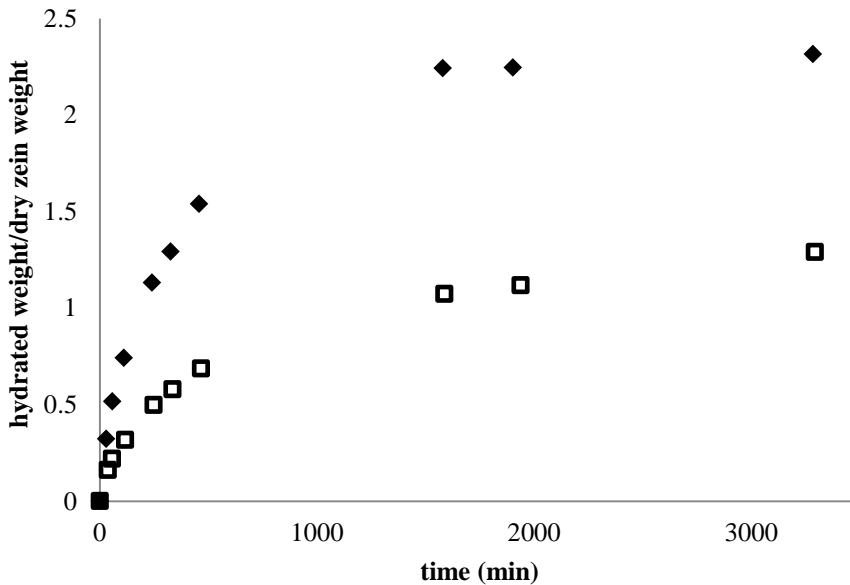


Figure 30: Monitoring of the hydration behaviour of caplets with 8.8% drug loading in HCl (pH 1) (◆) and phosphate buffer (pH 6.8) (□) using the weight based method.

The higher water uptake for the caplets in the HCl media may be explained by this mechanism. This could cause the diffusivity of the paracetamol in the zein network to

increase, thus resulting in faster dissolution rates in comparison to the results obtained using phosphate buffer media. This is confirmed by the *in vitro* drug release data shown below.

4.3.4. Evaluation of tuneability of *in vitro* drug release

The tuneability of drug release from zein-based caplets is studied *in vitro* by altering the drug loading and dimensions of the caplets. In Figure 31, the drug release profiles of the slices of zein caplets are displayed for four different drug loadings in two different dissolution media. The complete drug release is achieved over 30 hours in both media without initial burst release (data not shown), indicating that the zein matrix is a suitable candidate excipient for the preparation of sustained drug delivery systems. It can be observed in Figure 31, that the drug release is slower in phosphate buffer compared to 0.1M HCl. This could be attributed to the slower hydration rate and lower hydration values found in the weight based hydration experiments.

Slightly faster release rates can be observed for the samples with lower paracetamol loadings (4.4% and 8.8%) compared to the higher paracetamol loadings (22.2% and 45.1%). This may be partially attributed to the fact that paracetamol is molecularly dispersed in this formulations as indicated by the previous solid-state characterisation results. However, in the samples with higher drug loadings containing crystalline paracetamol, the dissolution of paracetamol crystals can form pores in the zein matrix, which could increase the sample porosity and subsequently the water penetration rates. This effect could be partially compromised again by the swelling of the zein which could close the pores. Although paracetamol crystals are present in the samples with high drug loadings, the thermodynamic driving force for dissolution is higher due to the high drug concentration in the matrix in comparison to the systems with lower drug loadings. There is therefore a balance of forces acting. Overall the release rates of the samples show weak dependence on paracetamol loading, indicating that the zein matrix can retain its slow release functionality for paracetamol concentrations up to 45.1%.

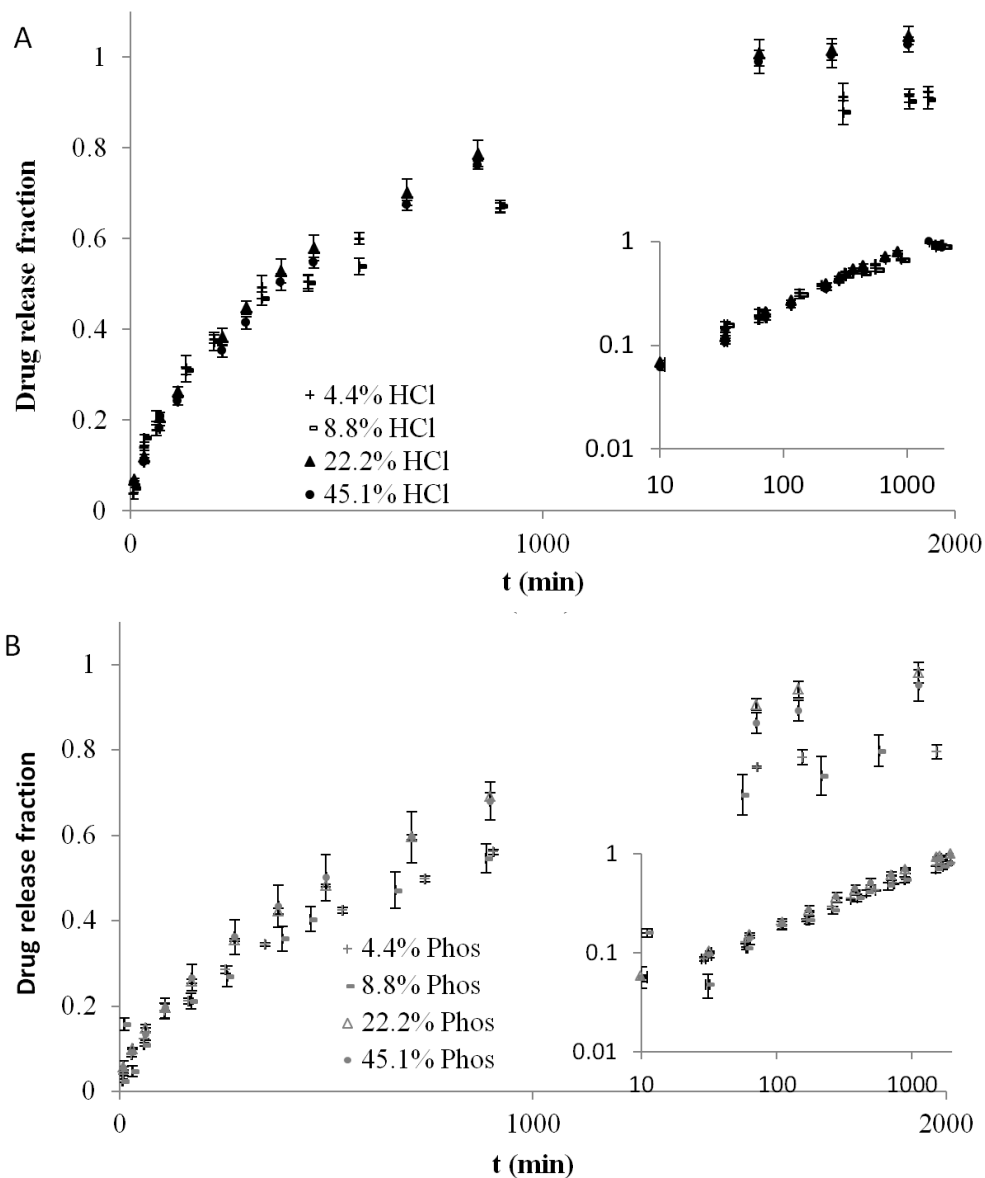


Figure 31: Release profiles for the caplets with different drug loadings (%) in A) 0.1M HCl and B) phosphate buffer (pH 6.8). Insert shows selected profiles fitted with a power-law function (equation [2]) and the Y- and X-axis are on log scale.

Model-fitting of the drug release data is performed in an attempt to reveal the dominating mechanism of the drug release from the zein-based caplets. In Figure 31, the inserted log-log plots of the drug release data show a linear correlation, strongly suggesting a power law

relationship applies. One of the well-known power law equations to explain the mechanism of drug release is the Peppas and Sahlin equation^[30, 31].

$$\frac{M_t}{M_\infty} = kt^n \quad [1]$$

where M_t is the mass of drug released at time t and M_∞ is the mass of drug release as time approaches infinity. Parameter t is time in minutes, k is a constant incorporating characteristics of the macromolecular network and the drug, and n is a diffusional exponent indicative for the transport mechanism. The value of n is dependent both on the geometry of the sample and the nature of the diffusion process. For the cylindrical geometry used in this study with a slice thickness-to-diameter ratio of 2.5, there are two limits to n : when the value n is 0.45, the drug release is dominated by molecular diffusion which is driven by a gradient in chemical potential (Fickian diffusion)^[30]. For this geometry when the value of n approaches 0.9, diffusion can be described by Case II diffusion, which is commonly associated with the glassy-to-gel state transition and relaxation of hydrophilic polymers which swell in water or biological fluids^[31]. In most cases the value of n is in between 0.45 and 0.9 in which a combination of Fickian diffusion and Case II transport applies. This type is often referred to as anomalous release. The power-law approximation is initially thought to be only valid in the short time limit^[32]. However, later it is shown the power-law approximation is valid up to 0.6 total fractional drug release^[30]. This means that the diffusional exponent n can only be correctly defined, when data fits are performed below 0.6 total fractional drug release. Model fitting results for the fractional drug release data up to 0.6 is shown in Table 4, where values of n and k are given. It can be observed that values of n are between 0.52 and 0.62 indicating anomalous release applies with a strong tendency to Fickian controlled release mechanism. This is further examined by comparing the rate of drug release with the rate of hydration of the drug-loaded caplets.

It can be observed in Figure 29c that hydration occurs at a significantly faster rate than the drug release of the same formulation. This suggests that the diffusion of paracetamol (carried out by the dissolution media) through the hydrated extrudate is slower than the hydration of the zein matrix and is the main rate-limiting factor for release. Therefore it is reasonable to predict that release would be driven purely by Fickian diffusion with a resulting diffusional exponent n of 0.45. However the swelling caused by water absorption results in a continuous change in the boundary conditions for diffusion which accounts for

the deviation from the ideal exponent. In addition as pointed out earlier for the samples with crystalline material present the dissolution of the crystals result in a higher porosity and surface area for drug release. This explains the slightly higher ($n > 0.45$) exponent values observed for the systems studied.

Finally to quantify the influence of caplet dimensions on the drug release profile, dissolution tests on caplet slices (diameter 6mm) with three different lengths are performed. As seen in Figure 32, the release rate decreases with increasing the caplet length. All samples show good linear correlation of release *v.s.* square root of time. This indicates that the drug release is predominately governed by Fickian diffusion [30, 33]. Table 5 shows the power-law fitting results and half-life ($t_{0.5}$) of the drug release for the samples with three different lengths. Fittings are only performed up to total fractional drug release of 0.6. From the n -values shown in Table 5, a correlation can be found between slice length (l) and constant (k), which is confirmed when comparing $t_{0.5}$ with slice length. The diffusional exponent n stays broadly the same with the change in dimensions indicating the release mechanism remains the same regardless the change of the dimensions of the drug delivery device.

Table 4: Fitting parameters of the drug release data of caplets with different drug loadings and in different media using power-law. Half-life values are determined using the fitting parameters.

Medium	Drug loading (%)	$k \cdot 10^2$ (min ⁻ⁿ)	n	$t_{0.5}$ (min)
HCl solution pH=1	4.4	2.3 ± 0.5	0.52 ± 0.03	373
	8.8	1.9 ± 0.6	0.55 ± 0.02	382
	22.2	1.6 ± 0.1	0.59 ± 0.01	342
	45.1	1.2 ± 0.1	0.62 ± 0.02	410
Phosphate buffer pH=6.8	4.4	1.4 ± 0.1	0.54 ± 0.01	751
	8.8	1.0 ± 0.1	0.60 ± 0.02	679
	22.2	1.3 ± 0.1	0.58 ± 0.01	541
	45.1	1.3 ± 0.1	0.59 ± 0.01	486

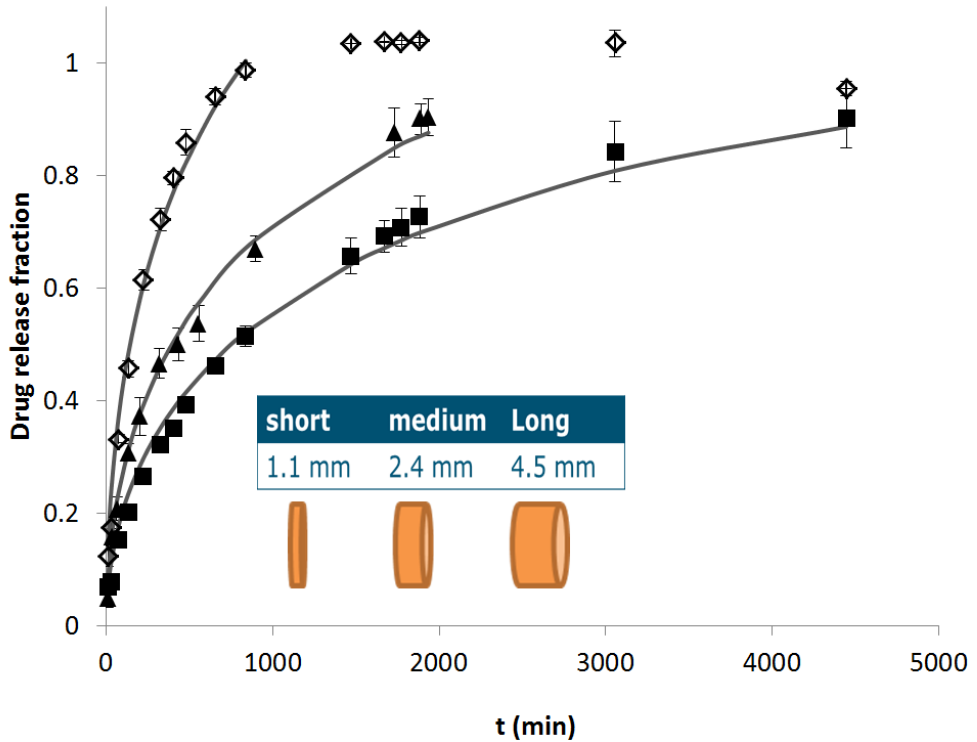


Figure 32: Dissolution of varying thickness zein/paracetamol caplet slices (8.8% drug loading, diameter 6mm) in HCl. Release is plotted versus time. Short, medium and long thickness are respectively indicated as \diamond , \blacktriangle and \blacksquare . The lines show data fits using the disk model: equation [2].

In an earlier study by Ritger and Peppas^[30] an exact expression is derived, describing release from disk-like geometries up to 0.9 fractional drug release:

$$\frac{M_t}{M_\infty} = 4 \left[\frac{Dt}{\pi a^2} \right]^{\frac{1}{2}} - \pi \left[\frac{Dt}{\pi a^2} \right] - \frac{\pi}{3} \left[\frac{Dt}{\pi a^2} \right]^{\frac{3}{2}} + 4 \left[\frac{Dt}{\pi a^2} \right]^{\frac{1}{2}} - \frac{2a}{l} \left[8 \left(\frac{Dt}{\pi a^2} \right) - 2\pi \left(\frac{Dt}{\pi a^2} \right)^{\frac{3}{2}} - \frac{2\pi}{3} \left(\frac{Dt}{\pi a^2} \right)^2 \right] \quad [2]$$

In this model the one-dimensional release equations of both slabs and long cylinders are summed up and additionally a coupling term is incorporated. M_t is the mass of drug released at time t and M_∞ is the mass of drug release as time approaches infinity, D is the diffusion coefficient. The symbols a and l are the disk radius and thickness respectively.

Table 5. Fitting parameters of the drug release data of 8.8% drug-loaded caplets with different slice lengths (shown in Figure 32) using Equation 2. Half-life values are determined using the fit parameters. Effective diffusion coefficients D are determined by fitting these release data to Equation 2.

Table 5: Fitting parameters of the drug release data of 8.8% drug-loaded caplets with different slice lengths (shown in Figure 32) using equation 2. Half-life values ($t_{0.5}$) are determined using the fit parameters. effective diffusion coefficients D are determined by fitting these release data to equation 2.

Slice length (mm)	$k \cdot 10^2$ (min ⁻ⁿ)	n	$t_{0.5}$ (min)	$D \cdot 10^{12}$ (m ² /s)
1.1	2.77 ± 0.4	0.57 ± 0.02	160	4.8 ± 0.4
2.3	1.86 ± 0.2	0.55 ± 0.02	407	5.0 ± 0.2
4.5	1.69 ± 0.2	0.51 ± 0.01	766	5.3 ± 0.2

By fitting the data to this model, the mutual effective diffusion coefficient D of paracetamol in hydrated zein could be approximated. In Table 5, it can be observed that D is around $5 \cdot 10^{-12}$ m²/s. Both the low variation in D for the different caplet lengths and the high correlation coefficient (R^2) values indicate that this model is highly suitable to explain the dependency of release kinetics on the device dimensions of this study. The value found for D is approximately 100 times higher than the diffusion coefficient of paracetamol in water ($\sim 4 \cdot 10^{-10}$ m²/s) estimated using the Stokes-Einstein relationship. This is a clear indication of reduced diffusion rate of dissolved paracetamol in hydrated zein matrix. The estimate of the effective diffusion coefficient allows the estimation of the release rates achievable by changing the device dimensions. Further manipulation of drug release may be made by the use of different plasticisers. However it should be noted that different drugs may have different effect on the release rates because molecular dimensions will result in changes in diffusion in the zein matrix. It is also noted in Table 5 that the half-life increases by 6-fold when the length of the extrudates increases from 1.1 to 4.5 mm. In comparison to this level of change, the changes in half-life observed in the samples with different drug loading is significantly less, being less than 0.3 fold when increasing the drug loading from 4.4 to 45.1%. These results indicate that stronger dimension effect on the drug release kinetics than the drug loading.

4.4. Conclusion

In this study paracetamol is successfully encapsulated into Fickian diffusion controlled drug delivery devices of zein by the use direct HME-IM. For lower drug loadings (4.4% and 8.8%) paracetamol is present as molecular dispersion in the zein matrix, whereas crystalline paracetamol are present in the formulations with higher drug loadings (22.2% and 45.1%). The drug release results confirmed that the zein caplets are suitable for controlled release, where release is found to be weakly dependent on drug loading but strongly dependent upon formulation dimensions. Both the power law fits to the release data as the real time hydration data indicated Fickian diffusion release to be the dominating mechanism. The strong dependence of drug release on formulation dimension can be used to manipulate the release rate by simply altering the dimensions of the device. The results of this study demonstrated the potential of using zein, a natural polymer from a sustainable source, as the sole excipient to create a Fickian diffusion controlled device suitable for tuneable controlled release by simple solvent-free HME-IM method.

4.5. Acknowledgements

This work is part of the Industrial Partnership Programme (IPP) Bio(-Related)Materials of the Stichting voor Fundamenteel Onderzoek der Materie (FOM), which is financially supported by the Nederlandse Organisatie voor Wetenschappelijk Onderzoek (NWO). The IPP BRM is co-financed by the Top Institute Food and Nutrition and the Dutch Polymer Institute.

4.6. References

1. Uhrich, K.E.; Cannizzaro, S.M.; Langer, R.S.; Shakesheff, K.M. Polymeric Systems for Controlled Drug Release. *Chemical Reviews* 1999, 99 (11), 3181-3198.
2. Grund, S.; Bauer, M.; Fischer, D. Polymers in drug delivery-state of the art and future trends. *Advanced Engineering Materials* 2011, 13 (3), B61-B87.
3. Liu, X.; Sun, Q.; Wang, H.; Zhang, L.; Wang, J.Y. Microspheres of corn protein, zein, for an ivermectin drug delivery system. *Biomaterials* 2005, 26 (1), 109-115.
4. Wang, H.-J.; Lin, Z.-X.; Liu, X.-M.; Sheng, S.-Y.; Wang, J.-Y. Heparin-loaded zein microsphere film and hemocompatibility. *Journal of Controlled Release* 2005, 105 (1-2), 120-131.
5. Georget, D.M.R.; Barker, S.A.; Belton, P.S. A study on maize proteins as a potential new tablet excipient. *European Journal of Pharmaceutics and Biopharmaceutics* 2008, 69 (2), 718-726.
6. Lawton, J.W. Zein: A history of processing and use. *Cereal Chemistry* 2002, 79 (1), 1-18.

7. Wang, Q.; Yin, L.; Padua, G. Effect of Hydrophilic and Lipophilic Compounds on Zein Microstructures. 2008, 3 (2), 174-181.
8. Belton, P.S.; Delgadillo, I.; Halford, N.G.; Shewry, P.R. Kafirin structure and functionality. *Journal of Cereal Science* 2006, 44 (3), 272-286.
9. Selling, G.W. The effect of extrusion processing on Zein. *Polymer Degradation and Stability* 2010, 95 (12), 2241-2249.
10. Breiteneder, H.; Mills, E.N.C. Plant food allergens - Structural and functional aspects of allergenicity. *Biotechnology Advances* 2005, 23 (6), 395-399.
11. Takagi, K.; Teshima, R.; Okunuki, H.; Sawada, J.I. Comparative study of in vitro digestibility of food proteins and effect of preheating on the digestion. *Biological and Pharmaceutical Bulletin* 2003, 26 (7), 969-973.
12. Zhang, M.; Reitmeier, C.A.; Hammond, E.G.; Myers, D.J. Production of textile fibers from zein and a soy protein-zein blend. *Cereal Chemistry* 1997, 74 (5), 594-598.
13. Selling, G.W.; Woods, K.K.; Biswas, A.; Willett, J.L. Reactive extrusion of zein with glyoxal. *Journal of Applied Polymer Science* 2009, 113 (3), 1828-1835.
14. Eith, L.; Stepto, R.F.T.; Tomka, I.; Wittwer, F. The Injection-Moulded Capsule. *Drug Development and Industrial Pharmacy* 1986, 12 (11-13), 2113-2126.
15. Deng, J.S.; Meisters, M.; Li, L.; Setesak, J.; Claycomb, L.; Tian, Y.; Stephens, D.; Widman, M. The development of an injection-molding process for a polyanhydride implant containing gentamicin sulfate. *PDA Journal of Pharmaceutical Science and Technology* 2002, 56 (2), 65-77.
16. Gilpin, R.K.; Zhou, W. Studies of the Thermal Degradation of Acetaminophen Using a Conventional HPLC Approach and Electrospray Ionization-Mass Spectrometry. 2004, 42 (1), 15-20.
17. Forato, L.A.; Bicudo, T.D.C.; Colnago, L.A. Conformation of α Zeins in Solid State by Fourier Transform IR. *Biopolymers* 2003, 72 (6), 421-426.
18. Georget, D.M.R.; Belton, P.S. Effects of Temperature and Water Content on the Secondary Structure of Wheat Gluten Studied by FTIR Spectroscopy. *Biomacromolecules* 2006, 7 (2), 469-475.
19. Fang, J.Y.; Chen, J.P.; Leu, Y.L.; Wang, H.Y. Characterization and evaluation of silk protein hydrogels for drug delivery. *Chemical and Pharmaceutical Bulletin* 2006, 54 (2), 156-162.
20. Ahlneck, C.; Zografi, G. The molecular basis of moisture effects on the physical and chemical stability of drugs in the solid state. *International Journal of Pharmaceutics* 1990, 62 (2-3), 87-95.
21. Peterson, M.L.; Morissette, S.L.; McNulty, C.; Goldsweig, A.; Shaw, P.; LeQuesne, M.; Monagle, J.; Encina, N.; Marchionna, J.; Johnson, A.; Gonzalez-Zugasti, J.; Lemmo, A.V.; Ellis, S.J.; Cima, M.J.; Almarsson, Ö. Iterative High-Throughput Polymorphism Studies on Acetaminophen and an Experimentally Derived Structure for Form III. *Journal of the American Chemical Society* 2002, 124 (37), 10958-10959.
22. Rossi, A.; Savioli, A.; Bini, M.; Capsoni, D.; Massarotti, V.; Bettini, R.; Gazzaniga, A.; Sangalli, M.E.; Giordano, F. Solid-state characterization of paracetamol metastable polymorphs formed in binary mixtures with hydroxypropylmethylcellulose. *Thermochimica Acta* 2003, 406 (1-2), 55-67.
23. Gopalakrishnan, T.R., Martin-Luther-Universität Halle-Wittenberg, 2010.

24. Gillgren, T.; Barker, S.A.; Belton, P.S.; Georget, D.M.R.; Stading, M. Plasticization of zein: A thermomechanical, FTIR, and dielectric study. *Biomacromolecules* 2009, 10 (5), 1135-1139.
25. Qi, S.; Avalle, P.; Saklatvala, R.; Craig, D.Q.M. An investigation into the effects of thermal history on the crystallisation behaviour of amorphous paracetamol. *European Journal of Pharmaceutics and Biopharmaceutics* 2008, 69 (1), 364-371.
26. Peterlin, A. Diffusion in a network with discontinuous swelling. *J. Polym. Sci. B Polym. Lett.* 1965, 3 (12), 1083-1087.
27. Thomas, N.L.; Windle, A.H. A theory of case II diffusion. *Polymer* 1982, 23 (4), 529-542.
28. Gallyamov, M.O. Sharp diffusion front in diffusion problem with change of state. *Eur. Phys. J. E* 2013, 36 (8), 92.
29. Yong, Y.H.; Yamaguchi, S.; Gu, Y.S.; Mori, T.; Matsumura, Y. Effects of Enzymatic Deamidation by Protein-Glutaminase on Structure and Functional Properties of α -Zein. *Journal of Agricultural and Food Chemistry* 2004, 52 (23), 7094-7100.
30. Ritger, P.L.; Peppas, N.A. A simple equation for description of solute release I. Fickian and non-fickian release from non-swellable devices in the form of slabs, spheres, cylinders or discs. *Journal of Controlled Release* 1987, 5 (1), 23-36.
31. Peppas, N.A.; Sahlin, J.J. A simple equation for the description of solute release. III. Coupling of diffusion and relaxation. *International Journal of Pharmaceutics* 1989, 57 (2), 169-172.
32. Alfrey, T.; Gurnee, E.F.; Lloyd, W.G. Diffusion in glassy polymers. *J. polym. sci., C Polym. symp.* 1966, 12 (1), 249-261.
33. Bird, R.B.; Stewart, W.E.; Lighfoot, E.N. *Transport phenomena*. John Wiley: Estados Unidos, 1976.

The maize corn protein zein has been suggested to be a suitable sustained release agent, in view of its heat-, pH- and microbial stability and its insolubility in water. Still, the range of drugs for which zein has been studied as an excipient is not extensive. In this study, zein is used as a sole excipient for a range of drugs differing in hydrophobicity and ionisation constants: indomethacin, paracetamol and ranitidine. Caplets are prepared by hot-melt extrusion (HME) and injection moulding (IM). Each of the three model drugs are tested on two drug loadings in various dissolution media. The physical state of the drug, microstructure and hydration behaviour are investigated in order to build up understanding about the release behaviour from zein based matrices for drug delivery. We find the zein matrix is able to stabilize the drugs in an amorphous state. This is potentially important for controlling the release kinetics, especially for poorly soluble hydrophobic drugs. However, the overall crystallinity of the drugs in the HME-IM caplets still increases with drug hydrophobicity. For ranitidine and indomethacin, swelling rates, swelling capacity and release rates are pH dependent as a consequence of the presence of charged groups on the drug molecules. Hence, electrostatic interactions between zein and drugs can also be used to tune release kinetics.

5. Controlled release from zein matrices: interplay of drug hydrophobicity and pH

¹Laboratory of Physical Chemistry and Soft matter and

²Physics and Physical Chemistry of foods, Wageningen
University, Wageningen, The Netherlands.

³School of Chemistry, University of East Anglia, Norwich,
United Kingdom.

⁴School of Pharmacy, University of East Anglia, Norwich,
United Kingdom.

This chapter is submitted as:

Bouman, J.^{1,2}; Belton, P.³; Venema, P.²; van der Linden, E.²; de Vries, R.¹; Qi, S.⁴
Controlled release from zein matrices: interplay of drug hydrophobicity and pH

5.1. Introduction

In the field of sustained and controlled release, biopolymers are increasing in popularity as compared to synthetic polymers, since they have the advantages of being biocompatible, environmentally sustainable and often inexpensive. An example is the maize corn protein zein, which has proven to be quite promising for sustained release applications. Indeed, it has been studied for controlled release in formats such as microcapsules^{[1],[2]}, fibers^{[3],[4]}, films^[5] and monolithic devices^{[6],[7]}. Sustained drug release is often required to maintain a steady drug plasma concentration for a longer period, or to target the drug release to the lower intestinal region in order to maximise absorption. Ideal polymers for sustained release are biocompatible, nontoxic, physically, chemically and microbiologically stable and most important of all, providing a slow but tuneable release^[8].

Zein is a major storage protein in maize corn and is a main by-product from bioethanol production by both wet and dry milling^[9]. It consists of α -, β -, γ - and δ -zein, which are proteins with different molecular weights and modes of extraction^[10, 11]. The α -zein is the predominant protein whose structure is a triple superhelix^[12]. The yellow colour of the powder is due to the lutein, localised in the non-polar interior of this helix. Possibly due to this structure, zein is relatively heat and pH stable^[13], water insoluble, but soluble in aqueous ethanol^[14]. The protein has hydrophobic and hydrophilic domains, but due to its insolubility in water, it is frequently considered to be a hydrophobic protein^[15]. However, the hydrated protein is found to absorb more water upon heating indicating a more hydrophilic nature^[14]. A similar conclusion is based on the calculated hydration energy of the protein on the basis of calculated hydration energies.^[14] The combination of these characteristics and its biocompatibility^[15] and anti-oxidative^[16] activity make it a good candidate as sustained release matrix material.

The use of zein micro- and nanoparticles as drug delivery devices (produced by the use of an anti-solvent precipitation process) has been reported by a number of groups^{[1], [2], [17]}. In these studies *in vitro* sustained drug release profiles are reported. However, in the presence of pepsin, quick degradation of zein occurs^[1], leading to equally quick disintegration and high drug release rates. The use of electrospinning and electro-spraying to create zein nanofibers and nanoparticles have also been reported^[3, 4, 15]. For these systems there are problems in maintaining the stability of the fiber- and particle morphologies that at this stage still need to be solved by crosslinking the zein^[15]. An interesting observation made in

these papers is that electrostatic interactions between the drug and the zein matrix contribute significantly to the compatibility between the drug and zein^{[15], [18]}.

The preferred and most widely used mode of drug delivery is still oral delivery in the form of tablets. Some work has already been performed on macroscopic zein based devices for oral administration^{[6],[7, 19]}. When engineering sustained release from macroscale zein devices, the effect of degradation of the zein network by pepsin is not as problematic, because hydration of zein itself already takes hours^[6]. Previously zein has been investigated as a tableting excipient for the sustained release of theophylline. It was found that compression of the zein led to high elastic recovery after pressing and resulted in unacceptable grooving inside of the tablets.^[7] To bypass such problems, we have recently investigated the use of zein as a hot-melt extrusion-injection moulded (HME-IM) caplet excipient^[6]. After HME-IM, zein caplets loaded with a model drug (paracetamol) showed close to diffusion-controlled sustained release: the release could be precisely tuned via the device dimensions, and was found to be nearly independent of drug loading.

Paracetamol is a moderately hydrophilic, uncharged model drug. In order to be useful as a general excipient it is crucial to understand how factors, such as, drug hydrophobicity and the presence or absence of charged groups on the drugs, affect the interaction with the zein matrix, and hence, the release profile. Therefore, we study the drug release behaviour of HME-IM zein caplets for a range of model drugs. In addition to paracetamol, we also investigate the highly hydrophilic drug ranitidine (which is positively charged at low pH) and the hydrophobic drug indomethacin (which is negatively charged at high pH). Zein has an isoelectric point (pI) around neutral pH values. Therefore we expect to find differences in release rates as a function of pH, caused by changes in the electrostatic interactions of the drugs with the zein matrix. This is the first report on the influence of drug hydrophobicity and pH on the mechanism of drug release from macroscopic zein matrices.

First we use DSC and PXRD to characterise the caplets in terms of drug crystallinity. X-ray tomography (XRT) is used together with scanning electron microscopy (SEM) to investigate the microstructures of the caplets before and during the drug release process. Finally, we study both the swelling- and drug release kinetics of the caplets, for a range of pH values.

5.2. Materials and methods

5.2.1. Materials

Purified zein protein flakes are obtained from Acros organics (Geel, Belgium). In order to decrease particle size to ensure good mixing with the different crystalline drugs, it is ground using a kitchen blender. The grinding process consisted of cycles of 15s grinding followed by a 20s of cooling, to minimise thermal damage to the protein as a result of frictional forces. Grounded zein powder particle size was roughly between 50-250 μm as estimated from microscopy images. The drugs used, i.e. paracetamol, indomethacin and ranitidine, are all obtained from Sigma Alldrich (Gillingham, UK).

5.2.2. Extrusion and injection moulding

Distilled water (10-12% of weight mixture) is mixed with the ground zein powder in a glass mortar and pestle, to lower the glass transition temperature (T_g) of zein, so hot-melt extrusion could be performed at a relatively low temperature. Drug is added to the zein-water mixture to obtain the mixes for formulations with drug loading of 4.4% and 22.2% (w/w). The ternary mixes (zein-water-model drug) are ground again prior to extrusion. A batch of 5-10g is processed using a HAAKE™ Minilab extruder (Thermo Fisher, Karlsruhe, Germany) with a co-rotating twin screw. Extrusion temperature is 80 °C, the screw speed is 100 rpm and no die is used. Extrudates are collected in a pre-heated injection moulding cylinder (80 °C) which is attached to the extruder. Also the IM process is performed at 80°C, under high pressure of 300-350 bar, where the still flexible extrudate is pressed into a caplet mould using a HAAKE™ MiniJet Pro Piston Injection Moulding System (Thermo Fisher, Karlsruhe, Germany). After the IM sequence, the mould is placed on aluminium foil positioned on dry ice for a rapid cooling. The caplet (5.9x4.4x19.7mm) is ejected out of the mould and stored in a sealed container at ambient conditions.

5.2.3. Differential Scanning Calorimetry (DSC)

DSC experiments are conducted using a Q2000 MTDSC (TA Instruments, Newcastle, DE, U.S.). A full range calibration is performed prior to sample testing. For the DSC samples, a caplet slice is cut and milled into smaller particles using mortar and pestle. Prior to the DSC measurements, all samples are dried in a desiccator above phosphorus pentoxide, for 4 days at room temperature, to minimize the effect of water evaporation during a DSC run. A standard heat-cool-heat sequence is applied for all samples, with 10.00 °C/min heating rate and 5.00°C/min cooling rate. In the DSC cell a nitrogen purge at a flow rate of 50 mL/min

is used. Analysis is performed using TA Universal Analysis software. To measure the amount of crystalline drug present, melting enthalpies are compared with the melting enthalpy of pure crystalline drug. Melting enthalpies for pure indomethacin, paracetamol and ranitidine are experimentally measured at respectively 98.0 ± 1.1 J/g, 181.0 ± 0.7 and 130.0 ± 2.1 J/g. For ranitidine melting is quickly followed by degradation. Therefore the apparent melting enthalpy may be heating rate dependent but, provided the rate is kept constant in all the experiments amounts of crystalline material may be estimated. The DSC measurement is only semi-quantitative as there may be dissolution of the drug during the heating process and the calculation neglects any contribution from the entropy of dissolution of the drug after melting. However as the mixture is unstirred during the heating process dissolution before melting is likely to be very small. Similar a significant error due to dissolution after melting would require a rapid diffusion of the drug away from its location and into the matrix which is not likely. Apparent melting enthalpy may be heating rate dependent but, provided the rate is kept constant in all the experiments a semi-quantitative estimate of crystalline material may be made.

5.2.4. X-ray Tomography (XRT)

XRT images are taken using a Phoenix v[tome]x m (General Electric, Wunstorf, Germany). This technique allows non-invasive measurement of the 3D structure of objects at spatial resolution below $1 \mu\text{m}$. A 3D image of a fixed particle can be reconstructed from a large series of two-dimensional radiographic images taken around a single axis of rotation^[20]. The following settings are applied: voxel size: $4 \mu\text{m}$, amount of images: 2000, Voltage 100kV, Current $110 \mu\text{A}$ and timing 500: ms

5.2.5. Powder X-Ray Diffraction (PXRD)

PXRD measurements are performed on caplets and pure powders using a Thermo Scientific™ ARL™ X'TRA Powder Diffractometer (Ecublens, Switzerland) fitted with a Cu (copper) x-ray tube. The following operating conditions are used: current, 40mA; voltage, 45kV; step size, 0.01° and acquisition time of 1.0 s/step.

5.2.6. Scanning electron microscopy (SEM)

Caplet pieces, cut using a razor blade, are attached to sample holders with carbon adhesive tabs (EMS, Washington, USA) and sputter coated with 10 nm Iridium (SCD 500, Leica, Vienna, Austria). Hereafter they are analyzed with secondary electron detection at 2 KV

and 6.3 pA with a high resolution scanning electron microscope (Magellan 400, FEI, Eindhoven, the Netherlands).

5.2.7. Dissolution and hydration media

Media with 4 different pH's are prepared. The pH 1 solution is a 0.1M HCl solution. The pH 5.5 medium is a sodium acetate-acetic acid buffer. Both the pH 6.8 and pH 7.8 media are phosphate buffers prepared from potassium dihydrogen phosphate and sodium hydroxide.

5.2.8. Hydration studies

Hydration is measured gravimetrically. Caplets (diameter 5.9 mm) are carefully cut into slices (thicknesses is 2.20 ± 0.03 mm) by the use of a razor blade. Slice thicknesses and weight are measured respectively using an electronic calliper and a microbalance. Caplets are immersed in a medium solution at 37°C with 50 rpm paddle rotation speed. At regular time intervals, a sample is removed from the dissolution bath. Excess water is gently removed using a piece of paper towel before weighing the sample. Subsequently the sample is immediately returned to the solution. The weight change of the sample is monitored over a period up to 70h. All hydration experiments are performed in triplicate.

5.2.9. Dissolution studies

Dissolution experiments are performed using the paddle method with 900 ml of dissolution media at 37.0 ± 0.5 °C and 50 rpm rotation speed of the paddles. Caplets are carefully cut into slices, measured and weight as in the hydration experiments. Release kinetics is measured at regular time intervals. 10 ml samples are taken and measured using a UV/vis spectrophotometer (S-22 Boeco, Boeckel and Co., Hamburg, Germany) at 243 and 314 nm corresponding to the λ_{\max} of respectively paracetamol and ranitidine. Because indomethacin has a low saturation concentration in water, a biphasic dissolution method needed to be applied on indomethacin loaded caplets to keep the chemical potential difference between the sample and the dissolution medium constant. Caplets are immersed in 600 ml medium, while on top a 300 ml octanol phase is present. Release is measured in the octanol phase by UV/vis at 319 nm, corresponding to a λ_{\max} of indomethacin. In dissolution media where pH is above pK_a (which is around 4.2) indomethacin is negatively charged, which could decrease uptake in octanol and theoretically disrupt the test. However when testing the release of drug crystals at pH of 6.8, it is found to be very fast compared to other pH's as

can be seen in Figure 41C. Therefore we have no reason to believe the charge of the drug will be disruptive for the test.

5.3. Results and discussion

5.3.1. Drug-zein compatibility

As zein protein has a complex structure, it is not possible to use theoretical Flory-Huggins based drug-excipient miscibility prediction methods, such as ground contribution and solubility parameters methods^[21], to assess the compatibility between zein and the model drugs. A first indicator for the drug-matrix compatibility is the influence of drug loading on the processability during hot-melt extrusion-injection moulding (HME-IM), as reflected by the extrusion torque. A higher torque indicates poorer zein-drug miscibility or poorer plasticisation of the zein matrix by the drug.

Our results for the extrusion torque for the model drugs (at two different drug loading) are shown in Table 6. We found that loading the zein matrices with the hydrophilic drug ranitidine reduces the extrusion torque. On the other hand, loading the matrix with the hydrophobic drug indomethacin increases the torque. For paracetamol we find an intermediate result, with little or no changes in the torque compared to the unloaded zein. As we will discuss more extensively in a later section, the changes in torque reflect the zein-drug miscibility at the temperatures at which extrusion occurs. We verified that small variation in moisture content (0.12-0.14 (w/w)) did not influence the torque values during extrusion (data not shown).

Table 6: Average extrusion torque for each drug loading. Extrusion torque increase with drug hydrophobicity. Paracetamol extrusion torque is most similar to that of unloaded zein.

Drug loading	Average extrusion torque (Ncm)			
	Zein	Indomethacin	Paracetamol	Ranitidine
No drug	30			
4.4% drug		40	30	20
22.2% drug		45	30	20

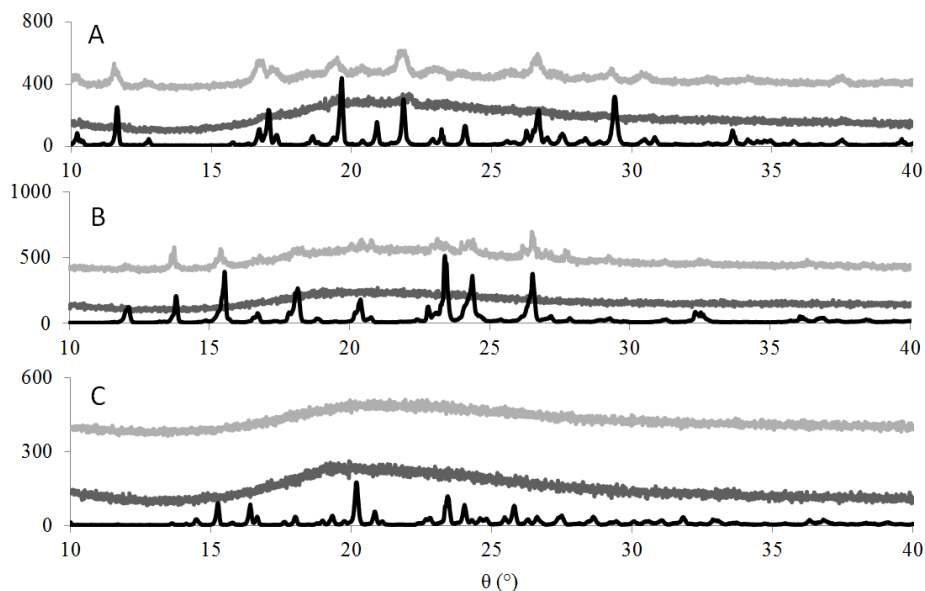


Figure 33: PXRD results of caplets containing different drug loadings (%), indicating crystallinity of the drug in the different caplets. Drugs loadings are 22.2% (—) and 4.4% (—) are displayed together with pure drug (—). Drugs used are A) Indomethacin, B) paracetamol and C) ranitidine. Results show increase in crystallinity with drug hydrophobicity in the HME-IM processed caplets.

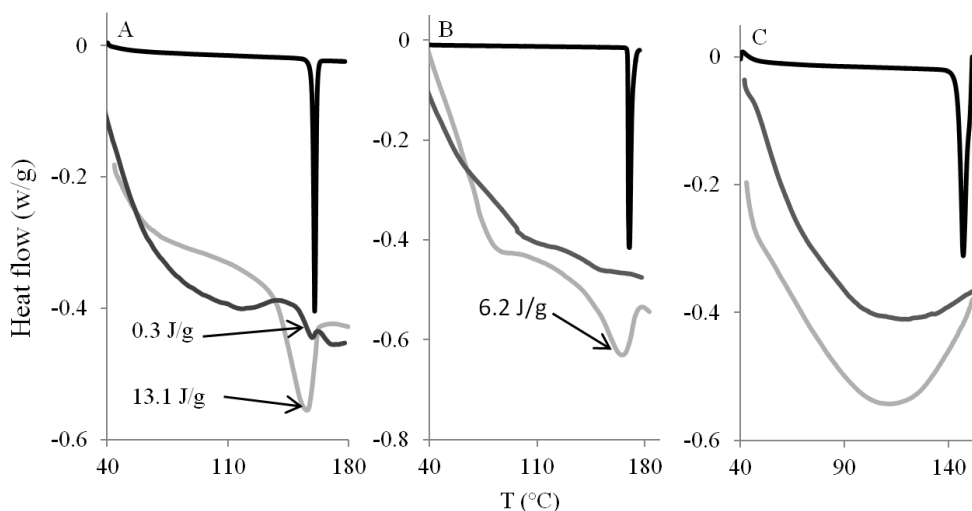


Figure 34: DSC thermograms of the zein/drug caplets containing different drug loadings: 22.2% (—) and 4.4% (—). Heat flow (W/g) is plotted vs Temperature T (°C). Drugs are A) Indomethacin, B) paracetamol and C) ranitidine. A reduced curve (—) of the pure drug is added as comparison. Melting enthalpy is displayed for caplets if melting peak is present.

The degree of crystallinity of the drugs in the caplets is determined using both PXRD and DSC. PXRD results are shown in Figure 33. For the most hydrophobic drug, indomethacin, we find some degree of crystallinity of the drugs in the caplets for both drug loadings (4.4% and 22.2%). For the paracetamol, only the caplets with a drug loading of 22.2% have some degree of crystallinity, in agreement with our previously published work^[6]. For the most hydrophilic drug, ranitidine, we find no indications of crystalline drug present in any of the caplets.

The corresponding DSC data is shown in Figure 34 and confirms the PXRD results. In addition, for the case of indomethacin, we use the DSC data to quantify the fraction of drug in a crystalline state, from the melting enthalpy of the crystalline drug melting peaks. This estimate is only semi-quantitative, as discussed above. We find that at 4.4% loading, the estimated degree of crystallinity is 0.3%. This increases to 13% at the higher drug loading of 22.2%.

Overall, our PXRD and DSC data show that the degree of crystallinity increases with hydrophobicity of the drug and also with drug loading. The degree of crystallinity is in line with the differences we observe in the HME processability of the three model drugs. The HME-IM temperature is set at 80°C which is still significantly (70°C - 90°C) below the melting points of the drugs. Crystals which remain undissolved during HME could act as a filler^[22] and this can explain the increase in extrusion torque for indomethacin. For the case of ranitidine, for which extrusion torques are lowest of all used mixes, we believe that the drug acts as a plasticizer of the zein. Note that the loss of crystallinity during extrusion is significant for all of the drugs we tested. We believe this cannot be caused by dissolution of the drug in the small amount of water used during the pre-mixing stage of the sample preparation, since the saturation concentrations of indomethacin, paracetamol and ranitidine around pH=6.5 are respectively 0.33 g/L^[23], 17.4 g/L^[24] and 660 g/L^[25]. Given the water contents of the mixes (which are below 0.14 w/w), the theoretical maximal dissolution of drugs in water at 20°C would be, respectively $3.9 \cdot 10^{-3}$ %, 0.2% and 7%. The increased solubility at the temperatures of extrusion (80°C) are also insufficient to explain the large decrease of the degree of crystallinity. For instance, we estimate that the theoretical maximal dissolution of paracetamol in the water present in the caplet at 80°C, can increase to only 1.5% at most, based upon extrapolation of published solubility curves^[26].

Therefore, the most likely explanation is that the zein/water matrix ‘solubilizes’ the drugs during extrusion. The amount of drug that is dispersed in the matrix may be expected to correlate inversely with the drug hydrophobicity. Nevertheless, even the hydrophobic indomethacin appears to be solubilized to a significant extent, as reflected by the large decrease of the degree of crystallinity upon incorporating the indomethacin in the zein matrix via HME. Therefore, we conclude that zein, processed using HME, is efficient at bringing a range of drugs into a non-crystalline state, which may be beneficial for drug delivery applications. This will be especially important when the dissolution of the drug crystals is slower than desired.

5.3.2. Microstructures of the drug-loaded caplets

We first investigate the structure of the drug-loaded caplets on the micrometer length scale, using XRT. Figure 36 shows XRT images (with a resolution of around $5\mu\text{m}$) of an unloaded zein caplet and of 3 zein caplets loaded with 22.2% of each of the three model drugs. For the caplets containing indomethacin and paracetamol, we observed domains with a significantly higher density than the background (indicated in red in Figure 36). For indomethacin the volume percentage of these domains is 9.1%, while for paracetamol the volume percentage of these domains is only 2.1%. In both samples the domains are largely homogeneously distributed in the bulk of the caplet. For indomethacin caplets it appears that there is a higher concentration of such domains close to the surface of the caplets. We found that during processing some air is included in the caplets, leading to some degree of porosity. Differences in porosity could influence the rate of hydration, but also the release rate as hypothesised in an earlier study on zein membranes^[5]. From the estimated volume percentage of pores (see Figure 36), the ranitidine and indomethacin loaded samples are found to have a higher volume percentage of pores than the paracetamol loaded and unloaded zein caplets. For all measured systems the overall volume fraction of the pores is in the order of a few percent.

Next we used SEM to investigate the same microstructures at an even higher resolution. Figure 37 shows representative SEM images for an unloaded zein caplet and for caplets loaded with 22.2% of each of the three model drugs. The images for the paracetamol loaded caplets are similar to those for the unloaded zein caplets. According to the SEM images, caplets with ranitidine appear to have a significantly smoother surface compared to the other caplets. Finally, for indomethacin loaded caplets, the SEM images clearly show the

presence of distinct particle-like structures, that could be the dispersed indomethacin crystals. The SEM images also demonstrate the presence of pores at smaller length scales than those probed by XRT. Hence the actual porosity of the caplets may be somewhat higher than the values estimated on the basis of XRT (see Figure 36).

An important observation is that the volume percentage of the domains with a higher electron density in XRT (shown in red in Figure 36) is similar to the degree of crystallinity as estimated on the basis of the DSC results. This strongly suggests that the dense domains in the XRT images can be identified as the drug crystals dispersed in a zein-drug matrix. The SEM images also confirm that only in the indomethacin caplets a significant fraction of crystals is present. It is also observed that many of these crystals are located in the pores of the caplet caused by the incorporation of a small fraction of air during the processing, as shown clearly in additional SEM image in Figure 35.

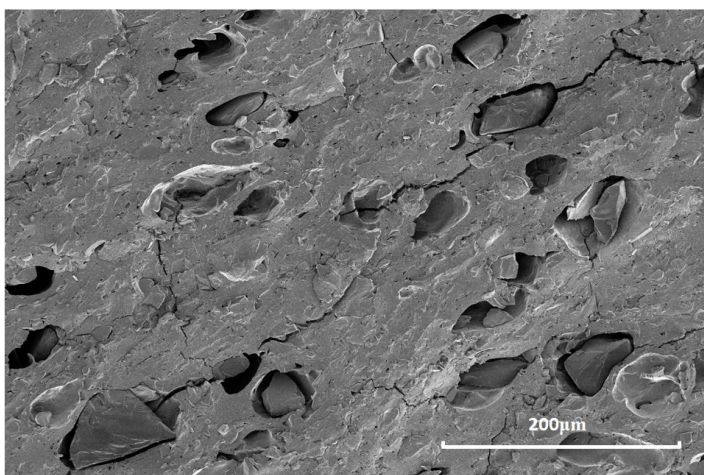


Figure 35: SEM images of cut cross sections of 22.2% loaded indomethacin caplets

The porosity due to the air incorporated in the caplets, is found to be higher for indomethacin and ranitidine than for the paracetamol and unloaded caplets. This may or may not be related to the fact that both indomethacin and ranitidine strongly influenced the extrusion torque. Even though the actual volume fraction of air that causes porosity is not high, the differences in porosity that we observe should be born in mind, in view of the large effect that such pores are suggested to have on release hydration and release properties .

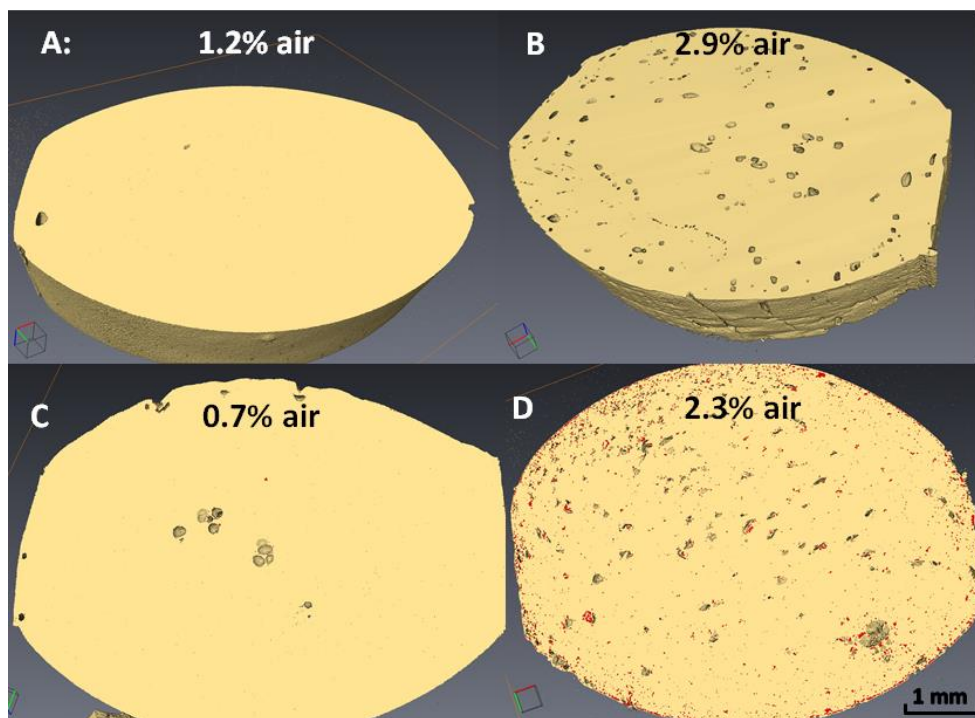


Figure 36: XRT images of caplets, showing presence and distribution of denser (drug) domain (in red) together with volume for air pockets. A) unloaded zein, B) 22.2% ranitidine, C) 22.2% paracetamol and D) 22.2% indomethacin. Volume of air pockets (%) is displayed for each caplet.

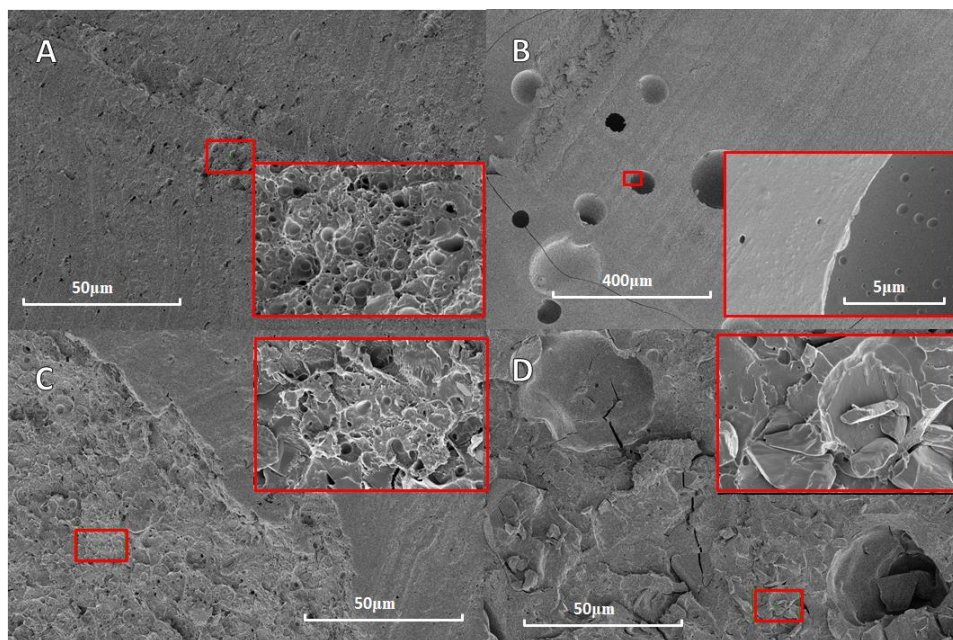


Figure 37 SEM images of drug-loaded zein caplet cross sections. A) unloaded zein, B) 22.2% ranitidine, C) 22.2% paracetamol and D) 22.2% indomethacin. The insert of each picture shows a zoom of the area displayed by the smaller red box.

5.3.3. Hydration and swelling kinetics

The hydration and swelling behaviour is expected to influence the release behaviour of matrix-based delivery systems. Water uptake of all samples is measured in two different dissolution media, HCl solution (pH 1) and phosphate buffer (pH 6.8), which are also used in the dissolution experiments (see Figure 38). The data is fitted to the Peleg^[27] equation, which is widely used as empirical equation to fit water uptake of matrices:

$$M(t) - M_0 = \frac{t}{K_1 + K_2 t} \quad [1]$$

where $M(t)$ is the moisture content (g_{water}/g_{zein}) at time t (min), M_0 is the initial moisture content, K_1 is the Peleg rate constant ($min \cdot (g_{water}/g_{zein})^{-1}$) and K_2 is the Peleg capacity constant ($(g_{water}/g_{zein})^{-1}$). The values of the fitting parameters $1/K_1$ and $1/K_2$ for the different caplets are shown in Table 7.

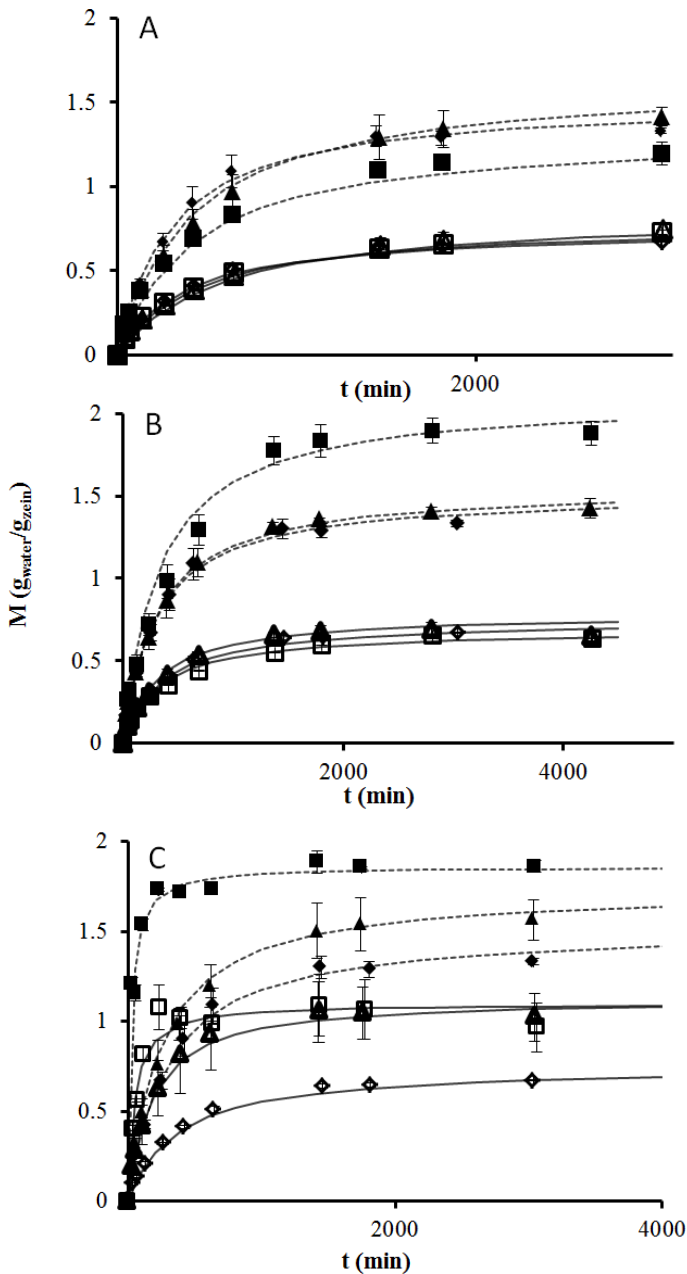


Figure 38: The water uptake M (g_{water}/g_{zein}) as a function of time t (min) for the different caplets used. Drug loadings at 4.4% ($\blacktriangle, \triangle$), 22.2% (\blacksquare, \square) and no (\blacklozenge, \lozenge) drug loading in pH 1 ($\blacktriangle, \blacksquare, \blacklozenge$) and pH 6.8 ($\triangle, \square, \lozenge$). The drugs tested are A) indomethacin, B) paracetamol and C) ranitidine. In all graphs, the water uptake curve of non-loaded zein caplets is added as comparison. The lines are fits using the Peleg model, Eq 1, to caplets in pH 1 (continuous line) and pH 6.8 (dashed line) medium.

Table 7: Fitting parameters of the caplet hydration data of A.) unloaded caplets and B.) caplets with different drug and drug loadings in different media. For fitting the Peleg equation (Eq1) is used, where $1/K_1$ displays initial hydration rate and $1/K_2$ is a measure of swelling capacity.

A.

	Zein	
	$10^2 \cdot 1/K_1$ $\frac{g/g\ zein}{min}$	$1/K_2$ $g/g\ zein$
pH=1	0.52	1.52
pH=6.8	0.21	0.75

B.

Drug loading, pH	Indomethacin		Paracetamol		Indomethacin	
	$10^2 \cdot 1/K_1$	$1/K_2$	$10^2 \cdot 1/K_1$	$1/K_2$	$10^2 \cdot 1/K_1$	$1/K_2$
	$\frac{g/g\ zein}{min}$	$g/g\ zein$	$\frac{g/g\ zein}{min}$	$g/g\ zein$	$\frac{g/g\ zein}{min}$	$g/g\ zein$
4.4%, pH=1	0.41	1.64	0.52	1.56	0.71	1.74
4.4%, pH=6.8	0.15	0.85	0.25	0.79	0.64	1.13
22.2%, pH=1	0.32	1.32	0.50	1.89	8.33	1.86
22.2%, pH=6.8	0.18	0.79	0.21	0.69	2.33	1.10

For all caplets, both the hydration rates ($1/K_1$) and the swelling capacity values ($1/K_2$) are much higher at pH 1 as compared to the values at pH 6.8. Hydration rates ($1/K_1$) of paracetamol caplets are comparable to those of unloaded zein caplets, while hydration rates ($1/K_1$) of indomethacin caplets are slightly lower and decrease with drug loading. For 22.2% loaded ranitidine caplets we find hydration rates that are much higher than those of unloaded caplets (~16.5 times higher at pH 1 and about 11 times higher at pH 6.8). As for the dependence of the swelling capacity ($1/K_2$) on the drug loading ratio, we find qualitatively different behaviour at pH 1 and pH 6.8. At pH 1 an increased drug loading has an increasing (for paracetamol and ranitidine) or decreasing (for indomethacin) effect on the swelling capacity. In contrast, at pH 6.8 caplets loaded with indomethacin and

paracetamol show very similar swelling capacity as compared to values for the unloaded zein caplets. This is not the case for ranitidine caplets, since they show an increase of $1/K_2$ at pH 6.8 compared to unloaded zein caplets.

The influence of pH on both hydration rate and swelling capacity can be related to the charge of the zein protein. The zein predominantly consists of α -zein, which has an isoelectric point of pI 6.8, hence at pH 1 zein is positively charged and at pH 6.8 it will be uncharged. As a result, at pH 1 the proteins will have more counter ions present which increases the osmotic pressure in the caplet and cause an increase in swelling^[28]. Another possible contribution to faster swelling at pH 1 may be the de-amidation of glutamine and asparagine amino acids of the zein^[29], which may also lead to a more open network. At identical drug loadings, both hydration rate and swelling capacity decrease with drug hydrophobicity, since the addition of the hydrophobic drugs to the zein matrix simply makes the combined system more hydrophobic. Probably, once the hydration takes place, the drug dissolution leads to an decrease of the chemical potential of the water in the matrix resulting in the uptake of water by the matrix.

Next, the dynamic changes in the microstructure of the caplets caused by hydration and swelling are studied in more detail using XRT. After 96 hours of hydration, the caplets are rapidly vitrified in liquid nitrogen and subsequently freeze-dried. XRT images of caplets that are hydrated at pH 1 and pH 6.8 are shown in Figure 39 and Figure 40. The similarity of the XRT images of the freeze-dried caplets and the light microscopy images of wet hydrated caplets (data not shown) confirmed that the freeze-drying process did not affect most of the interior microstructures of the caplets, with the exception of the formation of the radial cracks.

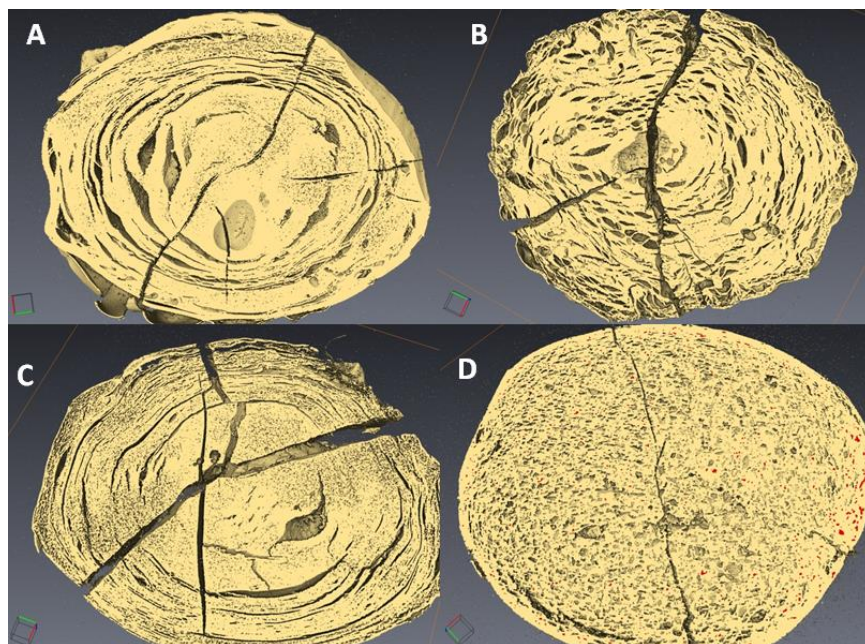


Figure 39: XRT pictures of caplets hydrated for 96h at pH 1 and subsequently vitrified and freeze dried. The zein caplets are loaded as follows: A: no loading, B: 22.2% rantidine, C: 22.2% paracetamol, D: 22.2% indomethacin. Radial cracks are most likely caused by the vitrification process.

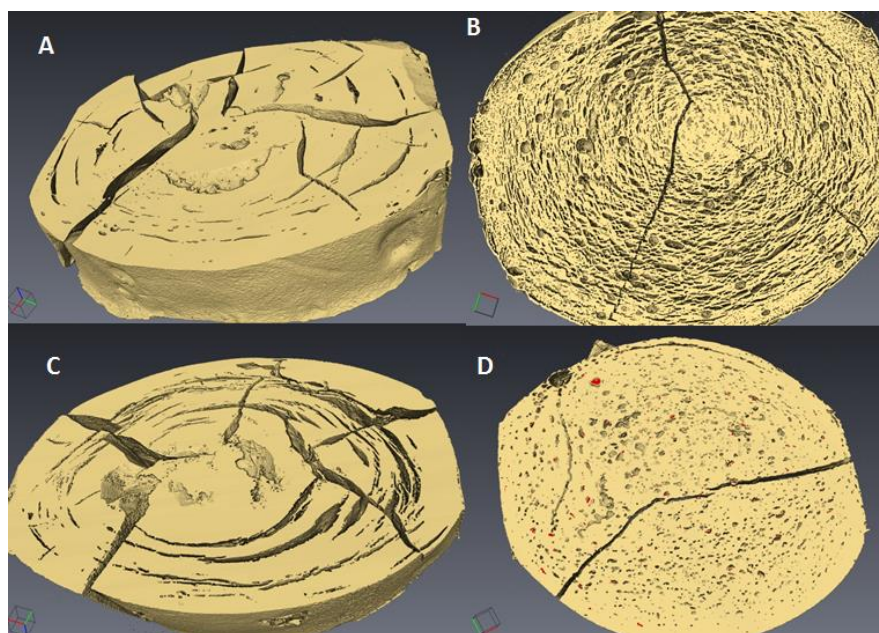


Figure 40: XRT pictures of caplets hydrated for 96h at pH 6.8 and subsequently vitrified and freeze dried. The zein caplets are loaded as follows: A: no loading, B: 22.2% ranitidine, C:22.2% paracetamol, D: 22.2% indomethacin. Radial cracks are most likely caused by the vitrification process.

In both Figure 39 and Figure 40, it can be observed that the zein and paracetamol-loaded caplets, show pronounced concentric circular cracks after hydration, similar to tree rings. For the ranitidine and indomethacin-loaded caplets, the cracks are much less pronounced. In the ranitidine sample the concentric circular cracks are still visible, while in the indomethacin sample they are only visible at the outer region close to the surface of the caplet. Previously, it is suggested that the cracks are a result of stresses on the network due to hydration^[30]. The correlation that we find between on the one hand hydration rates and capacities (Table 7) and on the other hand the occurrence of the circular cracks (Figure 39 and Figure 40) is therefore expected. The circularity of the cracks may be explained if we assume that hydration is controlled by case II diffusion^[6]. Since for case II diffusion there is a sharp boundary between the hydrated and unhydrated parts of the caplet, rupture is expected to take place at this boundary, that migrates inwards driven by the hydration process. For the ranitidine caplets the concentric cracks are much finer. This could be a consequence of the higher fraction of air and associated porosity of the ranitidine caplets.

The pores might relieve some of the stress due to the passing hydration front, leading to a finer crack structure.

5.3.4. Drug Release

Release profiles for paracetamol and ranitidine loaded caplets are measured by the conventional dissolution method, while for the caplets containing the poorly soluble indomethacin, the biphasic dissolution method is used^[31]. Here, an octanol phase is added to maintain sink conditions in the aqueous phase throughout the dissolution test. The indomethacin that is dissolved in the aqueous phase, is expected to be efficiently extracted by the octanol. For each drug an additional medium (with pH 7.8 or pH 5.5) is tested to further investigate the influence of pH on release kinetics. Results are shown in Figure 41 and also shown are fits of the release profiles to the Peppas equation^[32]:

$$\frac{Q(t)}{Q_{\infty}} = kt^n \quad [2]$$

Here Q is the mass of drug released at time t (minutes) and Q_{∞} is the mass of drug release as time approaches infinity. The parameter k depends on the characteristics of the excipient-drug network, while n is an exponent indicative for the transport mechanism. For the cylindrical geometry of the caplets with a slice thickness-to-diameter ratio of 2.7, two limited mechanisms can be identified. When the release kinetics is controlled by pure Fickian diffusion (driven by a chemical potential gradient^[33]), the expected value is $n = 0.45$. On other hand, when release is controlled by Case II diffusion (commonly associated with a glass-to-gel transition of the matrix, for which the matrix hydration step is controlling the release rate^[33]), the expected value is $n \sim 0.9$. The same value for n may also be found for very poorly soluble drugs, when release is limited by the dissolution rate of the drug. Values for the parameters k and n determined by fitting the Peppas model to the experimentally observed release kinetics for the three model drugs (up to a released fraction of 0.6) are given in Table 8. For ranitidine and paracetamol caplets, also values for the half-life (indicative for the typical release time) are given in Table 8.

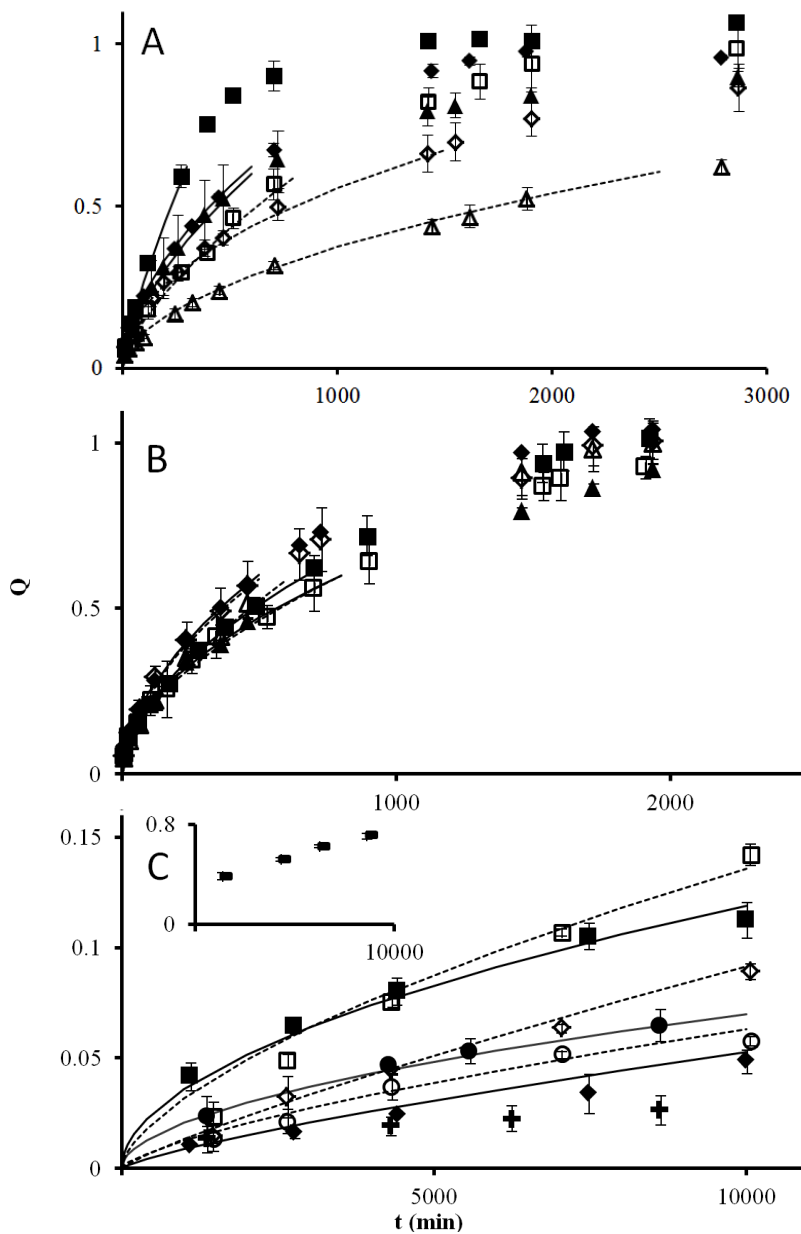


Figure 41: Release profiles for slices of caplets at pH 1 (◆,◇), pH 5.5 (○,●), pH 6.8 (■,□) and pH 7.8 (▲, △). The caplets are loaded with A) ranitidine, B) paracetamol and C) indomethacin, with a 4.4% loading (△,□,◇,○) and a 22.2% loading (▲,■,◆,●). The lines show data fits using the Peppas model, given by Eq. 2., to caplets with a 4.4% drug loading (dashed line) and a 22.2% drug loading (continuous line). In C), release from pure indomethacin crystals shown at pH 1 (+) and pH 6.8 (-) (see insert).

Table 8: Parameters describing the kinetics of release for the different caplets containing paracetamol, ranitidine or indomethacin. R^2 values of the fits are between 0.992 and 1.000. For indomethacin linear fits are applied giving a slope and intercept.

Drug loading, pH	Ranitidine			Paracetamol			Indomethacin		
	$k \cdot 10^2$	n	half-life (min)	$k \cdot 10^2$	N	Half-life (min)	$k \cdot 10^5$	n	Half-life ($\text{min} \cdot 10^{-4}$)
4.4% pH 1	2.16±0.45	0.47±0.04	761	1.93±0.27	0.55±0.03	358	4±0.6	0.84±0.04	7
22.2% pH 1	1.73±0.15	0.56±0.01	416	1.97±0.07	0.55±0.01	354	4±2	0.78±0.05	18
4.4% pH 5.5	-	-	-	-	-	-	10±5	0.70±0.05	19
22.2% pH 5.5	-	-	-	-	-	-	53±30	0.53±0.07	41
4.4% pH 6.8	0.67±0.07	0.67±0.07	600	1.98±0.65	0.51±0.06	553	41±8	0.63±0.05	7
22.2% pH 6.8	0.77±0.03	0.77±0.01	221	1.67±0.17	0.55±0.02	472	99±60	0.52±0.06	16
4.4% pH 7.8	0.96±0.10	0.53±0.02	1819	1.11±0.08	0.62±0.03	452	-	-	-
22.2% pH 7.8	1.21±0.35	0.61±0.07	454	1.62±0.11	0.54±0.02	594	-	-	-

A first observation is that for most paracetamol and ranitidine caplets, the exponent n is between 0.45 and 0.65, while for indomethacin caplets, the value of n is on average 15% higher. For paracetamol loaded caplets the release kinetics is almost independent of drug loading and release medium, in line with earlier results^[6]. For ranitidine, release rates drop significantly at the highest pH (pH 7.8), but increase with drug loading. With the exception of 22.2% loaded caplets at pH 6.8 and pH 7.8, the ranitidine caplets appeared to show slower release rates compared to paracetamol caplets. Not unexpectedly, indomethacin caplets showed a much slower release as compared to caplets containing paracetamol and ranitidine. The release rate for the indomethacin caplets is highest at pH 6.8, and lowest at more acidic pH values (lowest at pH 5.5 for 4.4% caplets and lowest at pH 1 for 22.2% caplets). Except at pH 1, the release kinetics is found to be quite insensitive to drug loading. The release kinetics of the paracetamol and ranitidine are found to be close to Fickian diffusion. The values of n that we find for indomethacin, at pH 1 indicate that here the limiting step is the dissolution of amorphous or crystalline drug particles. The solubility of indomethacin is known to be strongly pH dependent^[23] being less than 2.7 mg/L at pH 1. We have also tested release rates for indomethacin crystals ourselves and compared with the release rates from caplets, as shown in Figure 41. In the experiment, the crystals are kept in dialysis tubes to prevent their migration to the octanol phase. We confirmed that while at pH 6.8, release rates from crystals is much faster than from the caplets. For pH=1 it is just the other way around, suggesting that in the latter case the caplet preparation procedure has molecularly dissolved at least part of the drug into the matrix leading to faster release than from crystals.

A key factor influencing the pH dependence of the release kinetics is obviously the electrostatic interaction between the drugs and the zein matrix. In Figure 42, the pI of zein and the pK_a values of ranitidine and indomethacin are displayed together with their resulting charge at different pH values. Paracetamol is not included, because it is uncharged in all test media.^[34] If charges on the drug and the matrix have opposite signs, there is an electrostatic attraction and the release rate may be expected to become lower. Indeed, this is what is observed for ranitidine. For this case we find a significant difference in release rates between the case of pH 6.8 (where zein has no net charge) and pH 7.8 (where zein has a net positive charge), especially for 4.4% loaded caplets. Likewise, for indomethacin one would expect the slowest release between pH 4.5 and pH 6.8 where the drug and matrix

carry opposite charge signs. Indeed, for 4.4% loaded caplet we find that release at pH 5.5 is even slower than at pH 1.

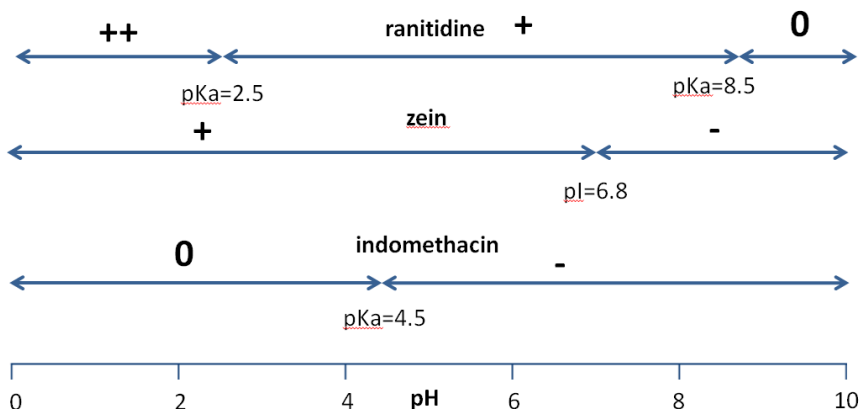


Figure 42: Schematic overview of the charge of ranitidine, zein and indomethacin at different pH's. pK_a and pI values for the compounds are also shown. Electrostatic attractions are higher between ranitidine and zein between pH 6.8 and pH 8.5 and higher between indomethacin and zein between pH 4.5 and 6.8.

The hydration rate and swelling capacity do not seem to directly correlate with the release kinetics. As shown in Figure 38, hydration rate and swelling capacity are much higher at pH 1 than at pH 6.8. However, for paracetamol caplets, release is only slightly faster at pH 1 than at pH 6.8. For ranitidine release is even slower at pH 1 than at pH 6.8. The water solubility of the drug does not seem to be the main determinant of release kinetics either, since release of paracetamol from the caplets is in most cases faster than the release of the much more soluble ranitidine (20 times more soluble). For the very poorly soluble indomethacin, solubility does appear to be a limiting factor, since for this case release is much slower as for the other drugs, and the diffusional exponent n that relates to the mechanism of drug release is much higher.

5.4. Conclusion

We conclude that extrusion followed by injection moulding is a suitable method for preparing sustained release caplets for a range of drugs, varying in hydrophobicity. The caplet preparation procedure leads to a reduction of crystallinity for all drugs, although the reduction is smallest for the most hydrophobic drug. We also find that electrostatic attractions between matrix and drug can significantly slow down release. We show that

depending on drug charge and hydrophobicity zein can show a wider variety of release characteristics.

5.5. Acknowledgements

This work is part of the Industrial Partnership Programme (IPP) Bio(-Related)Materials of the Stichting voor Fundamenteel Onderzoek der Materie (FOM), which is financially supported by the Nederlandse Organisatie voor Wetenschappelijk Onderzoek (NWO). The IPP BRM is co-financed by the Top Institute Food and Nutrition and the Dutch Polymer Institute. We thank Marise Hop for her contribution to this work.

5.6. References

1. Hurtado-López, P.; Murdan, S. Zein microspheres as drug/antigen carriers: A study of their degradation and erosion, in the presence and absence of enzymes. *Journal of Microencapsulation* 2006, 23 (3), 303-314.
2. Liu, X.; Sun, Q.; Wang, H.; Zhang, L.; Wang, J.Y. Microspheres of corn protein, zein, for an ivermectin drug delivery system. *Biomaterials* 2005, 26 (1), 109-115.
3. Jiang, Q.; Yang, Y. Water-Stable Electrospun Zein Fibers for Potential Drug Delivery. *Journal of Biomaterials Science, Polymer Edition* 2011, 22 (10), 1393-1408.
4. Huang, W.; Zou, T.; Li, S.; Jing, J.; Xia, X.; Liu, X. Drug-Loaded Zein Nanofibers Prepared Using a Modified Coaxial Electrospinning Process. *AAPS PharmSciTech* 2013, 14 (2), 675-681.
5. Oh, Y.K.; Flanagan, D.R. Swelling and Permeability Characteristics of Zein Membranes. *PDA Journal of Pharmaceutical Science and Technology* 2003, 57 (3), 208-217.
6. Bouman, J.; Belton, P.; Venema, P.; van der Linden, E.; de Vries, R.; Qi, S. The Development of Direct Extrusion-Injection Moulded Zein Matrices as Novel Oral Controlled Drug Delivery Systems. *Pharmaceutical Research* 2015 1-12.
7. Georget, D.M.R.; Barker, S.A.; Belton, P.S. A study on maize proteins as a potential new tablet excipient. *European Journal of Pharmaceutics and Biopharmaceutics* 2008, 69 (2), 718-726.
8. Grund, S.; Bauer, M.; Fischer, D. Polymers in drug delivery-state of the art and future trends. *Advanced Engineering Materials* 2011, 13 (3), B61-B87.
9. Lawton, J.W. Zein: A history of processing and use. *Cereal Chemistry* 2002, 79 (1), 1-18.
10. Shukla, R.; Cheryan, M. Zein: the industrial protein from corn. *Industrial Crops and Products* 2001, 13 (3), 171-192.
11. Argos, P.; Pedersen, K.; Marks, M.; Larkins, B. A structural model for maize zein proteins. *Journal of Biological Chemistry* 1982, 257 (17), 9984-9990.
12. Momany, F.A.; Sessa, D.J.; Lawton, J.W.; Selling, G.W.; Hamaker, S.A.H.; Willett, J.L. Structural characterization of α -zein. *Journal of Agricultural and Food Chemistry* 2006, 54 (2), 543-547.
13. Selling, G.W. The effect of extrusion processing on Zein. *Polymer Degradation and Stability* 2010, 95 (12), 2241-2249.

14. Belton, P.S.; Delgadillo, I.; Halford, N.G.; Shewry, P.R. Kafirin structure and functionality. *Journal of Cereal Science* 2006, 44 (3), 272-286.
15. Paliwal, R.; Palakurthi, S. Zein in controlled drug delivery and tissue engineering. *Journal of Controlled Release* 2014, 189 (0), 108-122.
16. Chiue, H.; Iwami, K.; Kusano, T.; Ibuki, F. Decreased Antioxidative Activity of Maize Zein in Response to Deamidation Rate. *Bioscience, Biotechnology, and Biochemistry* 1994, 58 (1), 198-199.
17. Podaralla, S.; Perumal, O. Preparation of zein nanoparticles by pH controlled nanoprecipitation. *Journal of biomedical nanotechnology* 2010, 6 (4), 312-317.
18. Xiao, D.; Gömmel, C.; Davidson, P.M.; Zhong, Q. Intrinsic Tween 20 Improves Release and Antilisterial Properties of Co-encapsulated Nisin and Thymol. *Journal of Agricultural and Food Chemistry* 2011, 59 (17), 9572-9580.
19. Oh, Y.K.; Flanagan, D.R. Diffusional properties of zein membranes and matrices. *Drug Development and Industrial Pharmacy* 2010, 36 (5), 497-507.
20. Herman, G.T. *Fundamentals of computerized tomography: image reconstruction from projections*. Springer, 2009.
21. Thakral, S.; Thakral, N.K. Prediction of drug-polymer miscibility through the use of solubility parameter based Flory-Huggins interaction parameter and the experimental validation: PEG as model polymer. *Journal of Pharmaceutical Sciences* 2013, 102 (7), 2254-2263.
22. Minagawa, N.; White, J.L. The influence of titanium dioxide on the rheological and extrusion properties of polymer melts. *Journal of Applied Polymer Science* 1976, 20 (2), 501-523.
23. Shen, T.-Y.; Winter, C.A.; Alma, B.S. Chemical and Biological Studies on Indomethacin, Sulindac and their Analogs. in *Advances in Drug Research*; Academic Press, 1977; 89-245.
24. Granberg, R.A.; Rasmuson, Å.C. Solubility of Paracetamol in Pure Solvents. *Journal of Chemical & Engineering Data* 1999, 44 (6), 1391-1395.
25. Kortejärvi, H.; Yliperttula, M.; Dressman, J.B.; Junginger, H.E.; Midha, K.K.; Shah, V.P.; Barends, D.M. Biowaiver monographs for immediate release solid oral dosage forms: Ranitidine hydrochloride. *Journal of Pharmaceutical Sciences* 2005, 94 (8), 1617-1625.
26. Fujiwara, M.; Chow, P.S.; Ma, D.L.; Braatz, R.D. Paracetamol crystallization using laser backscattering and ATR-FTIR spectroscopy: metastability, agglomeration, and control. *Crystal Growth & Design* 2002, 2 (5), 363-370.
27. Peleg, M. An empirical model for the description of moisture sorption curves. *Journal of Food Science* 1988, 53 (4), 1216-1217.
28. Katchalsky, A.; Michaeli, I. Polyelectrolyte gels in salt solutions. *Journal of Polymer Science* 1955, 15 (79), 69-86.
29. Yong, Y.H.; Yamaguchi, S.; Gu, Y.S.; Mori, T.; Matsumura, Y. Effects of Enzymatic Deamidation by Protein-Glutaminase on Structure and Functional Properties of α -Zein. *Journal of Agricultural and Food Chemistry* 2004, 52 (23), 7094-7100.
30. Islam, M.F.; Nobili, M.; Ye, F.; Lubensky, T.C.; Yodh, A.G. Cracks and topological defects in lyotropic nematic gels. *Physical Review Letters* 2005, 95 (14).
31. Sarode, A.L.; Wang, P.; Obara, S.; Worthen, D.R. Supersaturation, nucleation, and crystal growth during single- and biphasic dissolution of amorphous solid dispersions: Polymer effects and implications for oral bioavailability enhancement

- of poorly water soluble drugs. *European Journal of Pharmaceutics and Biopharmaceutics* 2014, 86 (3), 351-360.
32. Ritger, P.L.; Peppas, N.A. A simple equation for description of solute release I. Fickian and non-fickian release from non-swelling devices in the form of slabs, spheres, cylinders or discs. *Journal of Controlled Release* 1987, 5 (1), 23-36.
 33. Peppas, N.A.; Sahlin, J.J. A simple equation for the description of solute release. III. Coupling of diffusion and relaxation. *International Journal of Pharmaceutics* 1989, 57 (2), 169-172.
 34. Cairns, D. *Essentials of pharmaceutical chemistry*. Pharmaceutical Press, 2012.



6. General discussion

6.1. Outline

Proteins at lower water content can be found in many places in nature. A clear example are the storage proteins in seeds. Generally, these proteins serve as a source of amino acids for germination and plant growth. Protein contents in seeds can reach up 40% (w/w), while in domains within the seeds even much higher concentrations can be found^[1]. Recently, many of these proteins are under investigation due to a higher demand in plant based proteins as an alternative to animal based proteins, especially in the food sector. Knowledge about the proteins within the seed is important for their final application in products and the intermediate steps to acquire the proteins in the desired state. Another example from nature where proteins at low water content can be found, are spider webs mainly made of silk protein. These webs have the uniquely combination of high tensile strength and extensibility making them able to absorb large amounts of energy before breaking. Already for millennia silk is used in clothing however, recently many more applications are found^[2-4].

Both for the scientific pursuit, to increase understanding of natural materials, as well as for application purposes, investigations of protein behaviour at lower water content is gaining importance. Previous physico-chemical research has been more focussed on proteins in a dilute or semi-dilute state, e.g. to make gels or increase the viscosity of liquids. Much less studies focussed on understanding how proteins behave in the more concentrated regime. Protein behaviour changes significantly and often irreversibly, with lowering moisture content. This may either be undesired, e.g. when protein nativity needs to be preserved, or desired when the change in protein behaviour induces a useful functionality.

In this thesis we study changes in protein behaviour at low water content when hydrating or drying proteins. Drying dynamics is investigated for water soluble whey proteins in two different systems: coatings (**chapter 2**) and droplets (**chapter 3**). For coatings, the drying dynamics at different length-scales is investigated, while for droplets we mainly focussed on changes in droplet morphology during drying and remaining shell morphology after drying.

Drying and hydration of food proteins

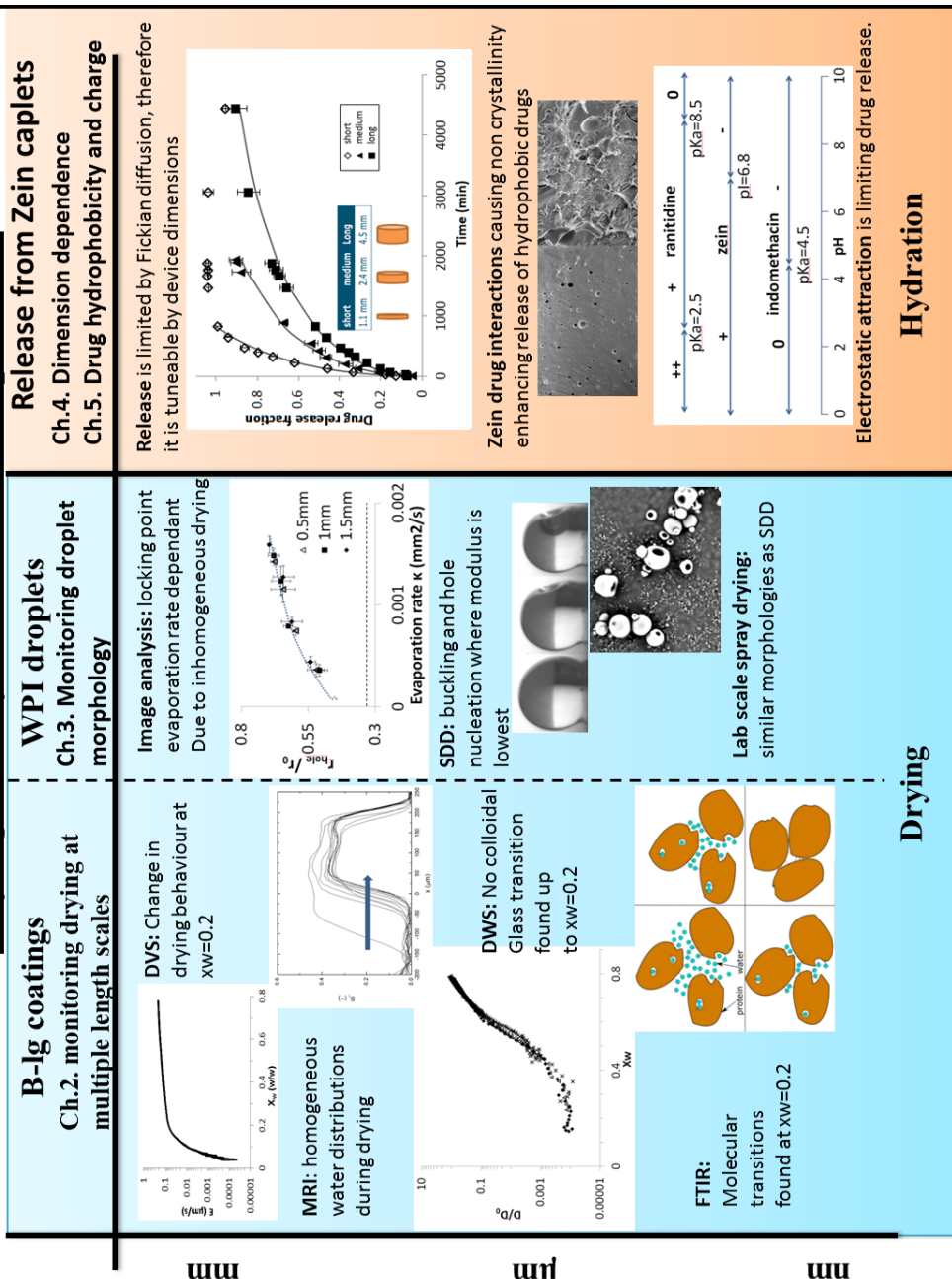


Figure 43: Graphical presentation of the thesis outline

Hydration behaviour is investigated for the water insoluble corn protein zein (**chapter 4** and **chapter 5**). Zein hydration is investigated to explore its potential as an excipient providing controlled release of active ingredients. In Figure 43, a graphical overview of the thesis content is shown.

In the current general discussion chapter, an overview of the thesis content and a discussion of the interrelations between the findings of each of the chapters is provided. For this, some additional supporting experimental data is presented. Finally, the practical relevance of our work in a broader context is discussed, as well as an outlook to future research.

6.2. Preparation of concentrated proteins: drying

The drying of aqueous protein mixtures by the evaporation of water (typically at elevated temperatures) is an important processing step for many applications. A typical example is the drying of protein coatings and films. These coatings and films may function as a barrier against moisture, gas or provide resistance to mechanical stresses^[5]. Additionally, films can be used as an encapsulation material for slow release purposes^[6]. Especially whey proteins are found to be suitable as a film and coating material due to their superior mechanical and barrier properties compared to other protein based or polysaccharide based films^[7]. Another reason to have proteins in a dry state is to give them higher stability against microbial spoilage or chemical degradation. Products that are dried for this reason include infant milk powder, whey protein isolate and many biologically active proteins (i.e. enzymes). A disadvantage of a drying process by heating is that it can change the conformation and even denature the protein. Also by means of other procedures, we should be aware that the removal of water replaces water-protein interactions with protein-protein interactions, automatically changing the internal structure of the protein (as discussed in **chapter 2**).

Many drying processes take place at elevated temperatures which can result in thermal denaturation of the protein. A drying process which reduces both thermal and dehydration damage is freeze drying. Prior to freeze drying the solution is vitrified, where, due to a fast freezing process, the rearrangement of the protein structure is minimised. During the freeze drying process the water is sublimated and because the sample remains in a frozen state, the dehydration damage is minimal. A major disadvantage of freeze drying is the huge energy cost involved.

A much more energy efficient process is spray drying. The solution liquid is dispersed into small atomised drops in top of a spray drying tower, while hot air is blown alongside the droplets. Due to the evaporative cooling, the droplet temperature, also referred to as the wet bulb temperature, remains relatively low. Therefore, this methods is also useful for thermal sensitive materials. Still, the dehydration process of the protein can cause denaturation and therefore it remains an important topic of investigation.

Most of the literature on protein drying relates to the final properties of protein films and powders. There is ample evidence that drying conditions have a profound influence on these final properties^{[8][9][10]}. The influence of the drying conditions on the final product properties, can only be properly understood by a detailed study of the whole process of drying and not just the final state. Therefore, there is a need to investigate the details of the dynamics of drying of proteins. This may seem like a rather fundamental research topic, further away from applications. However, we believe that a better understanding of the drying dynamics, is crucial for eventually being able to preserve protein native conformations and enzyme activity during drying and for being able to improve the barrier functionality of protein films.

6.2.1. Transitions in drying

In **chapter 2** and **chapter 3** of this thesis the drying dynamics of a protein solution, from high to low water contents, is explored. For proteins it is well known that generally a minimal (critical) amount of hydration water is necessary to maintain their functionality^[11]. However, proteins in aqueous environments are known to be chemically and microbiologically much less stable than dried proteins. Taking care of both aspects, some authors suggested that so called monolayer moisture content could be a measure for a critical moisture content where both functionality is maintained^[12,13], while still having good preservability^[14]. The monolayer moisture content is defined as the moisture content for which proteins are covered with a single layer of water molecules. The monolayer moisture content can be found by fitting sorption isotherm with the Guggenheim-Anderson-de Boer (GAB) model (**chapter 2**, equation 4) or with the older Brunauer–Emmett–Teller (BET) model. Later the topic is studied more in depth, investigating changes in the protein behaviour at low water content. In **chapter 2**, we find a transition during drying at much higher moisture contents than the monolayer moisture content both at macroscopic length scales (from DVS and MRI data) as well as at microscopic scales (from FTIR data). This

transition is not only found during drying, but also in equilibrated systems as observed using FTIR (**chapter 2**, figure 9). These higher values are not limited for β -Ig, but are also found for other proteins. For lysozyme^[15], a transition water content value (mass fraction) was found of $X_w=0.27$ from FTIR measurements. The importance of a critical moisture content is apparent from the fact that this is also the water content of the onset of enzyme activity. However, the lysozyme monolayer moisture content (X_w) based on the GAB fit from the sorption isotherm was found to be only $X_w=0.08$, more than 3 times lower. Also for gluten^[16, 17] a transition in both NMR as well as FTIR was found around $X_w=0.37$, while the monolayer moisture content value based on a GAB fit was only found to be $X_w\sim 0.08$ ^[18]. In a review work of Carreri^[13], the hydration of proteins is discussed based on a wide range of techniques, mostly based on lysozyme. In that review several levels of protein hydration are identified. At water content, X_w , below 0.15 the water only interacts with charged and polar groups, while for $X_w=0.15-0.25$ it was put forward that the long range connectivity of water molecules becomes apparent. From $X_w=0.25$, enzyme activity becomes observable, while only at and above $X_w=0.38$ the whole surface is covered with at least a monolayer of water. All these findings put the physical meaning of the monolayer moisture content based upon the GAB curve in question, since typical values yield a lower X_w (e.g. gluten yields $X_w=0.05$). Hence, one could argue that for proteins, this GAB value might be nothing more than just a fitting parameter.

Protein-water interactions remain complex, since they are dynamic, water can penetrate the protein, and water is not homogeneously distributed in the protein. Therefore the search for a critical moisture content for a wider range of proteins, which covers both functionality and stability, remains important. This would certainly contribute to a better understanding of the drying dynamics, and the associated transitions during protein drying. Besides deducing molecular transitions during drying as described above, one may also consider the characterisation of larger scale transitions in protein systems. For example, coatings or films prepared with only β -LG or WPI are brittle and unsuitable to use as a film or coating material. Krochta^[19] hypothesised that this brittleness is due to extensive protein-protein interactions, which are also observed in **chapter 2** below the critical water weight fraction of $X_w=0.2$. In order to decrease the brittleness, a plasticiser is needed to provide flexibility to the film or coating. One category of plasticiser forms hydrogen bonds with the protein, therefore replacing the protein-protein interactions with protein-plasticiser interactions.

Typical protein plasticisers are glycerol, polyethylene and also water. Another example in the characterisation of larger scale transitions is in the spray drying of protein solutions, during which sugars are often used as a plasticiser to prevent denaturation^{[20], [21]}.

In the following section, we mainly focus on the protein plasticisation by water. Protein plasticisation is a complicated topic, which is still poorly understood. The influence of a plasticizer can most clearly be seen from the changes it induces in the protein glass transition as a function of water content. Typically, protein glass transitions are measured using differential scanning calorimetry (DSC), by measuring the change in heat capacity, during a continuous increase of the temperature. The temperature at which the heat capacity changes to a different plateau value is referred to as the glass transition temperature or T_g . While for simple molecules, the thermal signature of a glass transition is often very clear, this is not the case for complex molecules such as globular proteins that have secondary and tertiary structures^[22]. As mentioned in **chapter 2**, we have been unsuccessful in measuring glass transitions at lower moisture content using modulated-temperature DSC (MTDSC). Therefore we attempt to measure thermal transitions during drying using MTDSC on a drying B-LG coating.

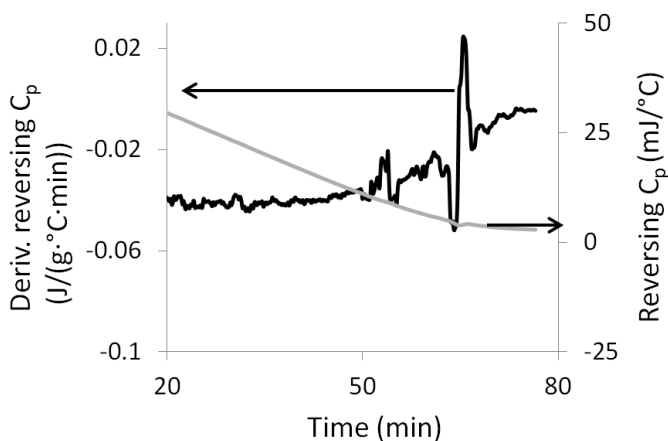


Figure 44: Measured heat capacity of a drying B-LG coating (initial concentration 20% (w/w)). Modulating temperature amplitude and period are 20°C, 0.424 °C and 80s, respectively. Both the reversed heat capacity and the derivative of the reversed heat capacity are displayed.

While modulating the temperature around 20°C (amplitude: 0.424 °C and period: 80s), we measure the heat capacity. A typical result is shown In Figure 44. Moisture contents at different drying times are determined gravimetrically. The dry weight of films is determined by the difference in weight before and after 3 days of oven drying at 80°C. Typically around 60 seconds a fluctuation occurs, as displayed most clearly in the derivative of the reversing heat capacity. During the drying process, no change in the non-reversing heat capacity could be found, again suggesting the absence of a clear glass transition. At the time of the fluctuation in the reversing C_p , moisture contents are found to be around 0.25, which is close to the transition moisture content of 0.2 measured from DVS and FTIR. After 60s of drying we always find cracks form through the coating. Therefore, we hypothesise that the fluctuations are caused by the energy release as cracks propagate through the coating, rather than that the fluctuations are signifying a glass transition. The data seem not to support the existence of clear glass transition.

6.2.2. Homogeneity of drying

When investigating the drying dynamics of proteins, the homogeneity of drying is an important factor to be considered. The development of inhomogeneities in protein concentration during drying, is likely to influence final product properties. In **chapter 3**, we show that for droplets, the inhomogeneity in protein concentration is a determining factor for the final particle morphology. In the spray drying process this directly relates to powder properties, such as bulk density and wetting behaviour. Also for films and coatings, inhomogeneity is of major influence and often causes challenges such as the formation of coffee rings^[23], which results in an inhomogeneous distribution of material after drying. Some fundamental work on the role of inhomogeneities during drying has been performed on drying colloidal suspensions^[24-27], while for proteins this issue has not yet been explored. One clear similarity between the colloidal and proteins systems is the invaginations in drying drops of colloidal suspensions as observed in one study¹⁹. These are very similar to the hole and vacuole formation we observe for drying whey proteins in **chapter 3**.

A common type of inhomogeneity for the film geometry is that of a protein concentration gradient from the interface towards the bulk, which is most apparent when evaporation rate is larger than diffusion of the protein. As a result, protein accumulation at the interface occurs. The relevant dimensionless number comparing evaporation rate to diffusion is the

so-called Peclet number (Pe). The value of the Peclet number is frequently used as a criterion for whether films may be expected to dry homogeneously or not. Pe is described as $Pe = b \cdot E/D$, where E (which can also be described as κ) is the evaporation rate, D is the diffusion coefficient of the solute and b is a factor which depends upon the geometry. When $Pe \gg 1$, drying may be expected to be inhomogeneous since then diffusion is not fast enough to equalize the concentrations, as compared to homogeneous drying, which sets up a concentration gradient at the interface. We use this criterion in **chapter 2** (equation 7) for films and in **chapter 3** (equation 3) for droplets. To compare the inhomogeneity of drying for both geometries, the Pe values found in this thesis for β -lg coatings and WPI droplets are displayed in Table 9.

φ	D (m^2s^{-1})	Pe coatings	Pe droplets no airflow	Pe droplet airflow
0.2	2.6×10^{11}	6	2	~ 10
0.3	7.7×10^{12}	~ 20	6	~ 40
0.4	3.3×10^{12}	~ 40	~ 20	~ 80

Table 9: Calculated protein diffusion coefficients (D) and Peclet (Pe) numbers of β -lg coatings and WPI droplets with and without the presence of an airflow (0.2ms^{-1}), at different volume fractions (φ) of protein.

The highest Pe values are found for droplets in the presence of an airflow, while the lowest Pe values are found for droplets without an airflow applied. Still, for both droplets, we have observed skin- and hole formation, which are hypothesised to be due to inhomogeneous drying. For thin coatings, we generally find homogeneous drying as indicated by NMR and DWS. It remains a possibility however that a thin skin, which cannot be detected by both methods, develops at the surface of the coatings during drying. In an earlier study on WPI droplets^[28], it is found that at a local concentration (close to the interface) of around 41%, the droplet surface starts to buckle. This concentration is close to the average protein concentration in the droplet at which hole formation is observed, as described in **chapter 3**.

6.2.3. Anomalous skin formation during protein drying

The implications of a protein “skin” layer for the morphological development of drying droplets can be profound. This becomes evident when drying a WPI droplets that contain an air bubbles at the start of drying process. In Figure 45 a time series of images is shown of a

droplet containing 20%(w/w) WPI, which is dried at 60°C and contains an air bubble.

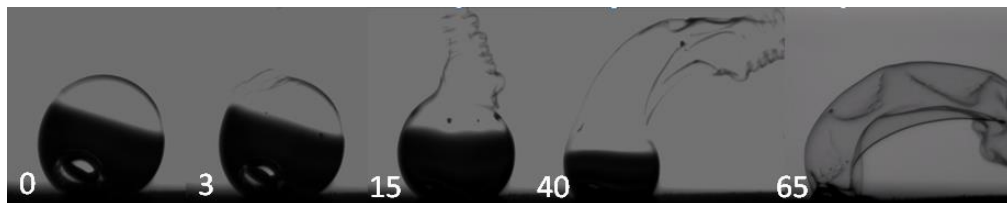


Figure 45: Time series of images of a drying droplet containing an air bubble at the start of drying. The initial radius of the droplet is 0.5 mm and the initial WPI concentration in the droplet is 20% (w/w). The droplet is dried with an airflow coming from the left, within the plane of the picture, with a streaming velocity of 0.2 ms^{-1} at 60°C. Time (s) after droplet disposition is displayed in the images. The air bubble is initially located at the left bottom side of the droplet.

It can be observed that after 3 seconds a “chimney” develops, that rises on top of the droplet. The air bubble that is initially present starts to vanish within seconds after droplet deposition. The chimney formation is observed for all tested drying temperatures, ranging from 20°C to 80°C. The growth rate and final size of the chimney increased with increasing drying temperature. In absence of an airflow, no chimney formation is observed. The formation of a chimney, so early in the drying process, indicates that an elastic skin can form very fast given to appropriate airflow conditions. Although chimney formation only occurs when an air bubble is present, the exact underlying mechanism is unclear. The chimney formation is probably triggered by a pressure difference between the top of the droplet and the surrounding air. Probably, the water vapour originating from the droplet causes the chimney to grow. The final volume can be up to 5 times (at 80°C) higher than the volume of the initial droplet (X-ray tomography results (data not shown)). This effect is of importance for spray drying processes. The inclusion of air bubbles, when droplets are atomised could lead to a radically different evaporation kinetics and a different final powder morphology.

6.3. Protein hydration

In many applications, protein hydration is an important factor when it comes to achieving a desired functionality. For spray dried protein powders a good reconstitution behaviour is an example of such a desired functionality, which is often obtained when during the drying, the protein denaturation is minimised^[29]. Another way of increasing powder reconstitution behaviour is to increase the agglomeration of powder particles during processing. As a

result, the wetting step will be increased due to capillary motion of water through the microspores between the particles. In contrast, for applications where films and coatings are used as a barrier material, hydration of the protein should be minimised. Both animal proteins (such as gelatine, casein and whey) ^[5, 6] and plant proteins (such as soy gluten and zein) ^[30] can be used for coatings and films. Proteins that have been used to create films and coatings include both water soluble and water insoluble proteins. To minimise hydration of final films, heat is often used in combination with drying^[5, 31], which gives rise to protein denaturation, leading to a more hydrophobic film. Protein-protein interactions are also enhanced and can even lead to network formation when the proteins are heat denatured. For these films and coatings, the addition of a plasticizer is necessary to ensure sufficient flexibility of the film. However, a plasticiser can also increase protein mobility, which is favourable for hydration^[32]. On the other hand, protein-glycerol interactions are hypothesised to be similar to protein-water interactions, therefore a plasticizer could compete with water on these protein binding sites, which could decrease hydration kinetics^[33].

Another application where hydration of dense proteins is important, is in the field of drug delivery. Here proteins can be used as slow release agent and examples are albumin, gelatine and collagen^[34]. For this purposes, a slow hydration and insolubility in water are often desired in order to provide a slow and sustained drug release. The corn protein zein has been suggested to be potentially useful as a slow release agent.^[35] In **chapter 4** and **chapter 5**, the potential of the corn protein zein as an excipient is investigated. The useful characteristics of this corn protein for pharmaceutical purposes is extensively discussed in the introductions of **chapter 4** and **chapter 5**. In the following paragraphs we discuss some key properties that make zein (and other proteins) suitable as excipients for slow release.

6.3.1. Hydrophobicity

A key determinant for proteins functionality is the hydrophobicity of the protein. It is an important factor for reconstitution behaviour of protein powders, barrier properties of coatings and films and the hydration and release behaviour of functional components from protein tablets and caplets. Since proteins have complicated secondary, tertiary and quaternary structures, and carry both hydrophobic and hydrophilic residues, the “hydrophobicity of a protein” is an ambiguous term, and there is no single good way of determining it. In principle, the hydrophobicity of a macroscopic substance can be defined

in terms of the contact angle the substance has, at an air-water interface. For protein hydrophobicity at smaller length scales, many alternative assays have been proposed, which are not always in agreement with each other. Zein is a protein where apparent contradictions about hydrophobicity exist and it is therefore a good example to discuss these in somewhat more detail. The Goldman–Engelman–Steitz (GES) scale^[36], determines the hydrophobicity of individual amino acids on the basis of their free energy of transfer from water to oil by calculating the surface area of each amino acid side chain in an α -helix. Based on this GES scale, 76.25% of the amino acids in α -zein are found to be hydrophobic^[37]. A disadvantage of this approach is that amino acids are counted as either hydrophobic or hydrophilic, without properly scaling amino acids of intermediate hydrophobicity. Another approach, which does use a continuous amino acid hydrophobicity scale is the grand average of hydropathicity index or GRAVY. The solubility of individual amino acids is evaluated in water where hydrophobic proteins give a positive index, while hydrophilic proteins give a negative index. Zein has a GRAVY index of 0.273, again indicating it to be a hydrophobic protein having overall more hydrophobic amino acids. Although the individual amino acids are indicating the protein to be hydrophobic, many of these hydrophobic residues will, of course, be hidden somewhere inside the globular structure of zein and will e.g. not be accessible to solvent. Hence, approaches that take the protein as a whole, can tell a different story. Already in **chapter 4** and **chapter 5**, we observe that zein is able to take up considerable amounts of water, which indicates that overall, globular zein has at least a somewhat hydrophilic properties. An approach to investigate the overall hydrophobicity is to follow the change in hydration, if temperature is changed. For purely hydrophobic proteins, since hydrophobic interactions increase with temperature, water should be expelled (from a hydrated protein sample) upon heating^[38]. Here, zein even takes up some more water upon increasing the temperature up to around 70°C,^[39]. According to Wang et al^[40], like many other proteins, zein can therefore be characterised as a polymeric amphiphile, since it can have both hydrophobic and hydrophilic properties.

The amphiphilicity of proteins is a key property, when it comes to applications of proteins as matrices for delivery of other compounds. For example, whey proteins have a good water solubility and hence, with regards to their dissolution properties, behave as hydrophilic^{[5],[41]}. After denaturation, the hydrophobic interior gets exposed to the solvent to a larger degree, leading to a more hydrophobic behaviour of the denatured proteins.

Through such changes, even hydrophilic whey proteins (in the form of particles of heat-denatured whey protein), can be used as a matrix for the slow release of e.g. hydrophobic aromas^[42]. To create these type of particles, heating conditions, pH and protein concentration are some of the crucial parameters that need to be tuned to reach an optimal functionality. Although milk proteins and in particular the whey proteins, are among the most widely explored protein for these purposes, there is now also a growing interest in plant-derived proteins such as zein, that are often much more hydrophobic. For these proteins, much less detailed investigations into their physico-chemical behaviour have been performed and many potential applications remain to be explored.

6.3.2. Plasticisation and co-plasticisation

Plasticisers are used as additives in particular in protein films to provide elasticity to an otherwise brittle system by lowering the glass transition temperature T_g . This allows for lower processing temperatures, a crucial property when heat sensitive ingredients are used such as drugs. For instance in **chapter 4** and **chapter 5**, water is used to plasticise the zein matrix resulting in much lower processing temperatures for hot-melt extrusion (HME) and injection moulding (IM). In these paragraphs we further discuss protein plasticisation by compounds other than water. There are two main groups of plasticisers^[43], the internal plasticisers and external plasticisers. Internal plasticisers are part of the polymer molecule, thereby making the polymer less ordered, which softens the molecules and lowers the glass transition temperature. External plasticisers are compounds which, without chemical reaction, interact with the polymer. In almost all cases, proteins are plasticised externally. In turn, external plasticizers can also be subdivided in two groups. Primary plasticiser or solvent plasticiser, enable the compound, under suitable conditions, to dissolve into the plasticiser even if the compound is crystalline. Non-solvent or secondary plasticisers only penetrate the amorphous regions of the a compound. In drug delivery, especially primary plasticisation is of importance. Many of the recent developed drugs are hydrophobic in nature. Poor dissolution properties of strongly hydrophobic drugs generally result in low systemic bioavailability. Keeping a hydrophobic drug in a non-crystalline state, could greatly enhance dissolution properties and thereby bioavailability. In **chapter 4** and **chapter 5** the zein/water matrix appears to solubilise drug molecules to some extent. Even the very hydrophobic indomethacin showed some loss in crystallinity after extrusion with zein. This could potentially explain the faster release of indomethacin caplets at pH 1

compared to dissolution of only the crystals (**chapter 5**). The extent of matrix plasticisation is important for both hydrophobic and hydrophilic drugs, since this has been shown to influence the drug release properties of the matrix^[44]. Therefore, when proteins are used as excipient or slow release agent, knowledge of its interaction with the drug could prove to be essential to understand or even predict dissolution kinetics, especially when hydrophobic drugs are used.

As an example, beyond what is already shown in **chapter 5**, we have investigated physical interactions in zein-drug powder mixtures (same drugs as in chapter 5) using DSC. A heat-cool-heat sequence is applied (rate is 10°C/min). In Figure 46 the glass transition temperature T_g are displayed for different zein/drug physical mixtures. The T_g is determined in the second heating step, during which all drug are found to be non-crystalline. The glass temperature T_g for ranitidine could not be determined since it decomposes after melting. In Figure 47 the melting range and the degree of crystallinity is displayed for the physical mixtures (i.e. the zein-drug powder mixes).

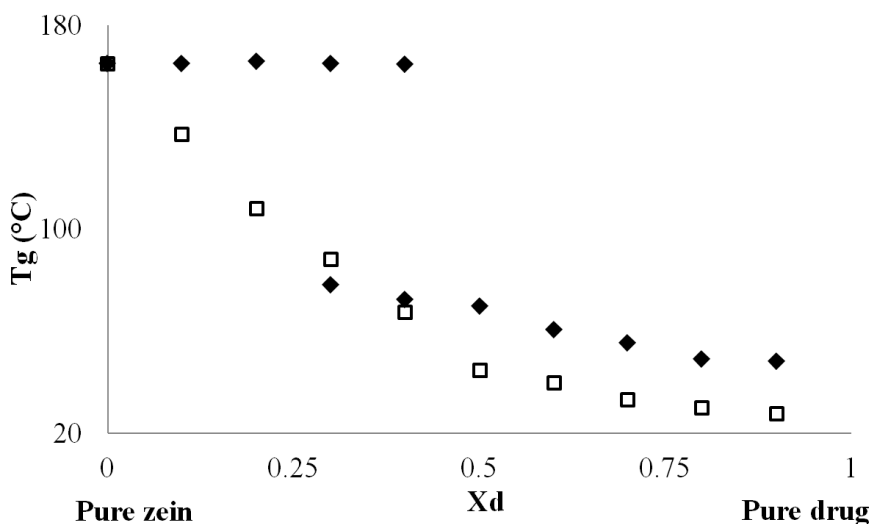


Figure 46: Glass transition temperatures T_g determined using DSC for zein/drug mixes. T_g is plotted versus drug content X_d (w/w). Drugs used are paracetamol (\square) and indomethacin (\blacklozenge). A heat-cool-heat sequence (rate is 10°C/min) is applied. T_g is determined during the second heating step during which no crystalline drug is present.

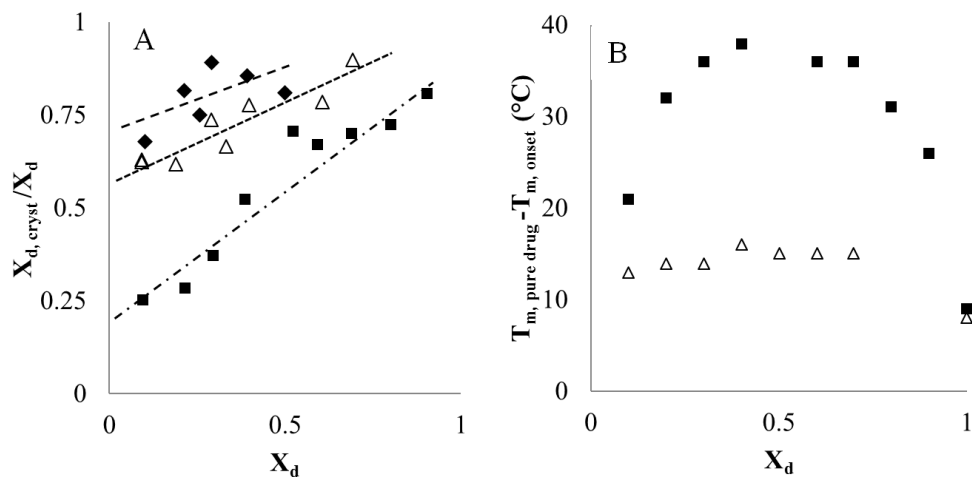


Figure 47:A) Drug crystallinity determined for different physical mixtures. Drug crystallinity $X_{d,cryst}/X_d$ (w/w) is plotted versus drug content X_d (w/w). B) Melting depression of the physical mixes $T_{m,pure\ drug} - T_{m,onset}$ is plotted versus drug content X_d (w/w), determined for different physical mixtures. Drugs used are paracetamol (■), indomethacin (△) and ranitidine (◆). Melting range is determined by subtracting the onset melting temperature of the physical mix from the melting temperature of the pure drug

When compared to the pure substance there is a widening of the melting range (often referred to as melting depression), which is often used as indicator of solubilisation of the drug into the matrix (Figure 47A). Here, a larger melting depression indicates better solubility. Another indicator of drug solubility in the matrix is the ratio of crystalline drug/total drug (Figure 47B). Here we assume that loss of crystallinity prior to melting can only be due to the drug dissolving into the matrix.

As shown in Fig. 4, for paracetamol the glass transition temperatures continuously decrease with increasing drug content. For indomethacin, at low loading the glass transition temperature is initially hardly affected, until at a drug content of 0.3-0.4 there is a clear break, and beyond this critical drug content the glass transition temperature for indomethacin decreases when further increasing the drug content. Fig. 5 shows the width of the melting transition (melting range) as a function of drug content in the zein matrices. The width increases much more for paracetamol than for indomethacin. Also the loss of crystallinity, shown in Figure 47B, is much higher for paracetamol than for indomethacin and ranitidine. All these results suggest that among the drugs tested, paracetamol is best

miscible with zein. It plasticises the zein to the largest degree, and has the lowest degree of crystallinity.

The poor plasticisation of zein by indomethacin and the relatively high crystallinity of indomethacin, could explain the relatively poor extrudability of indomethacin/zein mixtures as compared to paracetamol and ranitidine (as found in **chapter 5**). While for the physical (powder) mixtures, ranitidine shows behaviour that is intermediate between that of paracetamol and indomethacin, in **chapter 5** for the caplets it has shown to have the lowest degree of crystallinity. Hence, the added water probably plays a key role in further dissolving the highly water soluble ranitidine into the zein/water matrix. Co-plasticisation is therefore another potentially important topic for further investigations. In summary, the physical stability of drugs in matrices is a key consideration when there is a need to keeping drugs in a non-crystalline state.

6.3.3. Prevention of re-crystallization

Several mechanisms have been suggested to enhance the release of dissolved or dispersed drugs from a matrix^[45]. Two of the main mechanisms proposed are: 1) amorphous rather than crystalline state of the drug 2) good dispersibility of the drug in the matrix. A main argument against the use of solid dispersions (e.g. a drug dispersed in a solid matrix) is the often poor physical stability of the drug. In principle, non-crystalline states are thermodynamically unfavourable over the crystalline state, therefore re-crystallization often occurs. For pharmaceutical products this is undesired since this could alter product specifications e.g. drug bioavailability or even sensory properties, which makes it unsuitable for the market^[45]. So, if re-crystallization occurs, at least the timescale of this process needs to be investigated. As shown in **chapter 5**, when dispersing drugs in zein matrices, a significant fraction of the drugs is in an amorphous or molecularly dispersed state. In that chapter, we did not address the long term stability, which is crucial when this type of matrix is considered as a potential slow release formulation. Using DSC, we therefore compare the state of the drug of different samples of caplets 2 to 3 days after the HME and IM process while sample from the same batches is tested 9 months to 1 year later as well. The results are displayed in Figure 48.

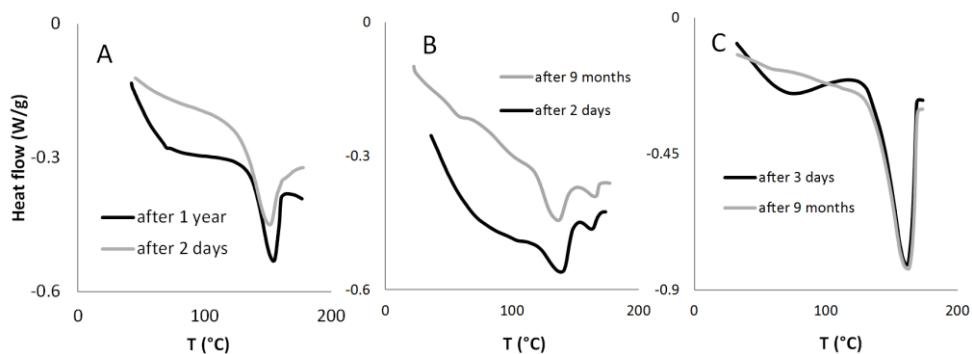


Figure 48: DSC results of 3 different caplets shown measured after long and short storage times. A) 22.2% indomethacin loading B) 22.2% paracetamol loading C) 45.1% paracetamol loading. Heat flow (W/g) is shown versus temperature T (°C). Heating rate is 10 °C/min.

For the timescales measured, our samples seem rather stable. Even for the 22.2% paracetamol loaded sample (Figure 48B) the peak around 130 °C, which we attribute to the crystalline form III, remained stable after 9 months of storage. This shows that the zein matrix is able to keep drugs into a non-crystalline state for prolonged periods of time.

6.3.4. Proteins as sustained release matrices

The use of natural polymers as sustained release agents has gained interest over the last decades. Advantages over synthetic polymers are better bio-availability and biodegradability. Additionally, they are perceived as being more natural and sustainable. Disadvantages compared to synthetic polymers are: fewer suitable natural polymers are known (for drug delivery purposes), and their properties are often not as tuneable. Also, many natural polymers still need modification^[46] before they are suitable to be used as an excipient. Here, starch is a well-known example of a polymer where modification is needed^[47]. Most proteins considered for slow release applications are used in the form of small beads or microcapsules. Examples of proteins used in this way include whey protein^[42], gelatin^[48] and zein^{[49], [50]}. Instead, we have investigated the potential of the corn protein zein as an excipient in solid dispersions, which is still the most common format of drug delivery. Indeed, in **chapter 4** and **chapter 5** we show that by using HME and IM, zein drug solid dispersion could be formed with a slow release profile, that is highly suitable for oral dosage forms. The release of a non-ionised drug (paracetamol) can be well approached by a 2D diffusion model^[51] as shown in **chapter 4**. We found release rates to be

precisely tuneable via the device dimensions, while pH and drug loading had no or only a minor influence on release. In many cases tuneability via pH is in fact required. A well-known synthetic excipient is Eudragit®^[52], a polymer that can be tuned to dissolve at different pH, thereby tuning release to occur at different pH's. In principle, proteins also have this ability to be tuneable by pH. For example, we show in **chapter 5** that the release kinetics of ionised drugs depends on pH via electrostatic interactions of the drugs with the zein matrix. A possibility to further tune this type of behaviour is by using multiple proteins to alter the effective pI of the protein excipient. Other heat stable and poorly water soluble proteins that might be used for this purpose are Karafin^[53] (pI~9)^[54] and silk^[55] (pI~2). Therefore investigating mixed protein systems as controlled release excipients is a promising research path to formulate novel protein excipient matrices.

6.4. General conclusion

In this thesis we have investigated various aspects of the physical chemistry of protein systems at low water content (see Figure 43). **Chapter 2** provides a fundamental view of changes in protein systems when drying towards low moisture contents. An important issue is found to be the homogeneity of drying and this also turned out to be a key issue in determining the morphologies of drying protein droplets, that we considered in **chapter 3**. For these droplets, small differences in drying rate over the droplet surface determine where hole- and vacuole formation occurs. Inhomogeneity over the whole surface is a large determinant for droplet size as the droplet diameter at the locking point increased with faster and thus more inhomogeneous drying. Here inhomogeneous drying and solute diffusivity will be key in understanding more complex multi component systems^[56], as in practice most spray dried systems are. The transition found for drying films in **chapter 2** on the molecular scale as observed with FTIR, is hypothesised to influence macroscopic drying behaviour as well, as observed in DVS. During the drying, protein-water interactions are replaced by protein-protein interactions decreasing the mobility of proteins. This effect of plasticisation that water has, is not only important in **chapter 2** and **chapter 3**, but also in **chapter 4** and **chapter 5** that dealt with zein matrices as excipients for drug delivery. Only after hydration (i.e. plasticisation) the zein matrix allowed for drug release. We also showed that to some extent drug molecules are miscible within the zein matrix and are able to plasticise it. This 'dissolution' of the drug into the zein matrix is a promising route to increase bioavailability of poorly soluble drugs. Along these lines, in **chapter 5** we

concluded that while zein matrices reduce the degree of crystallinity of the hydrophobic indomethacin to some extent, they would not yet be suitable to deliver this hydrophobic drug at high loading. Possibly, the miscibility of hydrophobic drugs such as indomethacin in zein matrices can be further improved by making the matrix more hydrophobic, e.g. by partial denaturation of the zein protein. Finally, proteins at low water content remain a promising topic where many further investigations are possible that are interesting both for fundamental science and for industrial applications.

6.5. References

1. Shewry, P.R.; Napier, J.A.; Tatham, A.S. Seed storage proteins: structures and biosynthesis. *The plant cell* 1995, 7 (7), 945.
2. Kim, U.-J.; Park, J.; Li, C.; Jin, H.-J.; Valluzzi, R.; Kaplan, D.L. Structure and Properties of Silk Hydrogels. *Biomacromolecules* 2004, 5 (3), 786-792.
3. Bunning, T.; Jiang, H.; Wade Adams, W.; Crane, R.L.; Farmer, B.; Kaplan, D. *Applications of silk*, 1994.
4. Kweon, H.-Y.; Cho, C.-S. Biomedical applications of silk protein. *International Journal of Industrial Entomology* 2001, 3 (1), 1-6.
5. Ramos, Ó.L.; Fernandes, J.C.; Silva, S.I.; Pintado, M.E.; Malcata, F.X. Edible Films and Coatings from Whey Proteins: A Review on Formulation, and on Mechanical and Bioactive Properties. *Critical Reviews in Food Science and Nutrition* 2012, 52 (6), 533-552.
6. Elzoghby, A.O.; Abo El-Fotoh, W.S.; Elgindy, N.A. Casein-based formulations as promising controlled release drug delivery systems. *Journal of Controlled Release* 2011, 153 (3), 206-216.
7. Khwaldia, K.; Perez, C.; Banon, S.; Desobry, S.; Hardy, J. Milk Proteins for Edible Films and Coatings. *Critical Reviews in Food Science and Nutrition* 2004, 44 (4), 239-251.
8. Alcántara, C.R.; Rumsey, T.R.; Krochta, J.M. Drying rate effect on the properties of whey protein films. *Journal of Food Process Engineering* 1998, 21 (5), 387-405.
9. Tapia-Blácido, D.R.; Sobral, P.J.A.; Menegalli, F.C. Effect of drying conditions and plasticizer type on some physical and mechanical properties of amaranth flour films. *LWT - Food Science and Technology* 2013, 50 (2), 392-400.
10. Denavi, G.; Tapia-Blácido, D.R.; Añón, M.C.; Sobral, P.J.A.; Mauri, A.N.; Menegalli, F.C. Effects of drying conditions on some physical properties of soy protein films. *Journal of Food Engineering* 2009, 90 (3), 341-349.
11. Rupley, J.A.; Gratton, E.; Careri, G. Water and globular proteins. *Trends in Biochemical Sciences* 1983, 8 (1), 18-22.
12. Marcos, B.; Esteban, M.a.A.; López, P.; Alcalá, M.; Gómez, R.; Espejo, J.; Marcos, A. Monolayer values at 30°C of various spices as computed by the BET and GAB models. 1997, 204 (2), 109-112.

13. Bellissent-Funel, M. Collective effects in hydrated proteins. Hydration processes in biology: theoretical and experimental approaches 1999, 305-143.
14. Rahman, M.S. State diagram of foods: Its potential use in food processing and product stability. Trends in Food Science & Technology 2006, 17 (3), 129-141.
15. Almutawah, A.; Barker, S.A.; Belton, P.S. Hydration of gluten: A dielectric, calorimetric, and fourier transform infrared study. Biomacromolecules 2007, 8 (5), 1601-1606.
16. Careri, G.; Gratton, E.; Yang, P.H.; Rupley, J.A. Correlation of IR spectroscopic, heat capacity, diamagnetic susceptibility and enzymatic measurements on lysozyme powder. Nature 1980, 284 (5756), 572-573.
17. Belton, P.S.; Colquhoun, I.J.; Grant, A.; Wellner, N.; Field, J.M.; Shewry, P.R.; Tatham, A.S. FTIR and NMR studies on the hydration of a high-Mr subunit of glutenin. International Journal of Biological Macromolecules 1995, 17 (2), 74-80.
18. De Jong, G.I.W.; Van den Berg, C.; Kokelaar, A.J. Water vapour sorption behaviour of original and defatted wheat gluten. International Journal of Food Science & Technology 1996, 31 (6), 519-526.
19. John, M.K. Proteins as Raw Materials for Films and Coatings. in Protein-Based Films and Coatings; CRC Press, 2002.
20. Santivarangkna, C.; Higl, B.; Foerst, P. Protection mechanisms of sugars during different stages of preparation process of dried lactic acid starter cultures. Food Microbiology 2008, 25 (3), 429-441.
21. Roos, Y.H.; Roos, Y.H. Chapter 4 - Water and Phase Transitions. in Phase Transitions in Foods; Academic Press: San Diego, 1995; 73-107.
22. Fuquay, J.W.; Fox, P.F.; McSweeney, P.L. Encyclopedia of Dairy Sciences 2nd Edition, Four-Volume set. Academic Press, 2011.
23. Deegan, R.D.; Bakajin, O.; Dupont, T.F.; Huber, G.; Nagel, S.R.; Witten, T.A. Capillary flow as the cause of ring stains from dried liquid drops. 1997, 389 (6653), 827-829.
24. Narita, T.; Hebraud, P.; Lequeux, F. Effects of the rate of evaporation and film thickness on nonuniform drying of film-forming concentrated colloidal suspensions. The European physical journal. E, Soft matter 2005, 17 (1), 69-76.
25. Baukh, V.; Huinink, H.P.; Adan, O.C.G.; Erich, S.J.F.; van der Ven, L.G.J. Predicting water transport in multilayer coatings. Polymer 2012, 53 (15), 3304-3312.
26. Boulogne, F.; Giorgiutti-Dauphine, F.; Pauchard, L. The buckling and invagination process during consolidation of colloidal droplets. Soft Matter 2013, 9 (3), 750-757.
27. Sugiyama, Y.; Larsen, R.J.; Kim, J.-W.; Weitz, D.A. Buckling and Crumpling of Drying Droplets of Colloid-Polymer Suspensions. Langmuir 2006, 22 (14), 6024-6030.
28. Sadek, C.; Pauchard, L.; Schuck, P.; Fallourd, Y.; Pradeau, N.; Le Floch-Fouéré, C.; Jeantet, R. Mechanical properties of milk protein skin layers after drying: Understanding the mechanisms of particle formation from whey protein isolate and native phosphocaseinate. Food Hydrocolloids 2015, 48 8-16.
29. Anandharamakrishnan, C.; Rielly, C.D.; Stapley, A.G.F. Loss of solubility of α -lactalbumin and β -lactoglobulin during the spray drying of whey proteins. LWT - Food Science and Technology 2008, 41 (2), 270-277.
30. Zhang, H.; Mittal, G. Biodegradable protein-based films from plant resources: A review. Environmental Progress & Sustainable Energy 2010, 29 (2), 203-220.

31. Wang, L.Z.; Liu, L.; Holmes, J.; Kerry, J.F.; Kerry, J.P. Assessment of film-forming potential and properties of protein and polysaccharide-based biopolymer films. *International Journal of Food Science and Technology* 2007, 42 (9), 1128-1138.
32. Sothornvit, R.; Reid, D.S.; Krochta, J.M. Plasticizer effect on the glass transition temperature of beta-lactoglobulin films. *Transactions of the American Society of Agricultural Engineers* 2002, 45 (5), 1479-1484.
33. Gao, C.; Stading, M.; Wellner, N.; Parker, M.L.; Noel, T.R.; Mills, E.N.C.; Belton, P.S. Plasticization of a Protein-Based Film by Glycerol: A Spectroscopic, Mechanical, and Thermal Study. *Journal of Agricultural and Food Chemistry* 2006, 54 (13), 4611-4616.
34. Pillai, O.; Panchagnula, R. Polymers in drug delivery. *Current Opinion in Chemical Biology* 2001, 5 (4), 447-451.
35. Georget, D.M.R.; Barker, S.A.; Belton, P.S. A study on maize proteins as a potential new tablet excipient. *European Journal of Pharmaceutics and Biopharmaceutics* 2008, 69 (2), 718-726.
36. Engelman, D.M.; Steitz, T.A.; Goldman, A. Identifying Nonpolar Transbilayer Helices in Amino Acid Sequences of Membrane Proteins. *Annual Review of Biophysics and Biophysical Chemistry* 1986, 15 (1), 321-353.
37. Cabra, V.; Arreguin, R.; Vazquez-Duhalt, R.; Farres, A. Effect of temperature and pH on the secondary structure and processes of oligomerization of 19 kDa alpha-zein. *Biochimica et Biophysica Acta - Proteins and Proteomics* 2006, 1764 (6), 1110-1118.
38. Grant, A.; Belton, P.S.; Colquhoun, I.J.; Parker, M.L.; Plijter, J.J.; Shewry, P.R.; Tatham, A.S.; Wellner, N. Effects of Temperature on Sorption of Water by Wheat Gluten Determined Using Deuterium Nuclear Magnetic Resonance. *Cereal Chemistry Journal* 1999, 76 (2), 219-226.
39. Belton, P.S.; Delgado, I.; Halford, N.G.; Shewry, P.R. Kafirin structure and functionality. *Journal of Cereal Science* 2006, 44 (3), 272-286.
40. Wang, Q.; Yin, L.; Padua, G. Effect of Hydrophilic and Lipophilic Compounds on Zein Microstructures. 2008, 3 (2), 174-181.
41. Onwulata, C.; Huth, P. *Whey processing, functionality and health benefits*. John Wiley & Sons, 2009.
42. Giroux, H.J.; Britten, M. Encapsulation of hydrophobic aroma in whey protein nanoparticles. *Journal of Microencapsulation* 2011, 28 (5), 337-343.
43. Edmund H, I.; Herman F, M. Principles of Plasticization. in *Plasticization and Plasticizer Processes*; American Chemical society, 1965; 1-26.
44. Bisharat, L.M.N.m., University of East Anglia, 2012.
45. Craig, D.Q.M. The mechanisms of drug release from solid dispersions in water-soluble polymers. *International Journal of Pharmaceutics* 2002, 231 (2), 131-144.
46. Grund, S.; Bauer, M.; Fischer, D. Polymers in drug delivery-state of the art and future trends. *Advanced Engineering Materials* 2011, 13 (3), B61-B87.
47. Chauve, G.; Ravenelle, F.; Marchessault, R.H. Comparative imaging of a slow-release starch excipient tablet: Evidence of membrane formation. *Carbohydrate Polymers* 2007, 70 (1), 61-67.
48. Khan, P.A.; Ismail, S.J.; Gani, S.R. Gelatin beads as sustained release drug delivery system.

49. Hurtado-López, P.; Murdan, S. Zein microspheres as drug/antigen carriers: A study of their degradation and erosion, in the presence and absence of enzymes. *Journal of Microencapsulation* 2006, 23 (3), 303-314.
50. Liu, X.; Sun, Q.; Wang, H.; Zhang, L.; Wang, J.Y. Microspheres of corn protein, zein, for an ivermectin drug delivery system. *Biomaterials* 2005, 26 (1), 109-115.
51. Ritger, P.L.; Peppas, N.A. A simple equation for description of solute release I. Fickian and non-fickian release from non-swellable devices in the form of slabs, spheres, cylinders or discs. *Journal of Controlled Release* 1987, 5 (1), 23-36.
52. Kadian, S.S.; Harikumar, S.
53. Wang, Y.; Tilley, M.; Bean, S.; Sun, X.S.; Wang, D. Comparison of methods for extracting kafirin proteins from sorghum distillers dried grains with solubles. *Journal of Agricultural and Food Chemistry* 2009, 57 (18), 8366-8372.
54. Kumar, T.; Dweikat, I.; Sato, S.; Ge, Z.; Nersesian, N.; Chen, H.; Elthon, T.; Bean, S.; Ioerger, B.P.; Tilley, M. Modulation of kernel storage proteins in grain sorghum (*Sorghum bicolor* (L.) Moench). *Plant Biotechnology Journal* 2012, 10 (5), 533-544.
55. Spiess, K.; Ene, R.; Keenan, C.D.; Senker, J.; Kremer, F.; Scheibel, T. Impact of initial solvent on thermal stability and mechanical properties of recombinant spider silk films. *Journal of Materials Chemistry* 2011, 21 (35), 13594-13604.
56. Meerdink, G.; van't Riet, K. Modeling segregation of solute material during drying of liquid foods. *AIChE Journal* 1995, 41 (3), 732-736.



Summary/Samenvatting

The concept of drying and hydration of dense proteins systems is introduced in **chapter 1.** Preparation of food or pharmaceutical products with desired product properties is often challenging when approaching higher protein concentrations. Dense proteins systems have been scarcely studied compared to proteins at lower concentrations. In this thesis we investigate the properties of dense protein systems during drying and hydration. In first part of this thesis (**chapters 2 and 3**), we will address drying behaviour where we focus on the use of whey protein isolate as a model system. In the second part (**chapters 4 and 5**), we focus on the hydration properties of drug filled matrices of the corn protein zein. In addition, the potential of zein as a slow release agent for pharmaceutical drug is investigated.

In **chapter 2**, we start to investigate drying in a more fundamental way, thereby focussing on the drying of a protein coating. In previous studies mainly the macroscopic properties of protein coatings after drying are investigated, leaving the drying dynamics virtually unexplored. Here we investigate the drying behaviour of the model protein β -lactoglobulin on multiple length scales with an unique combination of in-line techniques. On the microscopic length scale we use dynamic vapour sorption and magnetic resonance imaging while on a smaller length scales, we have applied diffusing wave spectroscopy and IR-spectroscopy to monitor the drying process. For all used techniques, the changes in the measured physical properties of the coating as a function of water weight fraction X_w from $X_w = 0.8$ down to $X_w = 0.2$ are gradual. However, using dynamic vapour sorption and IR-spectroscopy we measure a sharp change below water weight fractions of $X_w = 0.2$. We hypothesise that changes in the molecular interactions caused by dehydration of the protein results in a change in the drying kinetics of the film.

In **chapter 3**, protein drying is approached on a more applied level, where we study the drying of a spherical droplet. We use single droplet drying as a methods that can model the spray drying process in a simplified and well-controlled way. Sessile droplets are subjected to varying drying conditions such as temperature, initial protein concentration, presence of airflow and droplet rotation. During these experiments the morphological development is monitored by a camera. After drying, scanning electron microscopy and X-ray tomography are used to examine the particles that are formed after complete drying. Irrespective of the conditions used, we observe an initial droplet shrinkage, followed by the nucleation of a

hole in the droplet skin, which is followed by the formation of a vacuole. The drying conditions used, strongly influenced the location of the hole and the locking point prior to hole formation. We hypothesised that the location of the hole is caused by local inhomogeneity's in protein concentration causing a the nucleation of the hole where the local skin modulus is lowest. Also the locking point of the droplet is found to be due to a inhomogeneity over the hole droplet caused by rapid evaporation. These results can be of importance to understand powder structure and functionality as obtained in spray drying.

In **chapter 4** and **chapter 5** we have investigated the potential of zein as a sole excipient as obtained by hot melt extrusion (HME) and injection moulding (IM). Zein is good candidate as a sustained release agent, because it is insoluble in water, it is relatively heat and pH stable and it has a good microbial stability. In **chapter 4**, zein matrices were loaded with the drug paracetamol. Physical mixtures of zein, water and crystalline paracetamol are extruded and injection moulded into caplets. Characterisation of these caplets is performed using differential scanning calorimetry, IR- spectroscopy, scanning electron microscopy and powder X-ray diffraction. The hydration and drug release kinetics from the caplet slices is measured. We find that the drug release kinetics is broadly independent of the dissolution medium and drug loading. The release kinetics is diffusion limited and could be well described by a 2D diffusion model. The results demonstrate that the drug release rate from zein caplet slices can be tuned by its dimensions.

in **chapter 5**, a wider range of drugs differing in hydrophobicity is studied. Next to paracetamol, we have used two other model drugs, the hydrophobic indomethacin and the more hydrophilic ranitidine. The caplets are similarly characterised as in **chapter 4**. The zein matrix is capable to stabilize the different dugs in a non-crystalline state, which is promising especially for increasing the bioavailability of poorly water-soluble drugs. Overall crystallinity of the drugs in the caplets increases with its degree of hydrophobicity. For the poorly soluble indomethacin, dissolution rates at low pH were higher from caplet slices, compared to the dissolution rates of indomethacin crystals by themselves. In addition, we found that the electrostatic interactions between zein and drugs can also be used to influence the release kinetics.

Several aspects of drying and hydration behaviour of concentrated proteins are discussed in the general discussion (**chapter 6**). In particular, the homogeneity of drying

and hydration, the effect of protein plasticisation and the topic of protein hydrophobicity are discussed. Finally, we give recommendations for future research lines on spray drying and drug delivery.

Het belang van het drogen en hydrateren van geconcentreerde eiwitten systemen wordt geïntroduceerd in **hoofdstuk 1**. Bij het bereiden van levensmiddelen of farmaceutische producten, met een hoge eiwit concentratie, is het behalen van gewenste product-eigenschappen vaak een uitdaging. In vergelijking met eiwitten bij lagere concentraties zijn hoog geconcentreerde eiwitssystemen amper onderzocht, waardoor het gedrag onder hoge concentraties, relatief slecht begrepen is. In dit proefschrift onderzoeken we de eigenschappen van geconcentreerde eiwit systemen tijdens droog- en bevochtigingsprocessen. In het eerste deel van dit proefschrift (**hoofdstuk 2 en 3**), zullen we ons op het drooggedrag richten, waar we wei-eiwitten als modelsysteem gebruiken. In het tweede deel (**hoofdstuk 4 en 5**), richten we ons op de hydratatie-eigenschappen van met medicijn gevulde matrices bestaande uit het mais eiwit zeïne. Hierbij wordt de potentie van zeïne als excipiënt voor de langzame afgifte van farmaceutische geneesmiddelen onderzocht.

In **hoofdstuk 2** beginnen we op een meer fundamentele wijze eiwitdroging te onderzoeken. Hier richten we ons op het drogen van een eiwit laagje. In eerder onderzoek zijn met name macroscopische eigenschappen van eiwitlaagjes na het drogen onderzocht, terwijl dynamiek tijdens het drogen amper onderzocht was. In dit hoofdstuk onderzoeken wij het drooggedrag van het model eiwit β -lactoglobuline op meerdere lengteschalen met behulp van een unieke combinatie van in-line technieken. Voor de grotere lengteschaal (cm- μ m) gebruiken we dynamic vapour sorption (DVS) en magnetic resonance imaging (MRI) terwijl bij kleinere lengteschalen hebben we diffusie wave spectroscopie (DWS) en IR-spectroscopie gebruikt om het droogproces te volgen. Voor alle gebruikte technieken zijn de veranderingen in de gemeten fysische eigenschappen als functie van de water gewichtsfractie X_w van $X_w=0,8$ naar $X_w=0,2$ heel geleidelijk. Daarentegen, bij water gewichtsfracties lager dan $X_w=0,2$ meten we juist een sterke verandering met DVS en IR-spectroscopie. We veronderstellen dat veranderingen in de moleculaire interacties, die veroorzaakt wordt door dehydratatie van het eiwit, een verandering teweegbrengen in de macroscopische droogkinetiek van de film.

In **hoofdstuk 3**, wordt eiwitdrogen op een meer toegepast niveau benaderd waarbij we het drogen van druppels onderzoeken. Het drogen van enkelvoudige druppels wordt als methode gebruikt om het spreedroog-proces op een vereenvoudigde en goed gecontroleerde manier te modelleren. Sessiele (liggende) druppels worden gedroogd onder verschillende condities met als variabelen: temperatuur, initiële eiwitconcentratie

aanwezigheid van luchtstroom en druppel rotatie. Tijdens deze experimenten werd de ontwikkeling van de morfologie gevolgd door een camera. De deeltjes werden na het drogen onderzocht met elektronenmicroscopie en röntgen-tomografie. Voor alle gebruikte omstandigheden, zien we in de beginfase de druppels krimpen, gevolgd door de vorming van een gat, die zich uitholt tot een vacuole. De droogomstandigheden waren sterk bepalend voor 1) de plaats waar het gat zich vormde en 2) de grootte van de druppel tijdens de vorming van het gat. Onze hypothese is dat de locatie van het gat wordt veroorzaakt door plaatselijke inhomogeniteit in eiwitconcentratie waardoor het gat zich vormt op de plaats waar de lokale modulus van het vlieslaagje het laagst is. Ook de druppelgrootte tijdens de vorming van het gat wordt in grote mate bepaald door de inhomogeniteit, die veroorzaakt wordt door de snelle verdamping. De gevonden principes leveren meer inzicht in de poeder eigenschappen zoals verkregen na het sproeidrogen.

In **hoofdstuk 4** en **hoofdstuk 5** hebben we het onderzoek gericht op de potentie van zeïne als excipiënt (hulpstof) in caplets (tabletvormen) die gemaakt zijn door middel van hot-melt extrusie (HME) en spuitgieten (IM). Zeïne eiwit is een goede kandidaat om de vertraagde afgifte van medicijnen te bewerkstelligen. Het eiwit is onoplosbaar in water, relatief hitte en pH ongevoelig en het heeft een goede microbiële stabiliteit. In hoofdstuk 4 hebben we zeïne matrixen gemaakt met paracetamol daarin gedispergeerd. Poeder mengsels van zeïne, water en kristallijn paracetamol werden geëxtrudeerd en spuitgegoten in caplets. De caplets werden gekarakteriseerd door middel van differentiële scanning calorimetrie, IR-spectroscopie, scanning elektronenmicroscopie en röntgen verstrooiing. Vervolgens werden de hydratatie en medicijnafgifte van de caplets gemeten. We vinden dat de afgifte kinetiek in grote lijnen onafhankelijk is van het oplosmedium en de medicijn concentratie. De afgifte kinetiek is beperkt door het diffusie proces en kon goed worden beschreven met een 2D diffusie model. De resultaten tonen aan dat de (medicijn) afgiftesnelheid van zeïne tabletten kunnen gevarieerd door de afmetingen van de caplets aan te passen .

In **hoofdstuk 5** wordt een breder scala aan medicijnen met verschillen in hydrofobiciteit bestudeerd. Naast paracetamol, testen we de hydrofobe indomethacine en de meer hydrofiele ranitidine. De caplets worden op dezelfde wijze gekarakteriseerd als in **hoofdstuk 4**. We ontdekken dat de zeïne matrix in staat is de verschillende medicijnen in een niet-kristallijne toestand te stabiliseren. Deze vinding maakt zeïne als matrix veelbelovend voor het verhogen van de biologische beschikbaarheid van slecht (in water)

oplosbare geneesmiddelen. Verder neemt de totale kristalliniteit van de geneesmiddelen in de tabletten toe met de mate van hydrofobiciteit van het geneesmiddel. Bij lage pH was de afgifte snelheid van indomethacine uit caplets zelfs sneller dan uit het pure indomethacine kristallen. Bovendien vonden we dat de elektrostatiche interacties tussen zeïne en medicijnen kunnen worden gebruikt om de afgifte kinetiek beïnvloeden.

Tenslotte worden verschillende aspecten van drogen en hydratatie gedrag van geconcentreerde eiwitten wordt beschreven in de algemene discussie (hoofdstuk 6). Met name worden de homogeniteit van het drogen, het effect van eiwit plastificeren en het onderwerp: eiwitten hydrofobiciteit besproken. Tot slot geven we aanbevelingen voor toekomstig onderzoeklijnen op het gebied van sproeidrogen en drug delivery.

Acknowledgements

4 years and 2 months of PhD have ended. The experience was much like going through a tunnel. A long period of focusing on a small subject will create a tunnel vision. Like tunnel there is light on the end that is getting brighter and brighter when approaching the exit. The moment closes when I will go out..... a wide awakening. But before this moment, I will look back once more and will see many people which I would like to acknowledge.

In my thesis I had the luxury (and sometimes the burden) to have many supervisors/collaborators. I want to dedicate this section to thank all of you.

Allereerst Renko, vanaf het begin zei je dat dit PhD project veel zelfstandigheid vereiste. Vaak heb ik hier wel mee geworsteld, maar op een aantal beslissende momenten, wist je me weer helemaal te motiveren. Dank je wel hiervoor. Paul, je had altijd veel ideeën die het project meer diepgang gaven. Ook heb ik veel geleerd over klussen en verbouwingen, dank je wel voor alles. Erik, bedankt voor je energieke, optimistische, maar ook betrokken houding. Ik heb het enorm gewaardeerd!

Pete, you always had interesting and helpful ideas, which directly applied to my challenges. Next to this you were always a nice presence and I enjoyed your stories in Norwich and during the traveling. Sheng, many thanks for your involvement. I enjoyed and connected very well with your to the point attitude and your practical approach and I was impressed by your dedication to your work.

Laura, many thanks for your perseverance and care during the project. Maarten, wederom heb ik je efficiënte en betrokken aanpak gewaardeerd. Ook waren onze gezamenlijke conferenties en je pizza diner gezellig. Viktor and Henk, thanks for you technical skills and hospitality during my visits in Eindhoven.

Thanks as well to my 5 students: Matthijs, Jun, Chaojun, Marise and Erik. It was great to supervise you! I was always glad to meet you, at uni or at other places, also after you were finished.

Harry, Miranda, Martin, Peter, Remko Hamoen en Remko Fokkink, enorm bedankt voor jullie hulp met het experimentele deel. Ook veel dank aan Els, Mara en Josie voor de vele praktische ondersteuning en de goede gesprekken.

From the School of pharmacy, I would like to thank first of all Karol. Shortly we have collaborated which enjoyed a lot. Often we went to the pub on Friday evening or joined the group's movie nights, accompanied by Susana, Fabiane, Desire, Marco, Melania Carl and many others. These were great times! Also in the office and in the lab, I thank to Champ and Khaled, also for the nice trips we made to some English cities. Muqdad I liked all the enlightening discussions with you. Also many thanks to Cholpon, Sam and Lorina.

From Fysko, allereerst Sabine and Johan, mijn kantoorgenootjes: de combinatie van serieus werken met soms wat geks tussendoor was ideaal. Dmitry and Yunus, I really enjoyed our jamming time together (Arctic Monkeys.... still don't know how to play it). Christian, you always amazed me with your laidback approach to life, keep on going. Jeroen, Maria, Rui en Marcel, altijd een mooi sfeertje met jullie gezellig buiten met of zonder peukie. Wolf and Inge, bedankt voor de mooie Hawaii trip, rijdend in een cabrio, langs de zwarte stranden op weg om te gaan snorkelen. Also thanks to Tao, Harke, Armando, Monica, Lyakat (Mr Muscles), Lennart, Soumi, Gosia, Gosia, Merve, Hande, Natalia, Hanne, Helene, Juan, Jan Maarten and many others who joined the group later.

From Food physics my office mates (Jerome, Silvia, Elizabete, Pauline, Jinfeng, Alev and Min) at the many different offices we have been, many thanks to you. Kun, Anika Jinfeng and Min, thanks for the Canada holiday spotting a bear and many moose. Tijs, jouw humor was altijd een inspiratie voor me. Also thanks to Claire, Auke, Anika, Maria, Zhilli, Carsten, Vaida, Lenka, Kun, Leonard and Elke.

Verder aan mijn studievrienden Pascalle, Thomas, Milou, Nicole, Jacqueline, Inge en Marieke: vooral de ski-week zal ik niet vergeten, dank jullie wel. En natuurlijk de jaarclub: Jouke, Mikel, Caroline, Erik, Eline en Leendert. Hier vond ik iets dat echt reproduceerbaar is: geen weekend met jullie, zonder geniale en memorabele momenten.

Hans bedankt voor alle uitnodigingen naar die mooie party's, waar Lisette vaak ook bij was. Wim...sorry dat je nu plaats moet maken. Arjan, dat wildkamperen, gaan we zeker nog vaker doen. Elly, bedankt voor alle Rotterdam avonturen. Niet te vergeten ook pa en ma ook ontzettend bedankt voor alle steun en wijsheid. En natuurlijk mijn lieve Geraldine, misschien ben jij wel de grootste ontdekking van mijn PhD ;) :*.

About the author

Jacob Bouman was born in 's Hertogenbosch (The Netherlands) on April 3rd 1986. His secondary education took place at the Willem van Oranje College in Waalwijk, which he finished in 2004. Following his secondary school he started the bachelor levensmiddelentechnologie (food technology) at Wageningen university. In 2007 he wrote a thesis entitled *The kinetics of fibrillation of β -lactoglobulin* at the department of Physics and Physical Chemistry of Foods after which he finished his Bsc. Next, he started a gap year, where he did a one year study of Biblestudy and faithbuilding at the Wittenberg in Zeist. In 2008 he continued his studies in Wageningen and chose a master specialisation *process and product design*. His Msc. thesis on the topic, *rehydration of single food particles*, took place at the department of Food process engineering and was in collaboration with Friesland-Campina. For his internship he went to the United Kingdom, where he worked at the R&D department of Pepsico located at Beaumont park in Leicester. In September 2010, Jacob obtained his Msc. degree.



After a short job as logistical planner, Jacob started his PhD, which was a collaboration between Physical Chemistry and Soft Matter and Physics and Physical Chemistry of Foods. He studied drying and hydration behaviour of concentrated proteins. This PhD also entailed a collaboration with the school of pharmacy at the University of East Anglia in Norwich (UK), where he spend almost 1/3 of his PhD. The result from his four years of research are described in this thesis. Since September 2015, Jacob works at Nestlé in Nunspeet (NI) as process technologist in infant formula production.

Publications

Bouman, J.; De Vries, R.; Venema, P.; Van Der Linden, E.; Schutyser M.A.I. Hole and vacuole formation during drying of sessile whey protein droplets. *Submitted to journal*.

Bouman, J.; Belton, P.; Venema, P.; van der Linden, E.; de Vries, R.; Qi, S. Controlled release from zein matrices: interplay of drug hydrophobicity and pH. *Accepted*.

Alhijaj, M; Bouman, J; Wellner, N; Belton,P; Qi, S Creating drug solubilisation compartments via phase separation in multi-component buccal patches prepared by direct hot melt extrusion-injection moulding. *Submitted to journal*.

Bouman, J.; Belton, P.; Venema, P.; van der Linden, E.; de Vries, R.; Qi, S. The development of direct extrusion-injection moulded zein matrices as novel oral controlled drug delivery systems *Pharmaceutical Research*. **2015**, 1-12.

Bouman, J.; De Vries, R.; Venema, P.; Belton, P.; Baukh, V.; Huinink, H. P.; Van Der Linden, E. Coating formation during drying of β -lactoglobulin: gradual and sudden changes. *Biomacromolecules* **2015**, 16 (1), 76-86.

Kroes-Nijboer, A.; Venema, P.; Bouman, J.; Van Der Linden, E. Influence of protein hydrolysis on the growth kinetics of β -lg fibrils. *Langmuir* **2011**, 27 (10), 5753-5761.

Kroes-Nijboer, A.; Venema, P.; Bouman, J.; Van Der Linden, E. The critical aggregation concentration of β -lactoglobulin-based fibril formation. *Food Biophysics* **2009**, 4 (2), 59-63.

Overview of completed training activities

Disciplined specific activities

Courses

Advanced Soft matter, 2011, Wageningen

Han sur Lesse winterschool, 2011, Han-sur Lesse, Belgium

Conferences and Workshops

Euro food Water conference, 2012, Helsinki, Finland

Water Biophysics, 2012, Perugia, Italy

International drying Symposium, 2014, Lyon, France

APS PharmSci conference, 2014, Hatfield, UK

General Courses

Promotie in eigen regie, 2011, Utrecht

Endnote course, 2011, Wageningen

Matlab Fundamentals, 2014, Eindhoven

Nyenrode Business Week, 2014, Breukelen

Loopbaan orientatie, 2015, Utrecht

BCF career event 2015, Amsterdam

Optional courses and activities

Physical chemistry and colloid sciences group day 2011-2014

Physics and Physical chemistry of foods group day 2011-2014

Physical chemistry and colloid sciences study tour, 2013, USA (California)

Physics and Physical chemistry of foods, 2014, USA (east coast) and Canada

This research forms part of the IPP-Bio related materials program, funded by Foundation for Fundamental Research on Matter (FOM)

This thesis was printed by GVO drukker & vormgevers B.V, Ede, The Netherlands